REACTOR EXPERIMENTS AND RADIATION DETECTION

P. Frajtag, O. Pakari, G. Perret, M. Hursin, V. Lamirand, D. Siefman, A. Scolaro and A. Pautz

Lausanne, EPFL, 2025

Contents

List of Figures

List of Tables

1 Alpha particle detection

1.1 Introduction

This experiment gives an introduction into alpha particle physics and detection. Alpha particles are important to nuclear engineers because they are a large source of danger in radiation safety and because they are emitted by the major and minor actinides found in nuclear reactor waste. Additionally, alpha particles are used as a tool to artificially create neutrons with the (α, n) reaction. Such a reaction is used to create the neutrons necessary to start the chain reaction in nuclear fission reactors.

Alpha particles are unique in that they have a large biological effect, i.e. they are very damaging, but are also at the same time relatively easy to protect against as they rapidly lose energy when coming into contact with matter. A good rule of thumb is that human skin or a piece of paper is sufficient to stop an alpha particle. However, if they can reach sensitive tissue within a biological organism, they can cause serious damage because of their large size, electrical charge, and high energy. These facts are why it is possible to hold safely plutonium in one's hand and feel only a warm glow. Meanwhile in deadly contrast, ingesting plutonium and letting the alpha particles come into contact with sensitive pulmonary or digestive tissues will commonly prove to be fatal.

Students during this experiment will learn the principles of alpha particle decay, their behaviour when interacting with matter, the types of detectors that can be used to detect and characterize alpha particles, and the optimum construction of an alpha particle detection system that takes into account the unique features of alpha particle physics.

1.2 Theory

1.2.1 Alpha decay

Heavy nuclei are energetically unstable and tend to decay by the emission of an alpha particle. The reaction that emits an alpha particle is given in Equation 1.1, where X and Y are the initial and final nuclear species, or parent and daughter nuclides, and the He nucleus is the alpha particle.

$$ {}^{A}_{Z}X \rightarrow {}^{A-4}_{Z-2}Y + {}^{4}_{2}He \quad (alpha\ or\ \alpha) \tag{1.1} $$

For each distinct transition between initial and final state (from X to Y), a fixed amount of energy is released, called the Q-value of the reaction. This energy is shared between the alpha particle and the recoiling heavy nucleus, Y. The alpha particle takes an amount of energy given by *Q(A-4)/A*, A being the mass number of the parent, or decaying nucleus X. The rest of the energy, *Q(4/A)*, appears as the recoil energy of the daughter nucleus, Y. In other words, the alpha particle takes much more energy than the recoil nucleus and the energy of the alpha particle is mono-energetic at the fraction *(A-4)/A* of the reaction's Q-value.

Theoretically, an alpha particle's energy is unique for each transition and it is determined by the fraction *(A-4)/A*. However in the laboratory setting, an energy spread is measured for each alpha particle as seen in Figure 1.1, where an alpha particle appears to have multiple possible energies. This spread in measured energies is in one part due to both the particle's energy loss when it traverses the source it was created in and the energy loss occurring when it passes through other materials before reaching a detector. Additionally, an energy spread is caused by the resolution of the detection system, i.e. variations of the signal amplitude associated with the detection process itself.

Table 1.1 presents the characteristics of common radioisotope sources of alpha particles. It is important to note that one parent nuclide might decay in several different ways with varying degrees of probability. Each of these possible transitions has a different Q-value and therefore the alpha particle produced in the transition has a different energy, which usually lays in the range of 4 - 6 MeV.

Usually, the higher the energy of the alpha particle, the shorter the half-life. For nuclides emitting alphas of energy greater than 6.5 MeV, the half-life is expected to be less than a few days, limiting thereby their practical utility. On the other hand, if the energy of the emitted alpha particles is below 4 MeV, emission occurs less often, and the half-life is very large. This results in low specific activity or low source intensity, and hence, is of very limited application. Long half-life alpha-emitting radioisotopes have implications when handling nuclear reactor waste as they become determining factors in how long the waste needs to be stored. They are especially important when considering the severe biological effect upon being ingested. ^{239}Pu for instance, has a half-life of 2.4 x 10^4 years, meaning that waste containing this isotope must

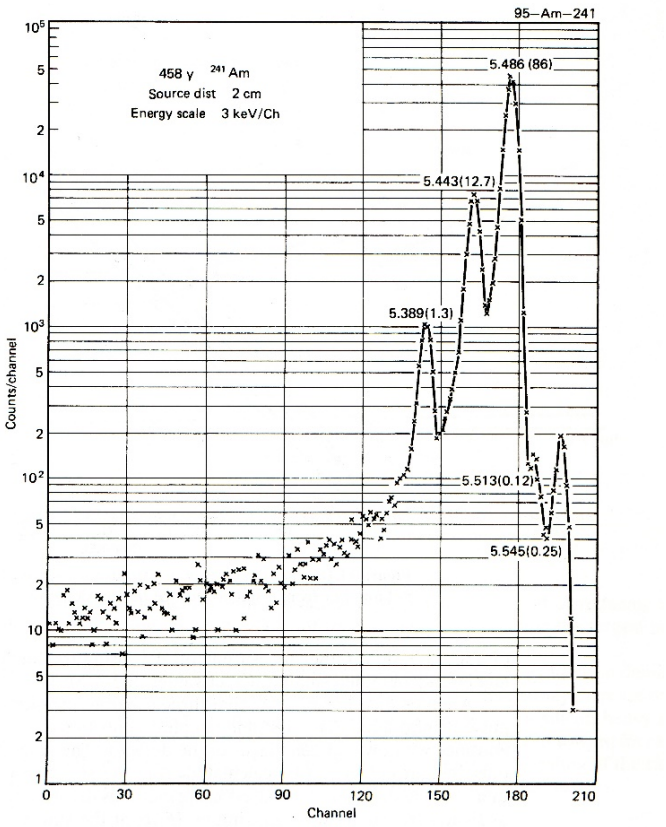

Figure 1.1: Alpha-energy spectrum from the decay of ^{241}Am, as measured by a silicon surface-barrier detector [1]. Each peak is identified by its energy in MeV and percent abundance (in parentheses).

be stored for at least that period of time, lest it be ingested by some unlucky organism.

Alpha particles lose energy rapidly while traversing a material, and therefore it is necessary to prepare such sources in the form of a very thin layer. Also, in order to protect and contain the radioactive material for operational safety, sources are usually covered with an extremely thin metallic or plastic foil, maintaining the condition of minimal energy degradation in the source itself. As an illustration, the linear range of 5.5 MeV alpha particles emitted from an ^{241}Am source is about 2.4x10^{-3} cm, or 24 μm, in aluminium (A = 27, ρ = 2.69 g.cm^{-3}). This range given in units of weight per unit area is 6.5x10-3 g.cm^{-2}. For understanding the process of alpha detection, the following section describes their interaction with matter.

Table 1.1: Examples of alpha-emitting radionuclides [1]

Source	Half-life	Energy [MeV]	%-Branching
^{232}Th	1.4 x 1010y	4.012	77
		3.953	23
^{238}U	4.5 x 109y	4.196	77
		4.149	23
^{235}U	7.1 x 108y	4.598	4.6
		4.401	56
		4.374	6
		4.365	12
		4.219	6
^{236}U	2.4 x 107y	4.494	74
		4.445	26
^{230}Th	7.7 x 104y	4.688	76.3
		4.621	23.4
^{234}U	2.5 x 105y	4.774	72
		4.722	28
^{231}Pa	3.2 x 104y	5.059	11
		5.030	20
		5.014	25.4
		4.952	22.8
^{239}Pu	2.4 x 104y	5.155	73.3
		5.143	15.1
		5.105	11.5
^{240}Pu	6.5 x 103y	5.168	76
		5.124	24
^{243}Am	7.4 x 103y	5.275	87.4
		5.234	11
^{210}Po	138 d	5.305	99 +
^{241}Am	433 y	5.486	85.2
		5.443	12.8
^{238}Pu	88y	5.499	71.1
		5.457	28.7
^{244}Cm	18y	5.805	76.4
		5.763	23.6
^{243}Cm	30 y	6.067	1.5
		5.99	5.7
		5.785	73.2
		5.742	11.5
^{242}Cm	163 d	6.113	74
		6.069	26
^{254m}Es	276 d	6.429	93
^{253}Es	20.5 d	6.633	90
		6.592	6.6

1.2.2 Interaction of alpha particles with matter

Heavy charged particles like alphas react primarily with matter through coulomb forces between the positively charged alpha and the negatively charged electron cloud of the absorbing medium. When the alpha particle interacts with the absorbing medium's electron cloud, it will either excite an electron/electrons, i.e. raise the electron to a higher energy shell, or remove the electron from the absorber atom, a process called ionization. Both of these reactions require energy, which comes at the expense of the alpha particle. As these reactions occur many times while traversing a medium, the alpha particle steadily loses energy and therefore its velocity decreases.

The slowing down of a charged particle like an alpha is described by its *linear stopping power, -dE/dX*. This is the differential energy loss per unit length for an incident particle, or the amount of energy lost by the particle per unit distance it travels. The linear stopping power is governed by the Bethe formula, given as Equations 1.2 and 1.3.

$$-\frac{dE}{dX} = \frac{4\pi z^2 e^4 NZ}{m_0 v^2}\left[ln\left(\frac{2m_0 v^2}{I}\right) - ln(1-\beta^2) - \beta^2\right] \tag{1.2}$$

Or,

$$-\frac{dE}{dX} = \frac{4\pi z^2 e^4 NZ}{m_0 v^2} B \tag{1.3}$$

where v and z are the velocity and charge of the incident particle, e is the charge of the electron, N and Z represent the number density and atomic number of the absorber, m_o and e are the electronic rest mass and charge, and $\beta = v/c$. The parameter I represents the weighted average excitation and ionization potential of the absorber, and is treated as an experimental constant for each absorber element. For a non-relativistic particle, β is small because $v \ll c$ and, as a result, only the first term in B is significant, which varies slowly with velocity. Thus, the specific energy loss for a given particle and absorber is mainly determined by the velocity of the incident particle, but also by the number density and atomic number of the absorber. Since the energy of the particle is continuously decreasing while traversing the medium, the specific energy loss increases as velocity decreases.

Equation 1.2 is valid only for high energies ($E/m \geq 1$ MeV/u). This is because as the energy of the alpha particle decreases, it tends to pick up more electrons from the medium it is crossing. Once the alpha particle's electron shell is full, the collisions between the alpha particle and electrons of the target atoms become nearly elastic. As the reactions between the alpha particle and absorber's electron cloud no longer result in large energy losses, the specific energy loss, $-dE/dX$, begins to decrease sharply.

An example of this behaviour is shown in Figure 1.2 for an alpha particle with an initial energy

of several MeV. This figure showing the alpha's energy loss is known as the Bragg curve. For most of the track, the alpha particle loses energy at a roughly $1/E$ rate as its charge is that of $2e^{-}$. Near the end of the track, the alpha particle loses its charge through electron pickup and the alpha particle can no longer lose energy as effectively through coulombic collisions. Figure 1.2 also shows two Bragg curves for a single particle vs. a parallel beam. The curves are different because an alpha particle's interactions occur stochastically and differ from particle to particle. Therefore, when comparing a single particle to the behaviour of the average particle (or the entire parallel beam), differences can occur.

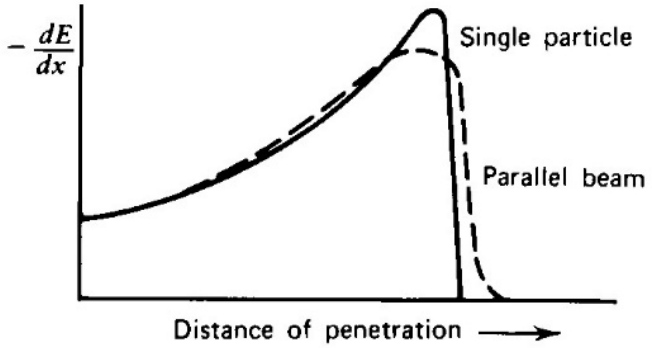

Figure 1.2: The Bragg curve, or the specific energy loss of alpha particles traversing a medium.

1.2.3 Principles of alpha detection

The detection of charged particles is usually done directly through ionisation in a given medium or via phenomena produced by ionisation. The different principles used in the detection of charged particles are summarised in Table 1.2. The first three detection methods fall into the category of on-line methods, whereas the last is an off-line method and has been found particularly useful for low intensity applications.

Table 1.2: Methods for detection of charged particles [4].

Detection method	Detector type	Detection medium
1. Charge carriers	Ionization chambers	Gases, semiconductors
	Proportional counters	Gases
	GM counters	Gases
2. Light sensing	Scintillation detectors	Inorganic crystals
		Organic liquids and plastics
		Noble elements
	Cerenkov detectors	Gases, transparent liquids and solids
3. Free carrier + light sensing	Hybrid detectors	Gases and liquids of noble elements
4. Track recorders	Track-etch detectors	Minerals, glasses and plastics

As mentioned earlier, alpha particles either get absorbed or lose a significant fraction of their energy while passing through materials. It is therefore important that, if a gas ionisation detector is used for their detection, it must have a very thin window for permitting the entry of these particles so that the alpha particle is not stopped before it reaches the detection medium. Solid-state detectors offer a much better energy resolution and a far thinner window for entry, and hence are generally preferred for alpha detection.

Detectors based on solid-state devices are far superior to ionisation chambers because of the lower energy required to produce a charge carrier. In addition, the high field is obtained because of their small dimensions and not necessarily due to higher applied voltage.

In a simplistic picture, one could say that a p-n junction is formed by establishing a heavily doped n-type layer on the surface of a p-type silicon wafer, as shown in Figure 1.3.

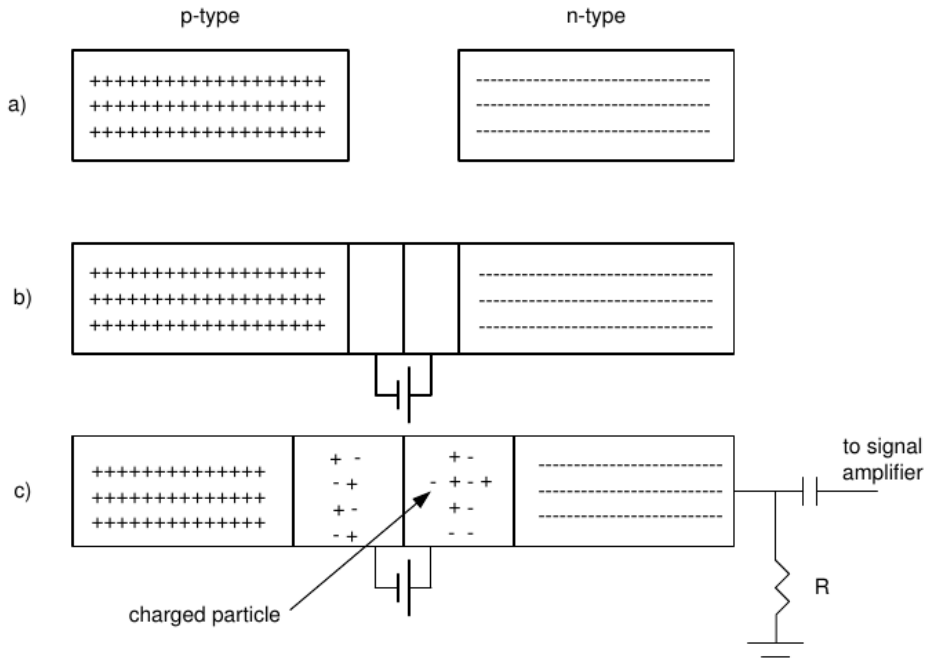

Figure 1.3: Formation and extension of depletion layer for particle detection.

One can obtain a region inherently depleted of free charge carriers (see Figure 1.3b), known as the depletion region. This region can be extended by applying a reverse bias, as shown in Figure 1.3c. Now, when a charge particle traverses this medium, producing a trail of electrons and holes, the applied bias will enable a quick removal of charges, and an appropriate charge-sensitive pre-amplifier and amplifier will then provide a pulse height proportional to the charge collected, i.e. to the energy of the incident particle. These detectors can be easily produced with depletion regions of a few hundred microns and hence are found suitable for most laboratory applications involving alpha particles.

In the current measurements, a surface barrier silicon detector will be used. This is essentially a

p-n junction, generally obtained by using an n-type silicon wafer which is stored in a humidity-controlled atmosphere after standard etching and mounting. The storage overnight results in absorbing oxygen, which yields a p-type surface. The electrical contacts are established by evaporating gold on the p-type, and aluminium on the n-type, surface. These detectors are characterised by a very thin dead layer, typically about 0.1 μm silicon equivalent, which corresponds to the loss of ~14 keV for a 5 MeV alpha particle.

A general layout of the complete detection system for the various detectors that will be employed in this laboratory course is depicted in Figure 1.4 The rectangle depicting an ionisation chamber in the figure will, in effect, be replaced by other detector types. In this experiment, the detector is a semiconductor.

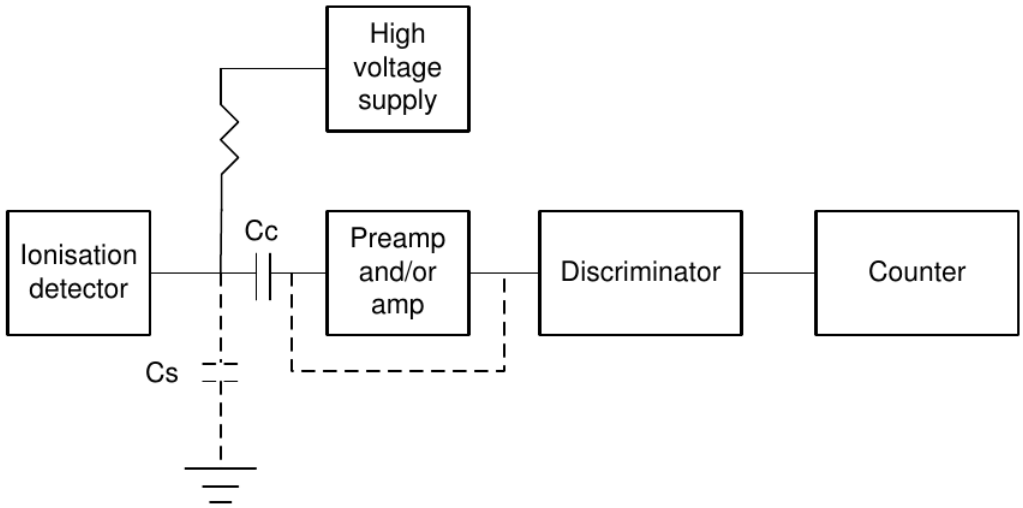

Figure 1.4: Block diagram of a typical counting setup for a gas ionisation detector.

1.3 Experiment description

The following experiments will be carried out using the alpha spectrometer:

- Experiment 1: Energy spectrum of an ^{241}Am alpha source
- Experiment 2: Degradation of spectrum with pressure and source-detector distance
  - Examination of the effects of air density and distance on the efficiency of the detector and the quality of the source's energy spectrum.
- Experiment. 3: Absolute source strength of an ^{241}Am source
  - Backtrack the strength of the source using the results from the detector

1.3.1 Important Precautions

The following precautions need to be followed at all times to ensure the safety of the experimenters and the equipment and to create high quality results.

1. Handle the radioactive source with care, following radiation safety principles.
2. Do not touch the surface of the silicon Surface-Barrier Detector (SBD).
    - The build-up of grease and dirt upon the surface attenuates the alpha particles.
3. Apply the specified voltage to the SBD, only after closing the vacuum chamber.
4. The voltage should be switched off before opening the vacuum chamber for any adjustments.
5. Do not connect/remove the power cable while the power is on.
6. Measurements without air should be carried out when the vacuum conditions are stabilised (usually takes 10-15 min).
    - Fluctuating pressure introduces uncertainties into the experimental results.
7. Switch off the vacuum pump at the end of the experiment.

1.4 Required setup

The following components are required for this experiment. Check to see if they are available. If they are not available, please speak with your lab instructor.

1. A portable vacuum system
2. A steel vacuum chamber - model-807
3. A silicon surface barrier detector
4. A calibrated ^{241}Am alpha source
5. An electronic unit.
6. Data acquisition system
7. A timer-counter electronic units ORTEC-871

This electronics unit processes detector pulses and has the bias supply, pre-amplifier and an amplifier, discriminator, and pulser unit (frequency 100 Hz) integrated into a single unit. The data acquisition system consists of an MCB-926 (Multi-Channel Buffer, single-width

bin module) coupled to a PC with MAESTRO-32 software, allowing use in a multi-channel configuration. The data acquired can be suitably treated with built-in options. The timer-counter is used for the source strength measurements.

1.5 Operational settings

Component	Setting
Surface-barrier detector bias	On
Vacuum conditions	Lowest possible when stable
Test pulser	Switch on whenever required
Preamplifier, amplifier and discriminator	All integrated in a single unit
MCB-926 input	To energy output of PAD

1.6 Measurement steps

1.6.1 Experiment 1: Energy spectrum of an ^{241}Am alpha source

The first step of this experiment is to obtain an energy spectrum for the ^{241}Am alpha source. The following steps should be followed to ensure good results.

1. Place the platform at a height such that the distance between the source and the detector is about 4 cm. Use the ruler and pincers at hand to measure the distance between the source and the detector.

    - **Note**: The distances between the platform and the detector and the source and the detector are not the same.
    - The surface barrier detector is mounted at the inner side of the top of the vacuum chamber. The alpha source can be placed at varying heights upon a platform within the vacuum chamber.

2. Turn on the vacuum system to evacuate the chamber. Do not begin measurements until the pressure is stable (typically between 30-50 mbar).

    - Lowering the air pressure, i.e. density, allows more and more alpha particles to reach the detector without losing significant energy in the intervening region, thus providing reasonably clear energy peaks corresponding to the various alpha energies.

3. Apply a specified high voltage to the silicon surface-barrier detector via the PAD unit.

4. Initialize the data acquisition in the MCB-926 multi-channel buffer unit. The energy spectrum of the ^{241}Am source is then obtained from the channel-count plot.

- Collect until approximately 10,000 counts to have good statistics. Record the exact number of counts.

5. Save the spectrum as ASCII SPE within the software. Make sure to indicate at which pressure and height it was obtained when saving.

1.6.2 Experiment 2: Degradation of spectrum with pressure & source-detector distance

The next step is to investigate the effects that the distance from the source to detector and the air density have upon the detector's efficiency and the quality of energy spectra. The distance is modified by moving the platform within the vacuum chamber. Students should vary the distance and pressure a sufficient number of times until they think that the phenomena are well characterized by the experimental results.

1. Make sure that the high voltage power supply is turned off before opening the vacuum chamber.

2. To change the pressure in the chamber first open the green valve then turn the yellow. Once the desired pressure is obtained, close the valves in reverse order first closing the yellow, then the green.

3. Initialize the data acquisition in the MCB-926 multi-channel buffer unit. The energy spectrum of the 241Am source is then obtained from the channel-count plot. Collect until approximately 10,000 counts.

4. Initialize the data acquisition is initiated in the MCB-926 multi-channel buffer unit. The energy spectrum of the ^{241}Am source is then obtained from the channel-count plot.

    - Collect until approximately 10,000 counts to have good statistics. Record the exact number of counts.

5. Save the spectrum as ASCII SPE within the software. Make sure to indicate at which pressure and height it was obtained when saving.

1.6.3 Experiment 3: Absolute source strength of the ^{241}Am source

In the final stage of the experiment, determine the absolute source strength of a ^{241}Am source. The source strength measurements should be carried out with the optimal source-detector distance and vacuum chamber pressure. Note, it may be possible to use measurements from the previous sections if the statistics are sufficiently good. The measurements are to be performed with the procedures outlined in Sections 1.6.1 and 1.6.2 .

1.7 Data analysis

1. *Energy calibration*: Use the saved ASCII file of the energy spectra to identify the channel number corresponding to each energy peak of the ^{241}Am source. Assign it to it the corresponding alpha energy (see Figure 1.1 in Section 1.2.1) and perform the energy calibration of the detector set-up. Use this to convert the channel numbers of the spectra to energies.

2. *Geometry* correction factor: Determine the geometry-efficiency correction factors for the various distances between the source and detector (for determining the absolute source strength). Use Equation 1.4

3. *Determine source strength*: Using the data from the ASCII files, integrate the number of counts under the peaks of each alpha particle. Use this integral and the geometry correction factor to determine the source strength.

The geometry factor G_{fx} for absolute source strength determination can be calculated from the relation given in Equation 1.4.

$$G_{fx} = G_1 \cdot [1.0 - G_2 + G_3]^{-1} \tag{1.4}$$

where

$$G_1 = \frac{4x^2}{a^2} \quad , \quad G_2 = \frac{3\left(a^2 + b^2\right)}{4x^2} \quad \text{and} \quad G_3 = \frac{5\left(a^4 + b^4 + 3a^2b^2\right)}{8x^4}$$

Here, a and b denote the detector and source radii, respectively, and x is the distance between source and detector. All distances are measured in the same units. The source radius is The source radius is $(3.00 \pm 0.05)mm$. The detector radius can be obtained by consulting the available information provided by the manufacturer, typically given as surface areas. It is important to also consider the thickness of the dead layer of the SBD.

The source strength (number of alphas emitted per second), S, can be calculated from the relation shown in Equation 1.5, where C_t stands for the integral counts over time t.

$$S = \frac{C_t G_{fx}}{t} \tag{1.5}$$

1.8 Expected results

1. ^{241}Am source energy spectra.

2. Change of the measured particles' energies and the absolute detector efficiency with changes in air pressure and distance. Preferably for two to three distances between the source and detector and two to three pressures.

3. Absolute source strength from the area under the energy peaks and calculated geometry factor. Provide the calculated geometry factors and the variables used in their calculation.
4. Identification of sources of errors.
5. A short note on the important conclusions.

1.8.1 Things to consider

- Why does the detector system use a vacuum?
- How important is the dead layer of the detector?
- Why is a semiconductor being used as a detector?
- Does the detector perform best when the source is as close possible? Why or why not?
- How is linear stopping power effected by the air pressure?
- Why do the alpha energy spectra look how they look?

2 Beta detection

2.1 Introduction

This experiment gives an introduction into beta-particle physics and detection. Furthermore, the experiment introduces students to the physics and use of liquid scintillator detectors. A good understanding of beta particles is essential for nuclear engineers because they are often found in many industrial and scientific settings. Beta-active nuclides are commonly produced by the bombardment of materials with neutrons, a common occurrence in nuclear fusion and fission reactors. For example radioactive tritium, ^{3}H, can be created when water or other hydrogen-rich materials are exposed to neutrons, which is common in water cooled or moderated nuclear reactors. In other cases, beta-emitters are purposefully created for a variety of engineering and medical applications; the isotope ^{99}Mo is commonly made in nuclear reactors or particle accelerators for use in medical procedures.

In this experiment, students will first use the liquid scintillator detector to identify five unknown beta sources based on their energy spectra and calculated source strengths. They will next investigate the possible contamination of the water in the Lotus experimental facility. The materials in the Lotus facility were exposed to neutrons and may be a source of non-negligible radioactivity. Students will compare Lotus' water to plain tap water and determine if radiation exposure has created radioactive elements. The exercise of identifying activated substances in a nuclear facility is a common practice of nuclear engineers, especially in the field of nuclear reactor decommissioning. Finally, the students will investigate the effects of quenching upon the quality and efficiency of liquid scintillation detectors.

2.2 Theory

2.2.1 Beta particle basics

A beta particle is a common form of radiation. This particle is essentially a fast electron that is emitted in the process given by Equation 2.1. Here X and Y are the initial and final nuclear

species, β is a beta particle, and $\bar{\nu}$ is an antineutrino.

$$ {}^{A}_{Z}X \rightarrow {}^{A}_{Z+1}Y + {}^{0}_{-1}\beta + {}^{0}_{0}\bar{\nu} \tag{2.1} $$

Each beta decay has a fixed decay energy, or Q-value, and this energy is divided between Y, β , and $\bar{\nu}$. The recoil nucleus Y receives a very small fraction of the Q-value. The energy of this recoil nucleus is usually so low that it is below the ionization threshold and, therefore, cannot be detected by any conventional method. The rest of the energy is shared between the beta particle and the antineutrino in a continuous manner. In other words, the beta particle can appear with an energy ranging from zero to the full Q-value of the reaction, often called the *endpoint energy*. This continuous range of possible energies results in a continuous beta spectrum as shown in Figure 2.1.

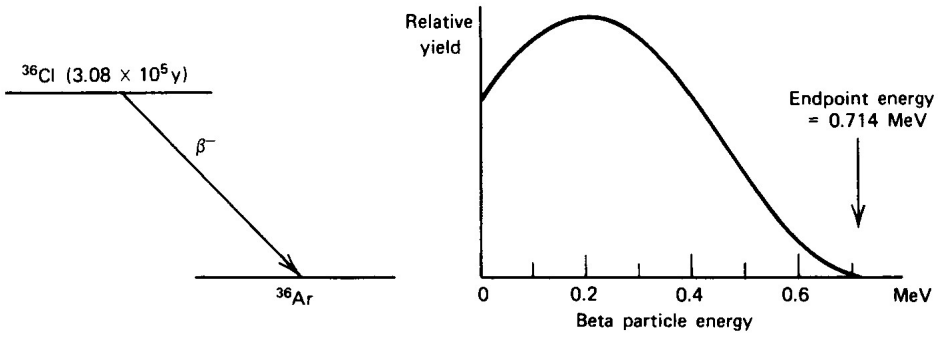

Figure 2.1: The decay scheme of ^{36}Cl and its beta particle's continuous energy distribution [1].

Beta-active radionuclides occur in many forms with a wide range of half-lives, ranging from thousands of years to tens of days. Some of the beta sources frequently used by nuclear engineers are summarized in Table 2.1

Table 2.1 shows purely beta-emitting radionuclides, meaning that the daughter nuclides decay directly to their ground state. However in other beta decays, the daughter nuclides are created in an excited state. Subsequent de-excitation usually occurs through the emission of gamma rays. These gamma rays' energies are essentially equal to the difference in energy between their initial excited state and the final and de-excited nuclear state. Because nuclear states have very well-defined energies, the energies of gamma rays emitted in de-excitation are also very specific, i.e. nearly monoenergetic. Common gamma-ray sources used in nuclear engineering applications are actually based on beta decay. These sources are generally limited to energies below about 2.8 MeV, and therefore have limited applications [1].

Table 2.1: Examples of pure beta-minus emitters [1].

Nuclide	Half-life	Endpoint energy (MeV)
^{3}H	12.26 y	0.0186
^{14}C	5730 y	0.156
^{32}P	14.28 d	1.71
^{33}P	24.4 d	0.248
^{35}S	87.9 d	0.167
^{36}Cl	3.08×10^{5} y	0.714
^{45}Ca	165 d	0.252
^{63}Ni	92 y	0.067
^{90}Sr/^{90}Y	27.7 y / 64 h	0.546/2.27
^{99}Tc	2.12×10^{5} y	0.292
^{147}Pm	2.62 y	0.224
^{204}Tl	3.81 y	0.766

2.2.2 Interaction of fast electrons with matter

Fast electrons, being charged particles, interact with matter in the same way as heavy charged particles: through coulombic interactions. While passing through matter, fast electrons suffer energy losses primarily by excitation and ionization of the target atoms. Fact electrons however typically lose their energy at a much lower rate than heavy charge particles. Additionally, they follow a much more erratic and winding path than heavy charged particles. A series of tracks emitted from a source of mono-energetic electrons might appear as sketched in Figure 2.2. The large deviations of the paths occur because the mass of an electron is equal to that of the orbital electrons it is interacting with and, therefore, the electron can lose a much larger fraction of its energy in a collision and scatter with significant angles. Furthermore, electron-nuclear reactions can occur, causing the electron to abruptly change directions.

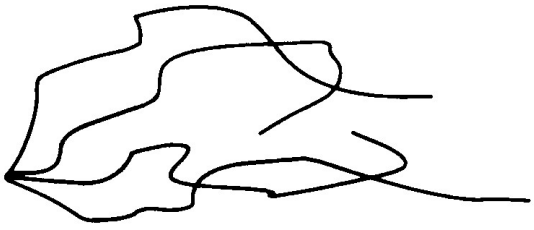

Figure 2.2: Path of fast electrons traversing a medium [1].

The energy losses created by coulombic interactions are often called *collisional losses*. The linear specific energy loss due to collisional losses is described by Equation 2.2 where $\beta = v/c$, with v and c being the velocity of the electron and of light respectively.

$$-\left(\frac{dE}{dX}\right)_c = \frac{2\pi e^4 NZ}{m_0 v^2}\left[ln\left(\frac{m_0 v^2 E}{2I^2(1-\beta^2)}\right) - ln(2)(2\sqrt{1-\beta^2} - 1 + \beta^2) + (1-\beta^2) + \frac{1}{8}\left(1-\sqrt{1-\beta^2}\right)^2\right] \tag{2.2}$$

Electrons differ further from heavy charged particles because they may lose a significant amount of energy through electromagnetic radiation known as *bremsstrahlung*. From classical electromagnetics, any charge accelerating must radiate energy. When a fast electron is deflected by coulombic collisions, it is accelerated and then emits bremsstrahlung in the form of photons. The linear specific energy loss due to bremsstrahlung is given by Equation 2.3. This equation shows why only fast electrons like betas emit significant bremsstrahlung radiation. For heavy charged particles, the m_0^2 term in the denominator becomes very large, reducing the amount bremsstrahlung emitted.

$$-\left(\frac{dE}{dX}\right)_r = \frac{NEZ(Z+1)e^4}{137 m_0^2 c^4}\left(4ln\left(\frac{2E}{m_0 c^2}\right) - \frac{4}{3}\right) \tag{2.3}$$

The variables Z and the electron energy E in Equation 2.3 show that radiative losses are more important at higher energies and for absorber materials of large atomic number. For fast electrons of interest in this experiment, energies are on the order of a few tens of keV. Radiative losses are, therefore, a small fraction of the total energy transferred to the absorbing medium in comparison to ionization and excitation losses. Bremsstrahlung radiation can become important however in influencing the response of detectors.

When fast electrons are deflected, their tracks tend to lead to a *backscattering* phenomenon. An electron entering a medium through a surface may undergo sufficient scattering that it exits the medium through the same surface it enters before being absorbed. Because the electron is not absorbed, it does not deposit all of its energy in the medium. This can have a significant effect on the response of detectors designed to detect electrons. Backscattering is significant for electrons with low incident energies, such as betas.

2.2.3 Liquid scintillators for beta detection

Due to the low energy of beta particles, their detection is usually carried out with either a gas-type ionisation chamber or a light-emitting scintillator. In the case of gas ionisation chambers, one employs either a thin entry window or a window-less counter. This is done to prevent the attenuation of electrons in the window and also to prevent their backscattering, which would cause the electrons to escape detection entirely. In this chapter's experiment, a liquid scintillator is used to help counteract these window-related problems. Because the detector is

the liquid itself, it needs no window and therefore backscattering losses are decreased and the detector's efficiency improves. Liquid detectors also alleviate problems related to the self-absorption of a particle within the source.

In the liquid scintillator detection scheme, the radioactive material is directly dissolved into a scintillator solution. This means that the radiation emitted by the source passes immediately through the detector allowing counting efficiencies to approach 100%. This fact makes liquid scintillation advantageous for low-energy radiations such as the beta particles emitted by tritium and ^{14}C, whose beta endpoint energies are 18.6 and 160 keV respectively. Both of these isotopes are important in chemical and biomedical applications, and therefore many applications of liquid scintillators are in these fields.

A liquid scintillator works by transferring the kinetic energy of fast electrons into light photons that can be measured via the excitation and subsequent de-excitation of the solution's molecules. A single beta particle, while travelling through the liquid scintillator, can produce several such light photons, as shown in Figure 2.3. These can be detected by two separate chains of electronic units, each consisting of a photomultiplier, pre-amplifier and an amplifier. The photomultiplier tube transforms the light produced by the scintillator into an electrical signal.

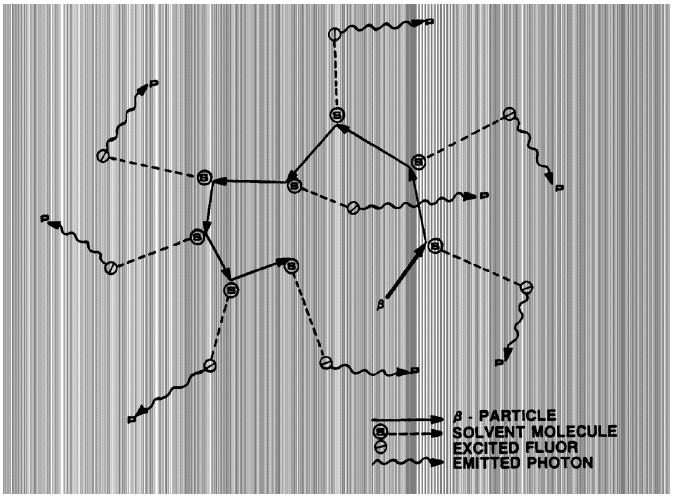

Figure 2.3: Illustration of the collision processes of a beta particle in a scintillator cocktail [2].

A common problem encountered with liquid scintillation is a reduction in the counting efficiency of the system due to an effect called *quenching*. The result of quenching is an energy loss in the liquid scintillation solution. This causes the detected energy spectrum from a radionuclide to appear to shift towards lower energies as seen at left in Figure 2.4. This change in energy distribution shows that the counting efficiency is dependent on the degree of quenching and therefore the nature of the sample, scintillator, and preparation method used in the detection process.

Quenching is primarily the result of three factors:

1. Photon quenching: Occurs when the transfer of energy from the beta particle to the solvent molecules is incomplete.

2. Chemical quenching (or impurity quenching): Beta energy is absorbed before it is converted into photons.

3. Colour quenching: Created by the attenuation of photons in the solution. A chemical species absorbs the light of a particular wavelength.

Colour quenching depends on the colour of the interfering chemical and the path length which a photon must travel. This means that for colour quenching, only certain photon energies are affected because of this dependence on wavelength of the photon. Chemical quenching on the other hand affects all energy radiations. This energy dependency is shown on the left of Figure 2.4.

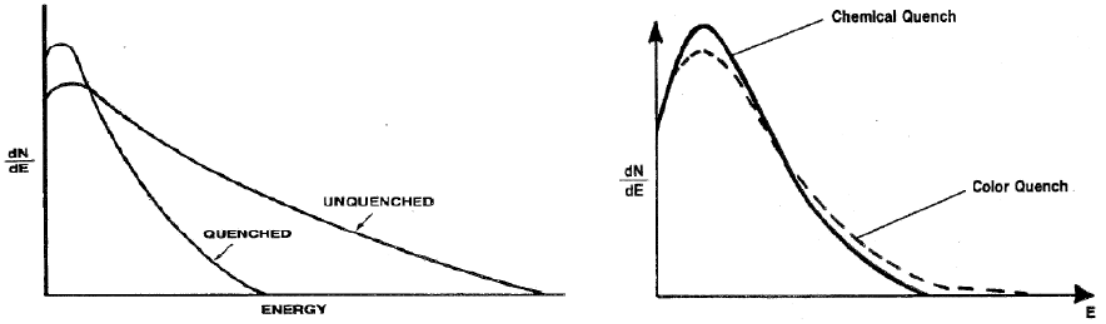

Figure 2.4: Left: Quenching Effect; Right: Chemical vs. colour quench [2].

An efficient detection scheme consists of two low thermionic-effect photomultipliers (PMTs), placed opposite each other, with a place for a sample vial at the centre. The vial and the PMT tubes are surrounded by lead of about 5 cm in thickness in order to reduce background. An appropriate cocktail mixture is filled in a standard plastic or glass vial and tightly secured after mixing uniformly with a beta source, also in the liquid phase. A fast coincidence circuit is incorporated, and the output of each tube is added after coincidence. This provides an excellent proportionality of the light output to the energy deposited in the sample; it is independent of the location of the energy deposition, and furthermore, it considerably reduces the background noise.

2.3 Experiment description

The following experiments will be carried out using the liquid scintillator.

- Experiment 1: Identification of ^{3}H and ^{14}C beta sources. Create beta spectra and determine source strengths.

- Experiment 2: Evaluation of contaminated water taken from the Lotus facility.
- Experiment 3: Evaluation of the effects of quenching on beta detection.

2.3.1 Important Precautions

The following precautions need to be followed at all times to ensure the safety of the experimenters and the equipment and to create high quality results.

1. Handle glass vials containing standard sources in the scintillation cocktail with the utmost care.
2. Report any problem when manipulating the vials (falls on the floor, broken glass, etc.).
3. Select a protocol corresponding to the beta source selected.
4. Glass vials should be placed in the designated rack corresponding to the actual protocol of the experiment.
5. Appropriate counting-statistics limits to be selected via the protocol.

2.4 Required setup

In this experiment, a computer controlled Packard Tri-Carb 1900 TR liquid scintillation spectrometer will be used. Its design is based on collecting a pulse height spectrum at a fixed gain over the entire energy range from 0 to 2000 keV. The system permits interrogation of the spectrum within any desired energy band while sample counting is in progress. Spectrum analysis of the detected events is made possible by the incorporation of micro-processor based electronics.

The spectrum analyser is directly calibrated in keV and the user can select any partition for storing, analysing and viewing the spectrum between 0 and 2000 keV. In the following studies, for example, 0 to 18.6 keV will be chosen for measuring the spectrum of ^{3}H, and 0 to 156 keV for ^{14}C.

The following components are required for this experiment. Check to see if they are available. If they are not available, please speak with your lab instructor.

1. A computer controlled Tri-Carb 1900 TR system located in the B-lab.
2. Five unknown beta sources.
3. The scintillation cocktail Ultima Gold LSC.
4. Contaminated water from the Lotus facility.

2.5 Operations

The use of the Tri-Carb detector system is given below. Detailed procedures can be found in Section 5 of the Tri-Carb's manual, which can be found in the laboratory.

The detector operates by manipulating black plastic racks in which radioactive samples are placed. Each rack is identified with a protocol by attaching a plug with the protocol's ID number. The detection system reads a bar code attached the protocol plug to determine which settings are to be used in the measurement. The protocol's settings are uniformly applied to all samples within a rack and therefore it is necessary to specify a protocol for each type of sample being analyzed so that the settings can be optimized. The protocol's settings are specified within the software system.

2.5.1 Counting samples

The following instructions should be followed for routine counting of samples:

1. Choose a sample rack and insert a protocol plug. The plug should be inserted at the end of the rack where the word "Varisette" is found.
2. Reset the counting flag on the protocol plug by pushing it to the left. If the orange marker is exposed, the counting flag is not set.
    - Note: Counting will not happen unless the counting flag is set.
3. Ensure that a protocol is defined within the software for the desired protocol plug's number chosen. Refer to Section 2.5.2 for more details.
4. Load the standards and/or sample into the rack taking care to record the order in which the samples are entered.
5. To initiate the counting, press the `F2-COUNT START` key on the status page.

2.5.2 Protocol definition and editing

To define a protocol, use the software following this procedure:

1. From the status page, select the `F1 EDIT PROTOCOL` key.
2. When the edit protocol page is displayed, enter the protocol number to be defined or edited and press the `ENTER` key.
3. Answer or change any/all parameter on the CPM page according to the setting desired for the samples being analysed.

- Note: The settings for ^{3}H and ^{14}C protocols are pre-programmed and do not need to be edited by students.

4. When editing is completed, press the `F1-EXIT EDIT` key twice to return to the system's status page.

5. Programming is now complete, follow the procedure in Section 2.5.1 for counting samples.

2.5.3 Saving spectra

Saving the created spectra requires transferring the data from the detector to a computer via a floppy disk. Students can then save the data from the computer in the lab to a personal device in order to perform analyses and to plot the spectra. To save a spectrum's data, follow the following instructions:

1. Insert a floppy disk into the disk drive on the front of the detector.
   - Note: this is drive `A:\`
2. To save the spectra, the program `SPECTRA1` needs to be run. To access the program, follow the following sequence on the keyboard.
   - `F10 - ETC`
   - `F3 - USER PROGRAM`
   - `F9 - SPECTRA1`
   - `Write the path:  C:\SPECTRA`
   - `ENTER`
   - `F3 - RUN`
3. In the program, the students can save the data with the following Instruction:
   - `F4 - File Management`
   - `Down Arrow`
   - `F3 - COPY FILES`
   - `F2 - A DISK`
   - `ENTER`
   - Note: For organization purposes, students can create their own directory on the floppy disk in the `A:\` drive.
4. Remove the floppy disk from the detector and transfer it to the computer in the laboratory to retrieve the data.

Each spectrum is saved with the format of `SP##S##.##`, which indicates the spectrum's protocol (`SP##`), the sample number in the given rack (`S##`), and the number of times it was counted (`.##`). For example, for protocol 12 with sample 2 counted once, the spectrum will be saved with the file name of `SP12S2.1`.

The data in a spectrum's file is saved in a histogram structure. The files give the number of counts measured in each energy bin of the histogram.

2.5.4 Preparing a sample

To prepare a sample, students need to find a clean vial and prepare the scintillator-source cocktail. The scintillator solution is called Ultima Gold LSC. This is to be mixed with the radioactive source. Special attention should be made to make the scintillator-source mixture be as transparent as possible to minimize the effects of quenching. When preparing a sample with water as a source, the water should only be 10-20% of the scintillator-source, with the scintillator being 80-90%. The scintillator-source solution also needs to be well mixed. To ensure well mixing, the vial must be placed in a centrifuge and mixed for ~20 minutes. Make sure to balance the centrifuge during mixing with another vial on the opposite side of the device.

2.6 Measurement steps

2.6.1 Experiment 1: Identification of ^{3}H and ^{14}C beta sources

The first step of this experiment is to identify unknown ^{3}H and ^{14}C sources. This is done by determining their source strengths and examining their energy spectra and then comparing them to specifications given in Table 2.2.

1. Identify the protocols in detector's software that correspond ^{3}H and ^{14}C sources.
2. Find the racks that correspond to given protocols' number. For example, protocol 12 in the software needs rack 12 in the detector.
    - Note: Two different protocols and two different racks need to be used for the ^{3}H and ^{14}C sources.
3. Initiate counting, measure the source strengths, and save the spectra for all samples following the instructions given in Section 2.5.

2.6.2 Experiment 2: Comparison of a contaminated water sample with tap water

Step 2 of the experiment examines the level of contamination in water from the Lotus experimental facility. This is done by preparing samples of both contaminated water and normal tap

water to identify if heightened levels of radioactivity were created by the Lotus' operations.

1. Prepare samples of contaminated water and tap water following the instructions given in Section 2.5.4
    - Note: The number of samples needed to reach conclusions about the degree of the water's contamination is up to the students to decide.
2. Identify the protocol in detector's software that corresponds ^{3}H sources.
    - Note: The main source of radioactivity in the water is ^{3}H.
3. Find the racks that correspond to given protocols' number.
4. Initiate counting, measure the source strengths, and save the spectra for all samples following the instructions given in Section 2.5.

2.6.3 Experiment 3: Evaluation of the effects of quenching on beta detection

Step 3 requires students to evaluate the effects that quenching has on the efficiency and effectiveness of the liquid scintillation detector. Students will prepare a series of samples with varying ratios of scintillator-cocktail-to-source volume in order to induce quenching effects. Students should use the same contaminated water that was used in Experiment 2. In general, adding more water increases the opacity of the sample, and therefore increasing the effects of quenching.

2.7 Data analysis

1. Perform spectrum and end-point energy analysis for each source using the spectrograph program.
2. Determine the source strengths for the unknown beta sources and identify them. Use Table 2.2 as a reference.
3. Analyse the contaminated water from Lotus and determine its activity.
4. Analyse the effect of quenching on the detector's performance (measurement statistics and spectra quality).

2.8 Expected results

The following results are expected:

1. Demonstration of the continuous-energy-spectrum nature of beta emission.

Table 2.2: Sources available during the experiment.

Source type	Source strength [dpm]	Reference date	Half-life [hrs]
^{14}C	120,900	07.09.1989	5.02E+07
^{3}H	249,200	29.08.1989	108,887
^{3}H	283,800	16.03.1998	108,887
^{3}H	87,450	18.12.2010	108,887
^{14}C	43,290	18.12.2010	5.02E+07

2. Comparison of measured and specified source strengths of the two sources, as well as of their end point energies.
3. Comparison of the suspicious water and tap water samples, discussion in terms of radiation protection.
4. Investigation of the effects of quenching on the counting efficiency.
5. Identification of sources of errors.
6. A short note on the important conclusions.

2.8.1 Things to consider

- Why are liquid scintillators interesting for measuring tritium and ^{14}C?
- What are the effects of quenching on the detection efficiency? On the spectra?
- What are the effects of bremsstrahlung radiation on the energy spectrums created?
- What are the effects of backscattering on the energy spectrums created?
- Why is the water from Lotus contaminated? Is this contamination a safety risk?
- Is it possible to make a quenching calibration curve to help adjust for quenching effects?

3 Gamma-ray spectroscopy and spectrometry

3.1 Introduction

Photons are an important type of radiation in nuclear engineering applications. They can be emitted in numerous ways, but the two main types of photons that are interesting to nuclear engineers are X-rays and gamma rays. X-rays are electromagnetic radiation emitted during the rearrangement of electrons in the outer shells of atoms. In contrast, gamma rays originate from transitions within the nucleus itself. Gamma rays are commonly emitted by radioisotopes as they decay, especially after beta decay when the daughter nucleus is left in an excited state. Gamma rays are therefore commonly found in radioactive environments, especially in spent nuclear fuel or other activated materials (e.g. materials surrounding a particle accelerator). Gamma rays are generally much more energetic than X-rays, and, therefore, more penetrating and, therefore, important in radiation safety and protection.

The chapter's experiment introduces the complex and important concepts surrounding the detection of photons and, in particular, focuses on gamma rays as they are often encountered by nuclear engineers. Students will learn how to use and calibrate a high-purity germanium, HP(Ge), detector with ^{152}Eu and ^{60}Co sources. Phase one of the lab uses a ^{152}Eu source to calibrate the detector and to make efficiency vs. particle energy curves. Phase two of the lab uses the ^{60}Co source so that students can measure the activity of the source with the detector and compare their results to theoretical values. Importantly the lab introduces students to the complex field of gamma-ray spectroscopy and spectrometry which involves creating and interpreting detailed gamma-ray energy spectra where overlapping effects such as Compton scattering, photoelectric absorption, and pair production can become very complicated.

3.2 Theory

3.2.1 Gamma-ray sources

Gamma radiation is emitted by excited nuclei as they relax into their lower-lying energy levels. In most cases, an excited nucleus is created from the decay of a radioactive element. Three common radioactive decays that lead to excited states are seen in Figure 3.1, which are beta-minus, beta-plus, and electron capture (EC). In each instance, the decay leaves an excited daughter nucleus that emits a gamma ray whose energy is equal to the difference between the initial and final nuclear state's energy.

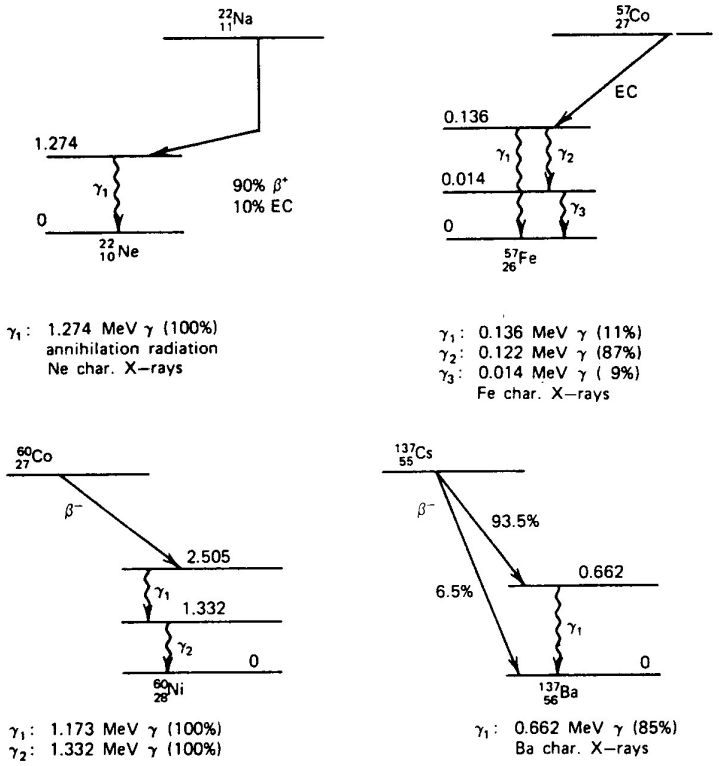

Figure 3.1: Decay schemes of a few commonly used gamma sources [1].

For the beta-emitting radioisotopes like ^{60}Co and ^{137}Cs in Figure 3.1, the beta decay process is typically slow with half-lives of hundreds of days or greater. The excited daughter nuclides, after decay, have a much shorter average lifetime, typically on the order of a few picoseconds. This means that the gamma-ray photons emitted by these beta decays have half-lives characteristic of the parent beta decays, but have energies that reflect the energy-level structure of the daughter nuclides. For example, in this experiment a ^{60}Co source is used. Gamma rays from a 60Co source decrease in intensity with the 5.26-year half-life of ^{60}Co, but in fact are released by the daughter nuclide ^{60}Ni produced by the decay.

Because the nuclear states of an excited nucleus have very well-defined energies, emitted gamma rays are nearly monoenergetic. This means that gamma-ray sources are often used by nuclear engineers as references for the precise energy and efficiency calibration of photon detectors. Gamma-ray sources usually have a strength of around 10^5 Bq and are encased in plastic disks. They are designed to be thick enough to prevent the radiation of the decay of the parent nucleus from being emitted, but allow the gamma radiation from the daughter nucleus to escape. However because the radiation from the parent decay still interacts within the source, often secondary radiation is created in the form of bremsstrahlung or annihilation photons.

3.2.2 Characteristic X-rays

In instances where orbital electrons are disrupted from their normal configuration by an excitation process, perhaps by the passing of ionizing radiation, the atom may exist an excited state. The atom's electrons tend to naturally rearrange themselves so that the atom returns to its ground state. The energy liberated during the electron's transition from the excited to ground state takes the form of a characteristic X-ray photon. This X-ray has an energy equal to the difference between the initial, excited state and the final, ground state. The energy of the X-rays is determined by where the vacancy in the electron shell was created and from which shell the electron that fills the vacancy comes from. For instance, if a vacancy is created in the K-shell of an atom, a K X-ray is emitted when that vacancy is filled. If that vacancy was filled by an electron from the L-shell or the M-shell, the energy of the K X-ray will be different because the binding energies in the L-shell and M-shell are different.

Characteristic X-rays are often generated by external sources of radiation like other X-rays, betas, or alpha particles. These particles strike a target and create excited or ionized atoms. These excited atoms subsequently de-excite and release characteristic X-rays. These characteristic X-rays become important in gamma-ray spectroscopy because they appear as detected photons on the energy spectrum. They may arise from the source itself (as a beta particle traverses the source and excites atoms) or from interactions of photons with structural materials or the detector itself. In any case, a nuclear engineer must be able to distinguish characteristic X-rays from gamma rays in a measured spectrum. Characteristic X-rays usually have energies in the keV range, as their energy is limited by the structure of the atom's electron shell.

3.2.3 Interactions of photons with matter

Gamma rays can interact with matter in many ways, but only three interactions are significant in gamma ray spectroscopy: photoelectric absorption, Compton scattering, and pair production. These reactions all play an important role in gamma spectroscopy and must be understood and identified by nuclear engineers. Each of these interactions is dominant in different energy ranges. The photoelectric effect dominates low-energy gamma rays (up to several hundred keV), pair production for high-energy gamma rays (5-10 MeV), and Compton

scattering for the range of energies between these two extremes. In addition to the gamma rays' energy being an important factor in determining the likelihood of one of these reactions, the atomic number of the absorber also effects the relative probabilities of these interactions to occur. For instance, the cross section for photoelectric absorption varies approximately with $Z^{4.5}$. The dependence of gamma-ray interaction cross sections on energy and atomic number is shown in Figure 3.2.

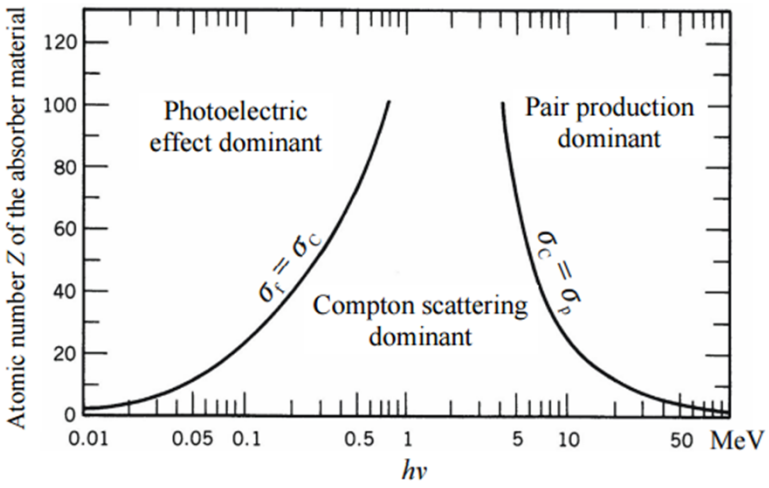

Figure 3.2: Dependence of gamma-ray interaction cross sections based on energy and atomic number.

Photoelectric absorption is an interaction in which an incident photon is absorbed by an atom and creates a photoelectron from one of the atom's electron shells. The energy of this photoelectron is the kinetic energy of the incident photon minus the binding energy of the electron in its original shell. A photoelectron is typically created from the K-shell, and will therefore have energies in the range of a few to tens of keV. During this process, a vacancy is created in the electron shell which is subsequently filled. This requires the liberation of binding energy in the form of a characteristic X-ray or Auger electron. In the case of the characteristic X-ray, the X-ray subsequently interacts through photoelectric interactions in the absorber. Because most of the gamma ray's original energy is carried by the photoelectron, almost all of the energy of the original gamma ray is deposited in the detector. If none of the characteristic X-rays escape, then all of the original photon's energy is deposited, making photoelectric absorption an ideal process for gamma-ray spectroscopy. This is because all of photon's energy is deposited in the detector and will therefore appear as a single peak on the spectrum. Because photoelectric absorption is the preferred mode of interaction, it is desirable to have detection materials with a high atomic number to increase the probability of the reaction to occur.

A Compton scattering interaction occurs when a photon interacts with an atom's electron cloud creating a recoil electron and a scattered gamma ray. The gamma ray's original energy is shared between the two and this energy division is dependent upon the interaction's scattering

angle. The interaction creates a spectrum of scattered gamma-ray energies which vary from the extreme of a grazing-angle scatter to a head-on collision. A grazing scatter results in a gamma ray that has nearly the same energy as the incident gamma and a recoil electron with very little energy. A head-on collision causes the incident gamma to backscatter in its origin's direction and the recoil electron to continue along the incidence direction. This head-on collision represents the maximum energy that can be transferred in a single Compton interaction. The spread of energies from a grazing angle to a head-on collision creates what is called a *Compton continuum* (see Figure 3.3) that ends at the *Compton edge*, where the maximum energy occurs from the head-on collision. This Compton continuum is commonly seen in gamma-ray spectroscopy and it is necessary for nuclear engineers to identify it in their analyses.

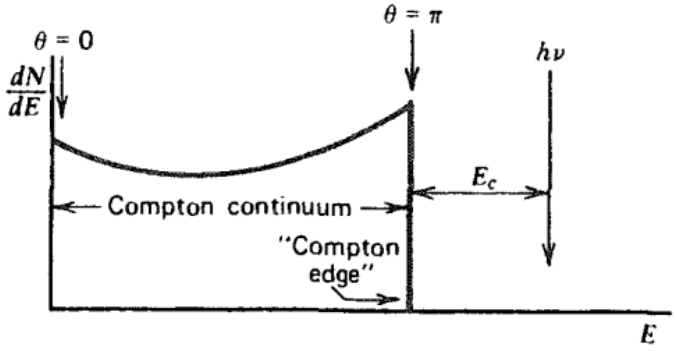

Figure 3.3: Sketch of the Compton scattering phenomenon [1].

The pair production reaction corresponds to the creation of an electron-positron pair when an incident gamma-ray interacts with a nucleus. An energy of $2m_0c^2$ is required for this reaction, or a photon energy of 1.02 MeV. When a gamma ray exceeds this energy threshold, its energy in excess of 1.02 MeV appears as the kinetic energy of electron-positron pair. Typically, all of the energy of the electron-positron pair is deposited in the detector. This creates a peak on the gamma-ray spectrum at a position of $h\nu - 2m_0c^2$, or at the difference in the original gamma ray's energy and the $2m_0c^2$ threshold. Additionally, the positron created in pair production may annihilate, or in other words, combine with a normal electron. When this occurs, both positron and electron disappear creating two annihilation photons with energies of m_0c^2 each (0.511 MeV).

3.2.4 Interpreting gamma-ray spectroscopy

When performing gamma-ray spectroscopy, the goal is to be able to identify the energy of a gamma-ray that hits the detector. Often if the gamma ray's energy can be accurately measured, it is then possible to identify from which radioisotope it came from. Distinguishing the incoming gamma ray from the variety of effects that occur in the detection process is the real challenge in gamma spectroscopy. A nuclear engineer must be able to distinguish the gamma

ray's peak from Compton scattering, characteristic X-rays, the peaks created by annihilation radiation, and from backscattering in structural materials.

A hypothetical gamma-ray detector and the spectra it might create are shown in Figure 3.4. First consider how the photoelectric effect appears upon a gamma-ray spectrum. A photoelectric absorption appears on the gamma-ray spectrum as something called a *full-energy peak*. This peak corresponds to a gamma ray depositing all of its energy in the detector in the form of a photoelectron via photoelectric absorption. The full-energy peak can also occur after a series of Compton scattering events. A photon may Compton scatter in the detector depositing its energy until its energy reduces enough for a photoelectric absorption to occur. In this case, a full energy deposition occurs and therefore a full-energy peak is still seen. A Compton continuum appears when, upon a Compton scatter, the scattered photon escapes from the detector only having partially deposited its energy. This continuum created from a single scattering event and then an escape exists up to Compton edge. Multiple Compton scattering events means that a photon can deposit more energy than that dictated by the first head-on collision, creating a second Compton continuum that stretches up to the full-energy peak.

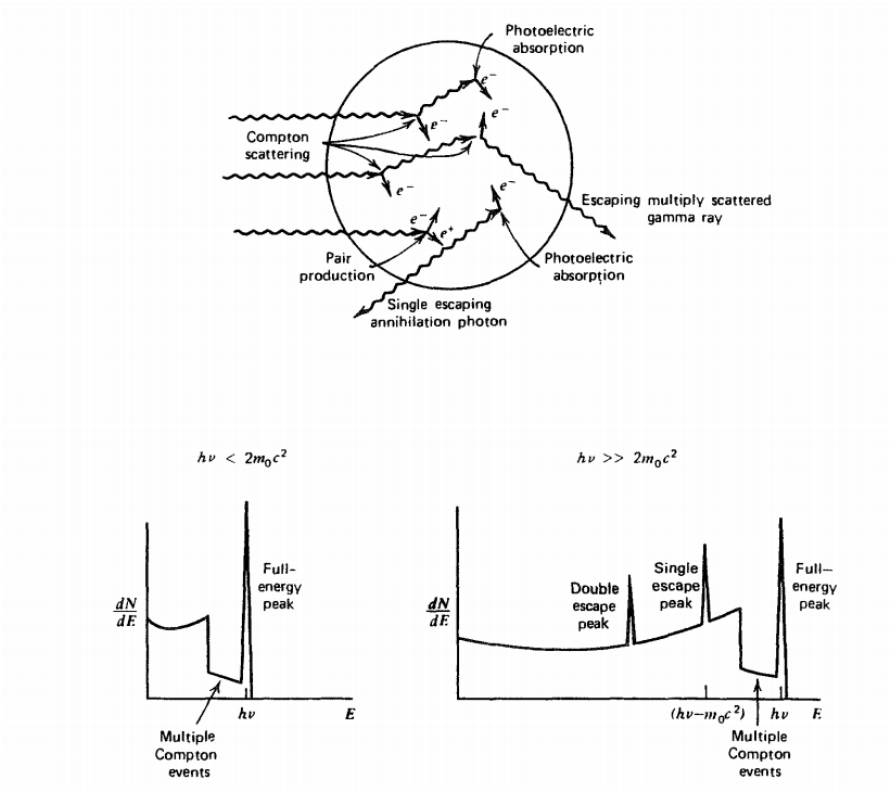

Figure 3.4: Description of effects occurring in gamma-ray spectroscopy and the different spectra that may occur [1].

If a gamma ray interacting with the detector exceeds the threshold energy for pair production ($> 2m_0c^2$), the effects of the subsequently created electron-positron pair may also be seen on

the spectrum as a *single escape peak* or a *double escape peak*. These peaks appear because of the creation and subsequent escape of annihilation photons. If one of these photons escapes, it does not deposit its energy and only the energy of electron-positron pair is deposited. If both photons escape, this corresponds to a double escape peak which appears on the spectrum at an energy of $h\nu - 2m_0c^2$. If one photon escapes and the other is absorbed, this corresponds to a single escape peak at an energy of $h\nu - m_0c^2$. If neither photon escapes, then all of the original photon's energy is deposited, meaning that a full-energy peak is created.

The spectra encountered in gamma-ray spectroscopy may also include secondary particles created in structural or shielding materials. Figure 3.5 shows a detector surrounded by a shielding/structural material and the effects that such materials can have upon a measured gamma-ray spectrum. An emitted photon may create a characteristic X-ray through photo-electric absorption, Compton scatter, or undergo pair production in the surrounding material. The characteristic X-ray appears on the gamma-ray spectrum as an X-ray peak. The Compton scattered photons may appear as a *backscatter peak*. Finally the annihilation photons as an *annihilation peak*.

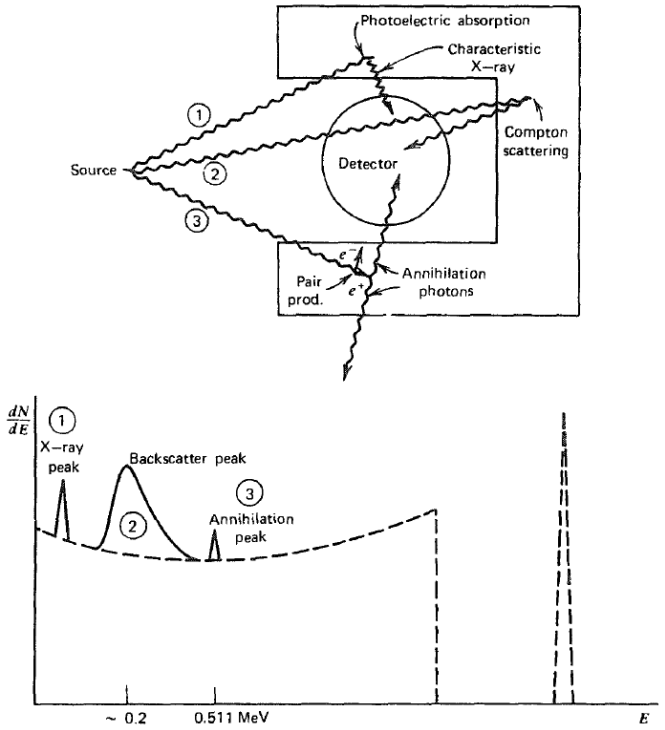

Figure 3.5: A typical experimental arrangement and generic features of the gamma spectrum. Shows influence of surrounding materials on the detector's response [1].

Real life gamma spectroscopy can be much more complicated than that shown in Figure 3.4 and Figure 3.5. This is because Figure 3.4 and Figure 3.5 show only spectra created by a monoenergetic photon. In real applications, one radioactive source may emit gamma rays of many different energies meaning that full-energy peaks, escape peaks, and characteristic

X-rays may all overlap onto one image. Furthermore, the problem can become even more complex if there are multiple radioactive isotopes present which each emit photons of different energies. The job of the nuclear engineer is then to analyse these spectra, find the full-energy peaks amongst the clutter of other phenomena, and find which photons correspond to these full-energy peaks thereby backtracking to the original radioisotope.

3.2.5 Energy resolution

The ability to identify all of the peaks previously described can be seriously hindered by the quality of the gamma-ray spectroscopy system's ability to resolve the appearance of a given photon. This quality is generally called the *energy resolution* of the detector and describes how well one can distinguish two peaks from each other. High energy resolution implies having very thin peaks that are easy to identify. Poor energy resolution results in very wide peaks that often merge together making it difficult or impossible to distinguish between them, or a sort of "blurring" of the measured peaks. The variations in peak widths reflect the fact that large fluctuations can occur from pulse to pulse in the detector despite the fact the same amount of energy is deposited in each event. Small fluctuations mean good resolution and a small peak that resembles a sharp spike or a mathematical Dirac delta function.

The energy resolution of a detector is determined by separate effects that include charge collection statistics, electronic noise, variations in the detector's response over its volume, and changes in the detector's operating parameters (e.g. temperature) during the measurements. For scintillators, intrinsic properties of the detection crystals can play an important role as well. Figure 3.6 shows the difference in resolution between an NaI and HP(Ge) detector. The different crystal properties create large difference in the energy resolution of the detectors. The NaI spectrum show significant blurring of the peaks that is common with lower energy resolutions. With this spectrum it is hard to distinguish between close-lying peaks. The HP(Ge) in contrast, has a much better energy resolution and the complex gamma-ray spectrum can be more easily identified. The choice of using an NaI vs HP(Ge) detector depends on factors like the cost of the detector, the acquisition time needed (HP(Ge) requires a longer acquisition time), the complexity of the gamma-ray spectrum, and the cooling requirements of the detector (the HP(Ge) needs to be cooled to a lower temperature). Therefore the type of detector to use is often an important choice for a nuclear engineer to make in terms of what kind of resolution they require for a given application.

The energy resolution of a detector is quantified by using the Full Width at Half Maximum (FWHM) of a given peak as shown in Figure 3.7. This represents the full width of the peak's distribution at a level that is at half the maximum ordinate of the peak. The energy resolution is then defined as the FWHM divided by location of the peak's centre, H_0. The energy resolution is therefore a dimensionless ratio commonly given as a percentage. Scintillators used in gamma-ray spectroscopy typically have an energy resolution range of 5-10%.

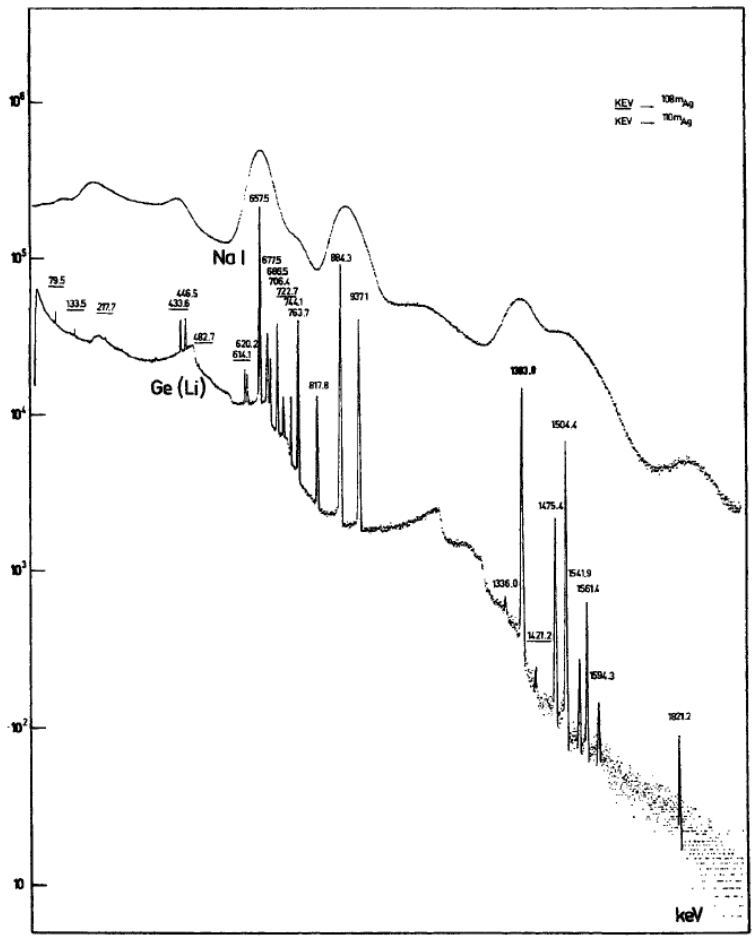

Figure 3.6: Comparison of gamma spectra obtained with NaI(Tl) and HPGe(Li) detectors [1].

3.3 Experiment description

The following experiments will be carried out using one of the HP(Ge) gamma detector systems:

- Experiment 1: Energy and efficiency calibration using a ^{152}Eu source
  - Calibrate the detector
  - Create gamma-ray energy vs. detector efficiency curves
- Experiment 2: Determining the source strength of a ^{60}Co source and the relative intensity of its two gamma rays.

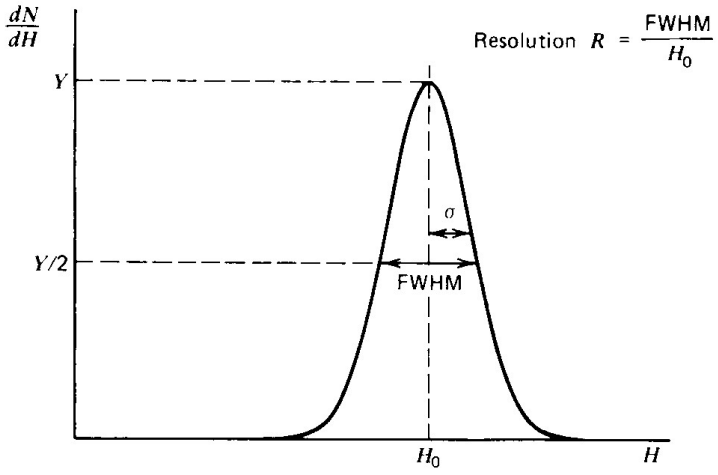

Figure 3.7: FWHM for expressing the energy resolution of a detector [1].

3.3.1 Important Precautions

The following precautions need to be followed at all times to ensure the safety of the experimenters and the equipment and to create high quality results.

1. Apply the specified high voltage (see Section 3.4) for the detector system chosen.
2. Handle gamma sources without touching the central active region.
3. Place the gamma source in the plastic holder slot at the appropriate distance.
4. Measurements should be carried out for a counting statistics of about 20,000.
5. Put the source back into the lead shielding container after use.

3.4 Required setup

This experiment requires a complete HP(Ge) detector system consisting of a detector, preamplifier, liquid nitrogen Dewar, and appropriate lead shielding. The LRS has two HP(Ge) detector systems, but only one will be used during this experiment. Note that the operating high voltage and other conditions are different for the two systems. Detector #01 requires an voltage of +4000V and detector #02 requires a high voltage of +3000V.

Each detector has its own data acquisition system (type DSA-1000, CANBERRA), connected to a PC (LRSPC3 and LRSPC13), with the following ID numbers:

- 2.1 DSA-1000, S/N: 11044024 (LRSPC3) DET #01
- 2.2 DSA-1000, S/N: 06041239 (LRSPC13) DET #02

3.5 Operational settings

3.5.1 Setting up the computer, software, and detector

First start the Windows XP virtual box on the computer. You will be prompted to enter a password, press *cancel*. You will then be prompted to enter a password again, press *okay* with the password field empty.

Next at the top of the virtual box there is a tool bar, at the middle of which is a *USB tab*. Click on the *USB tab* and then *attach all devices*. This will importantly mount the detector. You then will need to restart the *VDM service* (Areva/Canberra). Do so by right clicking on its tool bar in the bottom right hand corner of the screen.

After setting up the virtual box, open the *Gamma Acquisition software*. Once it is open, click on *file*, then *data source*, and select the detector. If you have not attached the detector in USB tab, it will not appear here in *data source*. Then you need to turn the high voltage power supply on by clicking on *MCA*, then *Adjust*, then *HVPS*, then *On*. You are now ready to begin detecting stuff! To do so, just press the green button (with a faint spectrum on it) in the program's tool bar to start the acquisition. Note: the gain needs to be adjusted in order to get accurate spectral data.

3.6 Measurement steps

The lab has two phases related to the sources used: ^{152}Eu and ^{60}Co. Phase one uses ^{152}Eu to calibrate the detector and to make efficiency vs. particle energy curves. Phase two uses the ^{60}Co source so that students can measure the activity of the source with the detector and compare their results to theoretical values.

3.6.1 Experiment 1: Energy and efficiency calibration using a ^{152}Eu source

The first step of this experiment is to calibrate the detector and determine the detector's efficiency for different particle energies. The efficiency must be determined at two different distance between the radioactive source and the detector. These distances are chosen by the students and need to be accurately measured.

Note: The energy calibration and efficiency measurements can be done for one distance at the same time, or with a single acquisition. In other words, a single acquisition can be used for the energy calibration and efficiency calculations.

The following steps should be followed for this phase of the experiment:

1. Place the ^{152}Eu source within the detector shielding, accurately measuring the distance from the source to the detector.

2. Begin an acquisition following the instructions given in Section 3.5.1 and manipulate the coarse grain of the detector system.

    - The gain is the amplification of the current signal in the system.
    - To see the whole gamma-ray spectrum, the gain must be correctly set.
    - The next steps cannot begin until the whole spectrum is visible.

3. Do the first energy calibration/efficiency acquisition with a collection time (strictly the live time) set to 15 minutes.

4. Once the acquisition finishes, the software can be calibrated by selecting *Calc*, then *Energy only calibration*. The channel numbers of the five prominent ^{152}Eu peaks need to be identified and then corresponded to theoretical energy of the peak to perform the calibration.

    - These peaks are shown in a laminated paper that present at the lab.
    - It is important that the calibration is accurate. Make sure that the peaks in the software's spectrum correspond to ±3 eV of the peaks' theoretical energy.
    - It is possible to zoom in on a peak to more accurately select a channel.

5. At the end of the every acquisition, print out a peak analysis report. This will integrate the counts under each peak, which are to be used in calculations. Save this peak analysis report.

6. Save the acquisition as .TKA and .CAM files. The .CAM files will allow to reopen the acquisition in the Gamma Acquisition software, and .TKA is exportable to Excel. Spectra can also be saved as .PDF files for use in reports.

7. Begin a second acquisition at a different distance between the source and the detector.

    - Acquisition time can be shortened to 10 minutes for this measurement.
    - Repeat steps 5 and 6 to save the peak analysis report and the acquisition data for this distance.

3.6.2 Experiment 2: Determining source strength of a ^{60}Co source and the relative intensity of its two gamma rays.

Next, the second phase of the experiment involves two acquisitions with a ^{60}Co source at the two distances previously used in Experiment 1. Each acquisition should last ~10 minutes and will follow the same procedure outlined in Section 3.6.1. The efficiency curves for each distance and these measurements are then used to calculate the ^{60}Co activity and the relative intensity of the two gamma rays of ^{60}Co. For each of these measurements, make sure to save all of data in the ways previously mentioned.

3.7 Data analysis

The following data processing should be carried out to determine the various parameters of interest:

1. *Energy and efficiency calibration*: The peak positions corresponding to the different ^{152}Eu gamma energies will be determined and the peak area analysis carried out using the built-in software (GENIE-2000), for the energy and efficiency calibration. For the efficiency calculation use the formula:

$$\epsilon(E) = \frac{N(E)/t}{A \cdot p(E)} \tag{3.1}$$

   where ϵ is the efficiency, E is the energy, N is the number of counts, t is the detection time, A is the sample activity and p is the emission probability for gamma with energy E.

2. *Dead time correction*: A dead time correction (if larger than about 1%) should be applied for each data set.

3. *Relative gamma intensity*: The peak areas and the corresponding efficiency values for the two ^{60}Co gamma rays will be used for determining their relative intensities. For the relative intensity use the formula:

$$\frac{I_1}{I_2} = \frac{N_1}{N_2}\frac{\epsilon_2}{\epsilon_1} \tag{3.2}$$

3.8 Expected results

The following results are expected:

- Spectra of each gamma-ray source, at different source-detector distances.
- Energy and efficiency calibration curves and equations at two different distances with the ^{152}Eu source.
- Relative intensity of the ^{60}Co gamma rays at two different distances.
- Strength of the ^{60}Co source at two different distances.
- Identification of the sources of error in each experiment.

3.8.1 Things to consider

- Does the detector's efficiency vary with gamma-ray energy? If it does/does not, why?

- Was it possible to see characteristic X-rays, backscattering, or annihilation photons from the shielding in the gamma-ray spectra?
- How do the relative intensities of the ^{60}Co gamma rays compare to their theoretical values? If they are different, why?
- How did adjustments in the gain affect the quality of the measured spectra?
- How well, statistically, does the energy calibration curve's equation fit to the experimental data?
- Is it possible to estimate the energy resolution of the detector?

4 Gamma-ray shielding and attenuation

4.1 Introduction

This experiment gives an introduction to the fundamentals of radiation protection against photons (e.g. gamma rays and X-rays). The processes that attenuate a photon are explored along with how attenuation varies with different materials, particularly Al and Pb. Photons like X-rays and gamma rays are commonly found in radioactive environments encountered by nuclear engineers. Additionally, they are very penetrating and have a significant biological effect, meaning that special care needs to be taken to protect against exposure to these kinds of particles. A common gamma-ray shielding problem encountered by nuclear engineers is the design of transport and storage casks for nuclear waste. Nuclear regulatory authorities require that the dose at the outside of a storage cask be below a certain limit. Companies must meet this regulation while also minimizing their costs. A nuclear engineer must then choose the appropriate quantity and type of shielding to meet these design constraints.

During this chapter's experiments, students measure the attenuation coefficients of gamma rays in two commonly encountered shielding materials: Al and Pb. Pb is commonly used in day-to-day radiation protection applications in industrial and research environments. Workers commonly create shielding with bricks of Pb in order to reduce their radiation exposure. Al is common shielding material in space applications to protect astronauts from cosmic rays. Al serves as an important and light-weight structural material while at the same time attenuates cosmic photons.

4.2 Theory

4.2.1 Attenuation of photons in matter

The basic mechanisms by which energetic photons interact with matter are the photoelectric effect, Compton scattering, and pair production. All of these processes result in either a partial or complete transfer of the photon's energy to the electrons of the target medium and thus

attenuate the photon. The fractional attenuation of a beam of photons passing through a material is described by Equation 4.1. Here, n photons pass per second normally through a foil of thickness dx containing N atoms/cm^3. The relative differential change in photon density attenuated by the beam, dn/n, is determined by the combined effects of either the photoelectric reaction, Compton scattering, and/or pair production, whose probabilities are described their microscopic cross sections σ_{ph}, σ_c and σ_{pp}. Often all of the microscopic cross sections are grouped into one term, μ, known as *linear attenuation coefficient*.

$$-\frac{dn}{n} = N(\sigma_{ph} + \sigma_c + \sigma_{pp})dx = \mu dx \tag{4.1}$$

The microscopic cross sections of the photoelectric effect, Compton scattering, and pair production depend on the photon's energy and the atomic number of the attenuating material. In terms of photon energy, the photoelectric effect has the largest cross section for low-energy photons (up to several hundred keV) and pair production has the largest for high-energy photons (5 MeV >). Meanwhile, Compton scattering has the largest cross section for the range of energies between these two extremes. The dependence of gamma-ray interaction cross sections on energy and atomic number is shown in Figure 4.1.

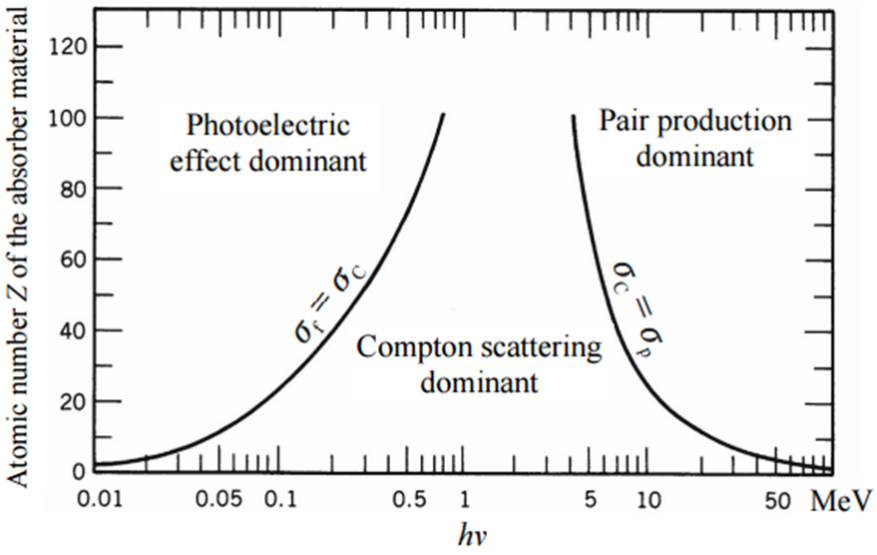

Figure 4.1: Dependence of photon interaction cross sections based on energy and atomic number.

The use of the linear attenuation coefficient is limited by the fact that it varies with the density of the target material, even though the material's composition remains the same. Therefore, the *mass attenuation coefficient* is more commonly used to describe photon attenuation and has units of g/cm^2. An advantage of the mass attenuation coefficient is that it does not change according to the physical state of an absorber. For example, it is the same for water whether present in liquid, solid, or vapour form. The mass attenuation coefficient, μ/ρ, is described

in Equation 4.2 in terms of the fractional reduction in a photon beam's intensity (n/n_0) when traversing an attenuating material of density ρ and thickness x.

$$\frac{n}{n_0} = exp(-\mu x) = exp\left(-\frac{\mu}{\rho}\rho x\right) \tag{4.2}$$

The mass attenuation coefficient for a compound or a mixture of elements can be obtained as in Equation 4.3, where w_i denotes the weight fraction of the ith type of isotope in the compound.

$$\frac{\mu}{\rho} = \sum w_i \left(\frac{\mu}{\rho}\right)_i \tag{4.3}$$

A photon's attenuation can also be characterized by a photon's mean free path λ, which is defined as the average distance travelled in the absorber before an interaction takes place. Its value can be obtained from Equation 4.4. The mean free path is simply the reciprocal of the linear attenuation coefficient. Typical values of λ range from a few mm to tens of cm in solids for common gamma-ray energies.

$$\lambda = \frac{\int_0^\infty x \;\; exp(-\mu x)dx}{\int_0^\infty exp(-\mu x)dx} = \frac{1}{\mu} \tag{4.4}$$

4.2.2 Photoelectric effect

Photoelectric absorption is an interaction in which an incident photon is absorbed by an atom and creates a photoelectron from one of the atom's electron shells. The energy of this photoelectron is described by T in Equation 4.5, where $h\nu$ is the kinetic energy of the incident photon, B_e is the binding energy of the electron in its original shell. In this process, the entire energy of the incident photon is transferred to an absorber atom's bound electron, usually an electron in the K or L shell, resulting in the ejection of the electron with energies in the range of a few to tens of keV.

$$T = h\nu - B_e \tag{4.5}$$

During this process, the energy B_e appears almost simultaneously as one of the characteristic X-rays of the target atom, because the electronic vacancy is quickly filled by electron transition within the atomic shells. In some cases, a fraction of the energy may appear as an Auger electron, which would again be quickly absorbed within a short distance from the site of production.

An approximate analytical expression for the photoelectric absorption cross section is given by

Equation 4.6, where K is a constant, and Z and $h\nu$ denote the atomic number of the medium and the energy of the incident photon, respectively. Equation 4.6 shows that the cross section has a strong dependence on Z. This leads high Z materials, like Pb, to be a shielding of choice for nuclear in radiation safety environments.

$$\sigma_{ph} = K\frac{Z^5}{(h\nu)^{3.5}} \tag{4.6}$$

4.2.3 Compton scattering

A Compton scattering interaction occurs when a photon interacts with an atom's electron cloud creating a recoil electron and a scattered gamma ray. The gamma ray's original energy is shared between the two and this energy division is dependent upon the interaction's scattering angle. From the energy and momentum conservation equations, the energy of the scattered photon is given by Equation 4.7, where $h\nu$ is the photon's energy, m_0c^2, is the mass-energy of an electron (0.511 MeV), and θ is the scattering angle of the reaction.

$$E'_\gamma = \frac{h\nu}{1+\frac{h\nu}{m_0c^2}(1-cos\theta)} \tag{4.7}$$

The energy of the scattered electron, T, is given by Equation 4.8, where $\alpha = h\nu/m_0c^2$.

$$T = E_\gamma - E'_\gamma = E_\gamma\frac{\alpha(1-cos\theta)}{1+\alpha(1-cos\theta)} \tag{4.8}$$

The maximum energy transfer to electrons takes place when the incident photon is scattered backwards, i.e. $\theta = 180°$, and the corresponding electron energy in terms of incident photon energy is given by Equation 4.9.

$$T = \frac{2\alpha E_\gamma}{1+2\alpha} \tag{4.9}$$

The probability of a Compton scattering per atom of an absorber depends on the number of electrons available in the target. The differential Compton scattering cross-section is given by the Klein-Nishina formula in Equation 4.10, where r_0 is the classical electron radius. Equation 4.10 shows a linearly increasing dependence of the cross section with Z. Again, the dependence on Z leads nuclear engineers to prefer high Z materials in for radiation protection against photons.

$$\frac{d\sigma}{d\Omega} = Zr_0^2\left(\frac{1}{1+\alpha(1-cos\theta)}\right)^2\left(\frac{1+cos^2\theta}{2}\right)\left(1+\frac{\alpha^2(1-cos\theta)^2}{(1+cos^2\theta)(1+\alpha(1-cos\theta))}\right) \tag{4.10}$$

4.2.4 Pair production

The pair production reaction corresponds to the creation of an electron-positron pair when an incident photon interacts with a nucleus. An energy of $2m_0c^2$ is required for this reaction, or 1.02 MeV. When a photon exceeds this energy threshold, its energy in excess of 1.02 MeV appears as the kinetic energy of electron-positron pair. The shared energy between the electron-positron pair is given by Equation 4.11.

$$T_e + T_p = E_\gamma - 2m_0c^2 \tag{4.11}$$

The pair production cross-section, σ_{pp}, is given by Equation 4.12, where σ_0 is the constant described by Equation 4.13.

$$\sigma_{pp} \approx Z^2\sigma_0\left(\frac{28}{9}ln\left(\frac{2E_\gamma}{m_0c^2}\right) - \frac{218}{27}\right) \tag{4.12}$$

$$\sigma_0 = \frac{1}{137}\left(\frac{e^2}{m_0c^2}\right)^2 \tag{4.13}$$

4.3 Experiment description

The following gamma attenuation coefficient experiments will be carried out with a ^{60}Co source and NaI(Tl) detector system.

- Experiment 1: Measuring the attenuation coefficient of Al
- Experiment 2: Measuring the attenuation coefficient of Pb

4.3.1 Important precautions

The following precautions need to be followed at all times to ensure the safety of the experimenters and the equipment and to create high quality results.

1. The material plates should be placed touching each other.
2. Do not change the detector-source geometry between measurements.
3. Keep the electronic settings fixed during the experiment.
4. Counting to be initiated with the control switch on ORTEC-773.
5. The number of counts should be maintained at a maximum of up to 20,000 for each plate thickness to finish the experiment within 2 hr.

6. Make sure that the power bin is neither overheated nor overloaded.

4.4 Required setup

The following tools and materials are needed for this experiment. If they are not present in the laboratory setting, please communicate with your lab instructor.

1. A NaI(Tl) detector and a ^{60}Co source.
2. A complete electronic setup consisting of a All-in-one Mirion Osprey NaI detector with integrated HVPS, preamplifier, and digital MCA photo-multiplier.
3. Ten Al plates with dimensions of 12 cm x 12cm x 1.04 cm and densities of 2.699 g.cm^{-3}.
4. Ten circular Pb plates with internal diameters of 9.77 cm, thicknesses of 0.2 cm and densities of 11.35 g.cm^{-3}, each embedded in an aluminium plate with an external dimension of 12 cm x 12 cm x 0.5 cm.

4.5 Operational settings

The operational settings in Table 4.1 should be used for the detector system.

Table 4.1: Operational settings of the NaI(Tl) detector.

Component	Setting
Operating voltage of the NaI(Tl) detector	540 V*
Amplifier settings (ORTEC-575)	cg=10, fg=0.8, to get ~5V pulses

4.6 Measurement steps

4.6.1 Experiment 1: Measuring the attenuation coefficient of Al

1. The NaI(Tl) detector and ^{60}Co source are in separate shielded arrangements, facing each other.
2. Follow the steps on the instructions sheet to turn on the detector. (As detector, use 'MCA' instead of 'DET1')
3. Adjust the operational settings as specified in Table 4.1.
4. Perform the transmission experiment by increasing in steps the thickness of the Al shielding between the source and detector by adding more plates.

4.6.2 Experiment 2: Measuring the attenuation coefficient of Pb

Repeat the steps described in Section 4.6.1, but with the Pb plates.

4.7 Data analysis

The ^{60}Co source has two photon energies of 1.17 and 1.33 MeV both emitted with equal probabilities. The data analysis should be done considering that the measurements with ^{60}Co lead to an attenuation coefficient of the average photon energy of 1.25 MeV.

Table 4.2: Mass attenuation coefficient for Al and Pb for different photon energies [1].

Photon energy[MeV]	μ/ρ **for Al** $[cm^2.g^{-1}]$	μ/ρ **for Pb** $[cm^2.g^{-1}]$
0.60	7.80E-02	1.25E-03
1.00	6.15E-02	7.10E-02
1.25	5.50E-02	5.88E-02
1.50	5.01E-02	5.22E-02
2.00	4.32E-02	4.61E-02

4.8 Expected results

1. Plot the count rate vs. material thickness for each material.
2. Determine the linear and mass attenuation coefficients for each material. (Perform linear fit taking the log of the count rate).
3. Compare the attenuation coefficient with the values in Table 4.2.
4. Identify the sources of errors for the attenuation coefficient.
5. Write a short note on the important conclusions considering radiation safety and the quality of these materials as shielding from gamma rays.

4.8.1 Things to consider

- What type of photon interactions are most important with a ^{60}Co source?
- How do Pb and Al compare in terms of their ability to attenuate gamma rays? Why would one material be used in the place of another?
- How much shielding of each material would be needed to successfully protect against a strong ^{60}Co source (1mSv/hr at 10 cm distance)? Consider the Swiss Radiological Protection Ordinance (814.501), which states that the public shall not be exposed to more than 1mSv per year. Assume 260 working days per year and a 7.5 hour work day.

What dose rate must a workplace therefore respect, and how much shielding of Al or Pb would you need to protect yourself adequately?

- Do the measured attenuation coefficients vary with the amount of shielding between the source and the detector? If so, why?
- The Pb plates are embedded in Al casings. Does this Al casing affect the measured Pb attenuation coefficients?

5 Neutron Detection

5.1 Introduction

As in the case of gamma rays, neutrons are uncharged and can therefore travel relatively large distances through matter without any interaction. When a neutron interacts, it does so with a nucleus of the material. As a result, it may disappear (be absorbed), or experience a change in energy and direction (be scattered). In each case, secondary radiation is produced (e.g. a capture gamma, a charged particle, a recoil nucleus, etc.).

5.2 Theory

5.2.1 Neutron Sources

The most common neutron source is a fission reactor, providing neutrons in a very wide energy band of 0.001 eV to about 10 MeV. In reactor physics, these neutrons are usually divided into three broad groups:

1. E < 0.2 eV, i.e. thermal neutrons,
2. 0.2 eV ≤ E ≤ 0.5 MeV, epithermal, and
3. E > 0.5 MeV, referred to as fast neutrons.

A typical prompt neutron spectrum resulting from the fission of ^{235}U by thermal neutrons is depicted in Figure 5.1. The shape of the spectrum is very similar for other fissile nuclei, e.g. ^{239}Pu, although the average neutron energy may differ slightly.

The fission neutrons' energy spectrum from about 0.0075 eV to 17 MeV has been shown to adequately follow Equation 5.1, where $\chi(E)$ represents the fraction of neutrons emitted with energy E MeV per unit energy interval (MeV).

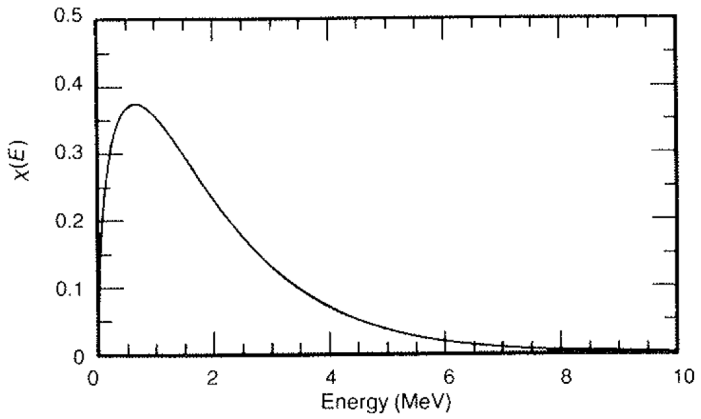

Figure 5.1: Energy spectrum of neutrons arising from the thermal fission of ^{235}U.

$$\chi(E) = 0.453e^{-1.036E}\sinh(\sqrt{2.29E}) \tag{5.1}$$

Although, most of the neutrons have energies of 1-2 MeV, there are some with energies in excess of 2 MeV. The neutron spectrum gets strongly modified within the reactor due to the various neutron interactions and, as a result, is found to vary from location to location.

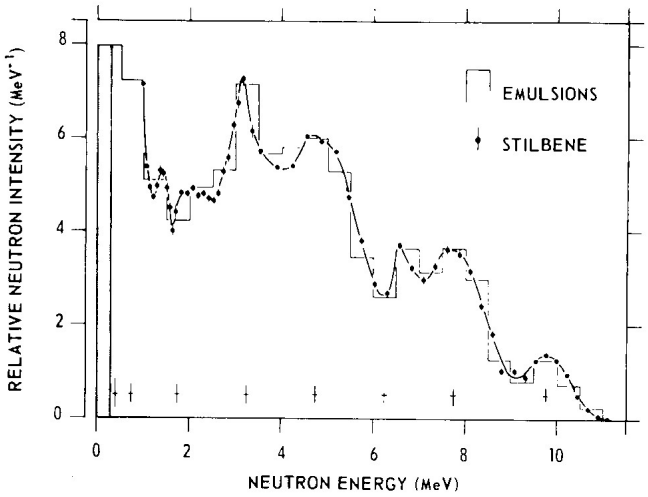

Figure 5.2: Measured energy spectrum of a Pu(α, n)Be source.

Apart from reactors, neutrons can also be made available in the laboratory from charged-particle reactions using an accelerator or from isotopic sources. Examples of the latter are a nucleus which fissions spontaneously (such as ^{252}Cf) or a mix of an alpha-emitter and neutron-producing nuclides (e.g. a mixture of ^{239}Pu and ^{9}Be; see Figure 5.2). The nuclear reactions for neutron production are

$$^{X}_{94}\mathrm{Pu} \rightarrow {}^{X-4}_{92}\mathrm{U} + {}^{4}_{2}\mathrm{He} \tag{5.2}$$

$${}^{4}_{2}\mathrm{He} + {}^{9}_{4}\mathrm{Be} \rightarrow {}^{6}_{12}\mathrm{C} + {}^{1}_{0}\mathrm{n} \tag{5.3}$$

A typical design of a Pu(α, n)Be source is depicted in Figure 5.3.

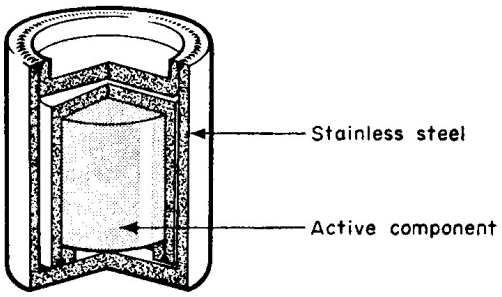

Figure 5.3: A typical double-walled Pu(α, n)Be neutron source.

The specifications of the source used in this experiment are shown in Table 5.1

Table 5.1: Characteristics of the Pu(α, n)Be neutron source available for the measurements

Parameter	Value
Diameter (mm)	33.3
Length (mm)	69
Maximum neutron energy (MeV)	10.6
Average neutron energy (MeV)	3.5
Energy of gamma rays (MeV)	4-5
Isotopic composition of plutonium	
^{239}Pu	91.76%
^{240}Pu	7.52%
^{241}Pu	0.69%
^{242}Pu	0.03%

5.2.2 Principles of neutron detection

Neutrons are either detected actively, via nuclear reactions resulting in the production of charged particles, or passively by measuring the radioactivity induced in appropriate samples after neutron absorption. A typical active neutron detector consists of a converting medium, integrated into a conventional charged particle detector, while passive detectors consist of activation samples in the form of foils, wires, etc., of different shapes and sizes. In the latter case, measurement of the associated activity is carried out after irradiation of the sample (foil/wire). A list of activation detectors usually employed to cover the slow-neutron energy

range is presented in Table 5.2. Also, a list of threshold activation detectors employed for the detection of fast neutrons is given in Table 5.3.

Table 5.2: Materials used as slow-neutron activation detectors [1].

Element	Isotopic Abundance [%]	Thermal activation cross section [10^{-28} m^2]	Induced activity	Half-life
Manganese	^{55}Mn (100)	13.2 ± 0.1	^{56}Mn	2.58 h
Cobalt	^{59}Co(100)	16.9 ± 1.5	^{60m}Co	10.4 min
		20.2 ± 1.9	^{60}Co	5.28 y
Copper	^{63}Cu(69.1)	4.41 ± 0.20	^{64}Cu	12.87 h
	^{63}Cu(30.9)	1.8 ± 0.4	^{66}Cu	5.14 min
Silver	^{107}Ag(51.35)	45 ± 4	^{108}Ag	2.3 min
	^{109}Ag(48.65)	3.2 ± 0.4	^{110m}Ag	253 d
Indium	^{113}In(4.23)	56 ± 12	^{114m}In	49 d
		2.0 ± 0.6	^{114}In	72 s
	^{115}In(95.77)	160 ± 2	^{116m}In	54.12 min
		40.2 ± 1	^{116}In	14.1 s
Dysprosium	^{164}Dy(28.18)	2000 ± 200	^{165m}Dy	1.3 min
		800 ± 100	^{165}Dy	140 min
Gold	^{197}Au(100)	98.5 ± 0.4	^{198}Au	2.695 d

Since neutron interaction processes leading to charged particles strongly depend on the neutron's energy, separate techniques have been developed to detect neutrons of different energies. The selection of the medium for detection is generally based on the energy range of interest. In the current experiments, we will confine ourselves to the detection of slow neutrons (energy < 0.5 eV) using gas detectors. The two widely used nuclear reactions for such on-line neutron detection are

$$^{10}_{5}\mathrm{B} + ^{1}_{0}\mathrm{n} \rightarrow \begin{cases} ^{7}_{3}\mathrm{Li} + ^{4}_{2}\mathrm{He} + 2.792\ \mathrm{MeV}\ (6\%) \\ ^{7}_{3}\mathrm{Li}^{*} + ^{4}_{2}\mathrm{He} + 2.310\ \mathrm{MeV}\ (94\%) \end{cases} \tag{5.4}$$

$$^{3}_{2}\mathrm{He} + ^{1}_{0}\mathrm{n} \rightarrow ^{3}_{1}\mathrm{H} + ^{1}_{1}\mathrm{H} + 0.764\ \mathrm{MeV} \tag{5.5}$$

Each of the neutron detectors employed in this lab uses one of the above reactions in a gas ionisation chamber. The first reaction is obtained using BF_3 as the filling gas, while the latter employs ^{3}He. Since, in each case, both the charged particles produced are liberated within the detector, the net response provides information about the total energy liberated in the reaction and not about the energy of the incoming neutron.

Since a gas detector can be operated at different high voltages, there are different modes

Table 5.3: Materials used as fast-neutron activation detectors [1].

Material	Reactions of Interest	Isotopic Abundance (at %)	Half-Life	γ Energy (MeV)	γ Abundance (%)	Threshold (MeV)
F	$^{19}F(n, 2n)^{18}F$	100.0	109.7 min	0.511+	194°	11.6
Mg	$^{24}Mg(n, p)^{24}Na$	78.7	15.0 h	1.368	100	6.0
Al	$^{27}Al(n, \alpha)^{24}Na$	100.0	15.0 h	1.368	100	4.9
Al	$^{27}Al(n, p)^{27}Mg$	100.0	9.46 min	0.84–1.01	100	3.8
Fe	$^{56}Fe(n, p)^{56}Mn$	91.7	2.56 h	0.84	99	4.9
Co	$^{59}Co(n, \alpha)^{56}Mn$	100.0	2.56 h	0.84	99	5.2
Ni	$^{58}Ni(n, 2n)^{57}Ni$	67.9	36.0 h	1.37	86	13.0
Ni	$^{58}Ni(n, p)^{58}Co$	67.9	71.6 d	0.81	99	1.9
Cu	$^{63}Cu(n, 2n)^{62}Cu$	69.1	9.8 min	0.511+	195°	11.9
Cu	$^{65}Cu(n, 2n)^{64}Cu$	30.9	12.7 h	0.511+	37.8°	11.9
Zn	$^{64}Zn(n, p)^{64}Cu$	48.8	12.7 h	0.511+	37.8°	2.0
In	$^{115}In(n, n')^{115m}In$	95.7	4.50 h	0.335	48	0.5
I	$^{127}I(n, 2n)^{126}I$	100.0	13.0 d	0.667	33	9.3
Au	$^{197}Au(n, 2n)^{196}Au$	100.0	6.18 d	0.33–0.35	25–94	8.6
Li	$^{7}Li(n, \alpha n')t$	92.58	12.3 y	0–0.019×	100×	3.8

of operation, the corresponding detector response regions being indicated as a function of applied voltage in Fig. 5.4. A typical detector design (proportional counter type) is shown in Fig. 5.5.

The selection of the applied voltage depends on the desired application. It may be noted that there are several gases available that can be used in a gas ionisation detector, and one of the important criteria is the energy required to produce an ion-pair. The characteristics of some of the gases generally used in ionisation-type detectors are summarized in Table 5.4. As indicated earlier, we have chosen different types of gas ionisation detectors for the present neutron detection experiments. In each case, the gas serves the dual purpose of being a target material for the production of charged particles, as well as a medium for their detection. The detectors will be operated in the proportional region to get a response proportional to the ionizing particle energy, in each case. Typical outputs from a large and a small-size BF_3 detector, for incident thermal neutrons, are shown in Figure 5.6

Since the total energy deposition occurs in the gas for most of the events in the case of a bigger detector, the wall effect continuum is reduced in comparison to that for a small-size detector, where a significant number of events involve energy loss in the detector wall, rather than in the gas, due to the proximity of the wall to the site of the neutron reaction. From the conservation

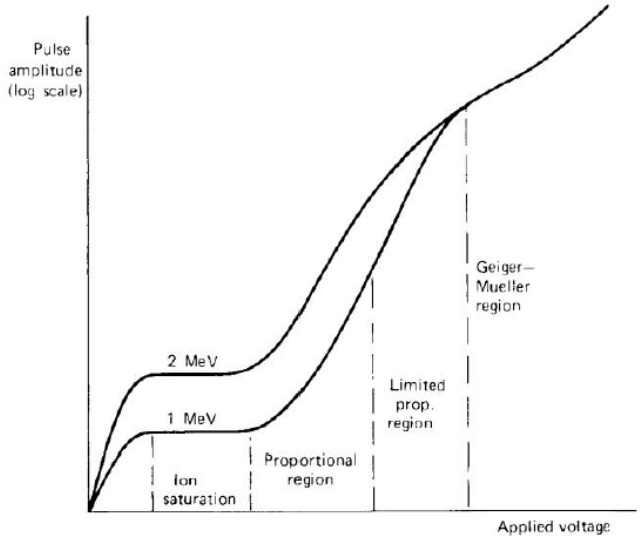

Figure 5.4: The different regions of operation of a gas-filled detector.

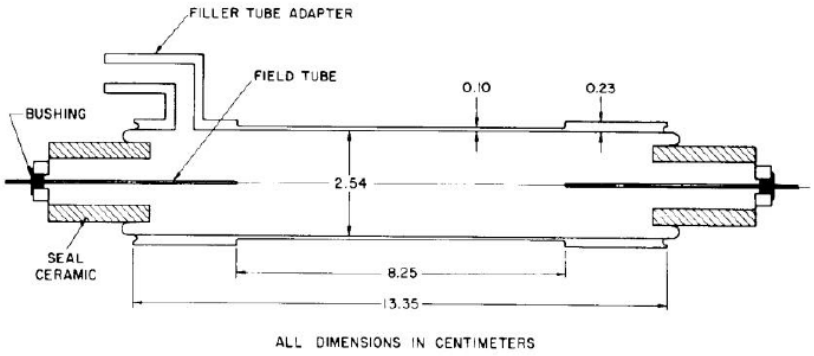

Figure 5.5: Cross-sectional view of a typical proportional counter tube.

of energy and momentum applied to the dominant reaction type (94%) in Equation 5.4 the energies received by the resultant charged particles ^{7}Li and ^{4}He are found to be 0.840 and 1.47 MeV, respectively. These energies effectively represent the threshold limits of the wall-effect continuum (corresponding to the situation where the neutron reaction occurs at the wall and only one of the particles can deposit its energy in the gas).

Similarly, the response of a medium size 3He gas detector to slow neutrons is shown in Figure 5.7

For an infinitely large detector, the response to thermal neutrons will be a single, well-defined peak, corresponding to a total energy of 764 keV. The corresponding wall-effect continuum threshold limits are 191 and 573 keV due to ^{3}H (tritium or triton) and ^{1}H (proton), respectively.

From the number of full-energy peaks obtained with each detector employed in the current

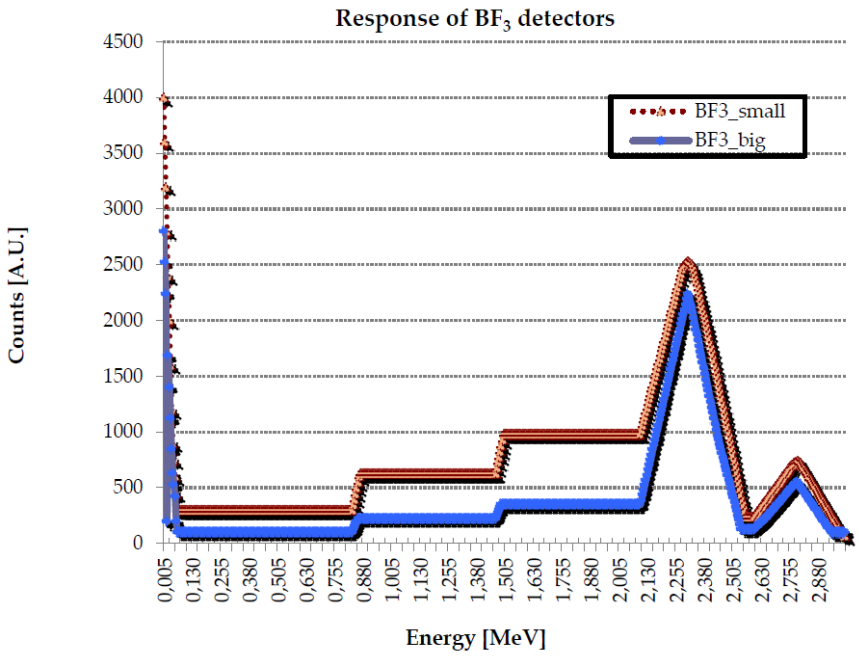

Figure 5.6: Pulse height spectra of BF_3 detectors: distribution from a large-diameter detector (blue) and from a small-diameter detector (red), showing continuum due to wall effect.

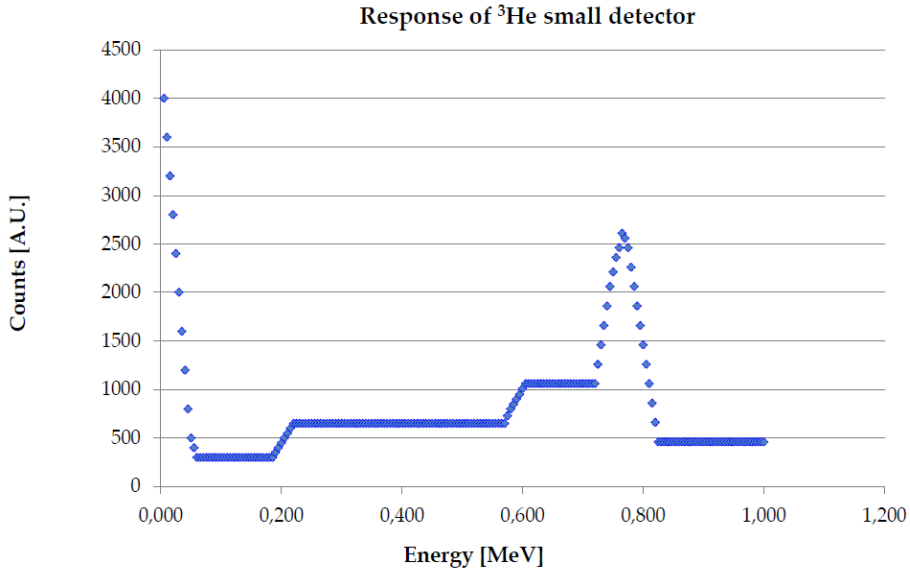

Figure 5.7: Differential energy spectrum of charged particles produced in a ^{3}He detector, resulting from neutron interactions with ^{3}He.

measurements, it is simple to identify the type of detector. Thus, there will be a single peak (corresponding to 0.764 MeV) in the case of ^{3}He, while two distinct peaks (corresponding to 2.792 and 2.310 MeV) occur in the case of a BF_3 detector.

Table 5.4: Energy dissipation per ion pair of different gases.

Gas	First ionization potential (eV)	W-value (eV/ion pair)	
		Fast electrons	Alpha particles
Ar	15.7	26.6	26.3
He	24.5	41.3	42.7
H2	15.6	36.5	36.4
N2	15.5	34.8	36.4
Air	33.8	35.1	32.2
O2	12.5	30.8	32.2
CH4	14.5	27.3	29.1

The fraction of events appearing under the wall-effect continuum essentially depends on the reaction products, their energy distribution, the detector diameter and the pressure of the gas used for detection. For the current analysis, a simple definition can be used to quantify the wall effect in terms of the wall-effect continuum factor, defined as the ratio of the area under the continuum regions to the net area (from the start of the continuum up to the end of the dominant peak).

5.3 Experiment description

The following experiments will be performed using the two different types of gas-filled, slow-neutron detectors:

- Experiment 1: Identification of detector type
- Experiment 2: Characterisation of wall-effect continuum
- Experiment 3: Quantitative estimation of reaction type in BF_3 detector

Each experiment consists of positioning one of the neutron detectors in the vicinity of a Pu(α, n)Be neutron source located in the CARROUSEL facility and measuring the pulse height spectrum using a multi-channel analyser.

5.3.1 Important precautions

The following precautions need to be followed at all times to ensure the safety of the experimenters and the equipment and to create high quality results.

1. The voltage should be raised and lowered slowly, and in small steps.
2. The high voltage must be switched off during changing of the detectors.

3. The coarse and fine gains of the amplifier must be adjusted to keep the maximum pulse heights in the range of 4 to 5 V.

5.4 Required setup

The following components are required for this experiment. Check to see if they are available. If they are not available, please speak with your lab instructor.

- High voltage unit
- Pre-amplifier
- Amplifier
- Multi Channel Analyser
- Three neutron detectors (two BF_3 neutron detectors)
- PC with MAESTRO 32 software for data analysis

5.5 Measurement steps

5.5.1 Experiment 1: Identification of the detector type

The first experiment involves determining the type of gas fill used in the neutron detector. The multi-channel analyser response (pulse height spectra) will be studied to see the differences in the response of the various detectors. The number of peaks observed (corresponding to total energy deposition) will form the basis for identifying the type of gas filled in the detector. An oscilloscope is provided to visualize the pulses coming out of the various stages of the setup.

The following steps should be followed.

1. Verify that the HV is turned off.
2. Place one of the ionisation detectors in its plastic tube and install it in the CARROUSEL facility; be sure that the detector is correctly placed within its tube.
3. Switch on the power supply, set the appropriate HV voltage corresponding to the detector considered (~ 1000V). With the oscilloscope, record and sketch in the report the output of the pre-amplifier.
4. Connect the pre-amplifier to the amplifier. The coarse and fine gains must be adjusted to get appropriate pulse heights out of the amplifier. With the help of the oscilloscope, adjust the settings so as to obtain a 4-5 V pulse out of the amplifier. Record and sketch in the report the output of the amplifier. Report the coarse and fine gains used.

5. Connect the output of the amplifier to the multichannel analyser. Acquire data in the multi-channel analyser to get sufficient statistics. Save the pulse height spectrum for analysis.

6. Switch off the power supply unit by lowering the voltage in small steps.

7. Replace the detector by the second and then third detector (changing voltage and amplifier conditions appropriately as specified in steps 3 and 4), and acquire data for the same pre-set time in each case. The high voltage must be switched off before to change the detector. Report HV, fine and coarse amplifier gains.

8. Sketch the measurement setup in your report

9. Conclude on the type of gas filled in each detector.

5.5.2 Experiment 2: Characterization of wall-effect continuum

The second experiment involves characterizing the wall-effect continuum for each of the neutron detectors provided. The shape of the region below the dominant peak will be studied to infer the characteristics of the wall-effect continuum, i.e. the size of the detector. An oscilloscope is provided to visualize the pulses coming out of the various stages of the setup.

The following steps should be followed.

1. Verify that the HV is turned off.

2. Place one of the BF3 detectors in its plastic tube and install it in the CARROUSEL facility; be sure that the detector is correctly placed within its tube.

3. Switch on the power supply, set the appropriate HV voltage corresponding to the detector considered (~ 1000V).

4. Connect the pre-amplifier to the amplifier. The coarse and fine gains must be adjusted to get a 4-5 V pulse out of the amplifier.

5. Connect the output of the amplifier to the multichannel analyser. Acquire data in the multi-channel analyser for about 20 minutes to get sufficient statistics. Save the pulse height spectrum for analysis. Report dead time. Eventually correct the position of the detector with respect to the source to have a dead time lower than 1%.

6. Switch off the power supply unit by lowering the voltage in small steps.

7. Replace the detector by the second BF_3 detector (changing voltage and amplifier conditions appropriately as specified in steps 3 and 4), and acquire data for the same pre-set time in each case. The high voltage must be switched off during branching of the detector. Report HV, fine and coarse amplifier gains as well as dead time.

8. Qualitatively compare the two pulse height spectra.

9. Report the ratio of the area under the continuum regions to the net area (from the start of the continuum up to the end of the dominant peak) as well as the associated uncertainty. Decide which detector has the largest diameter based on the spectra.

5.5.3 Experiment 3: Quantitative estimation of reaction type in BF_3 detector

Estimate the branching ratio of the B(n,α) reaction (see Equation 5.4). The percentage contribution due to each reaction type in the case of a BF_3 detector can be obtained from the spectrum by measuring areas under the two full-energy peaks. An oscilloscope is provided to visualize the pulses coming out of the various stages of the setup.

The following steps should be followed.

1. Verify that the HV is turned off.

2. Place one of the BF_3 detectors in its plastic tube and install it in the CARROUSEL facility; be sure that the detector is correctly placed within its tube.

3. Switch on the power supply, set the appropriate HV voltage corresponding to the detector considered ($\sim$ 1000V).

4. Connect the pre-amplifier to the amplifier. The coarse and fine gains must be adjusted to get a 4-5 V pulse out of the amplifier.

5. Connect the output of the amplifier to the multichannel analyser. Acquire data in the multi-channel analyser for about 20 minutes to get sufficient statistics (maybe it is not needed to redo such acquisition; old results could be used...). Save the pulse height spectrum for the analysis. Report dead time. Eventually correct the position of the detector with respect to the source to have a dead time lower than 1%.

6. Report the ratio the area under each of the two full energy peaks and divide by the total area under both peaks. Estimate uncertainty and compare to the reference values (94%/6%)

5.6 Expected results

1. HV, fine and coarse amplifier gains for each detector

2. Pulse height spectra for each detector

3. Estimation of the branching ratio of the BF_3 reaction

4. Characterization of wall-effect

6 Fast neutron detection via Pulse Shape Discrimination

6.1 Introduction

In this lab session, you will learn the fundamentals of organic scintillator detectors. Organic scintillators are a class of materials widely employed in radiation detection and measurement because of their ability to emit detectable bursts of light when exposed to ionizing radiation (scintillation). These materials consist of organic molecules or polymers/plastics doped with luminescent compounds that become excited upon interaction with charged particles. As a result, they emit photons that can be detected that can provide information about the type, energy, and intensity of incident radiation. Organic scintillators have applications in fields ranging from nuclear physics and medical imaging to homeland security and environmental monitoring. For instance, the IAEA uses organic scintillators for fresh fuel verification measurements [8]. Special nuclear material (SNM) such as plutonium and enriched uranium is identifiable through the detection of neutrons and photons emitted from spontaneous and induced fission events, and some organic scintillators can detect both particle types.

Organic scintillators are typically lightweight, exhibit fast response times, and are well-suited for detecting fast neutrons and gamma radiation. In contrast, inorganic scintillators consist of crystalline materials such as sodium iodide (NaI) or cesium iodide (CsI), which exhibit scintillation in the crystal lattice. Inorganic scintillators tend to have higher density and better energy resolution, making them more suitable for detecting gamma and X-ray radiation. The choice between these two types of scintillators depends on the specific requirements of the radiation detection task at hand.

6.1.1 Physics of organic scintillators

Gamma-ray interactions within scintillators typically can be summarized to stem from three principal phenomena: Photoelectric effect, Compton scattering, and Pair Production (please see Experiment 3 for more details on gamma-ray interactions with matter).

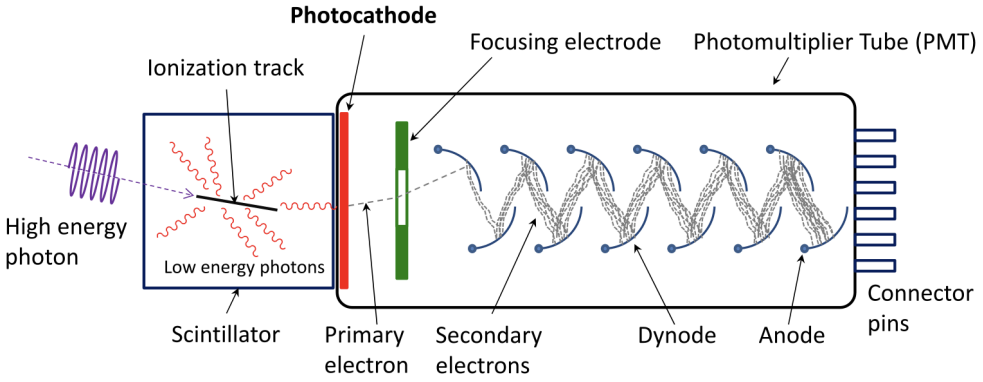

Figure 6.1: Concept of using a photomultiplier tube (PMT) top detect radiation induced scintillation light. By Qwerty123uiop, CC BY-SA 3.0, https://commons.wikimedia.org/w/index.php?curid=62426194

The photoelectric effect, in which the gamma ray is entirely absorbed by an atomic electron, leads to the emission of a photoelectron in the scintillators. In Compton scattering, a gamma ray imparts only part of its energy to an atomic electron, causing it to recoil and the gamma ray to change direction. In this case, the energy deposited within the scintillator is shared between the recoiling electron and the resulting scattered gamma ray, which may undergo further interactions. Both interactions result in the excitation of the scintillator material, with a subsequent emission of scintillation light, typically in the visible or ultraviolet range, which is then detected and converted into an electrical signal for analysis. The light is often collected via photomultiplier tubes (see Figure 6.1). An interesting difference between organic and inorganic scintillators is the fact that low Z materials exhibit significantly lower cross sections for the photoelectric effect. This means that organic scintillators often do not exhibit the usual photo-peak and Compton continuum pulse height shapes, but rather only a Compton continuum. This makes organic scintillators not very suitable for source identification tasks, as photopeaks are usually used to assign energies and thus determine an emitting isotope. However, their fast scintillation decay makes them good timing devices, e.g., for multiplicity counting (a standard IAEA procedure for Pu mass verification [9]).

Some organic scintillators, depending on the composition of the crystal or plastic, exhibit significantly different pulse shapes from neutron interactions compared to gamma-ray interactions (see Figure 6.2). The organic scintillators detect neutrons mainly through elastic scattering on protons, as opposed to gamma rays which primarily interact through Compton scattering on electrons. The two types of radiation are distinguishable because of the ratio of prompt and delayed scintillation light. Most of the scintillation light comes from prompt fluorescence (few nanoseconds), but the higher stopping power (dE/dx) of a proton in the active volume leads to an increased density of triplet states that deexcite through delayed fluorescence (hundreds of nanoseconds).

Because of the delayed fluorescence, the pulse die-away time for neutron scatters will be

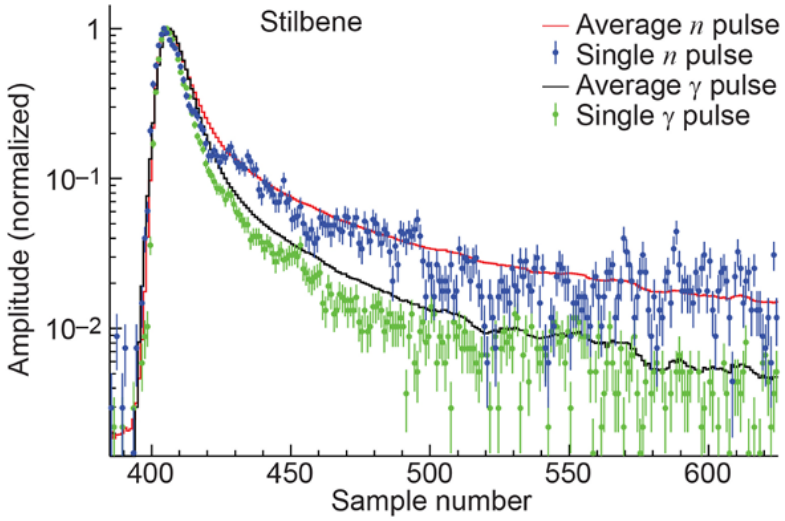

Figure 6.2: Average pulse shapes from a stilbene organic scintillator [3].

longer than that of photon scatters of equivalent light output, which may be quantified by either pulse height or pulse integral. Thus, we can discriminate between the two types of interactions with charge-integration pulse-shape discrimination (PSD). Figure 6.2 displays the clear difference in the tail region of neutron and photon pulses for a typical organic scintillator (stilbene). For a neutron and photon signal of equivalent pulse height, the tail region of the neutron signal will have a higher integral value. The same remains true for a neutron and photon signal of equivalent pulse integral. This characteristic highlights the significant amount of delayed fluorescence associated with neutron signals relative to photon signals.

Organic scintillators with the right composition can therefore be used as dual particle - fast neutron and gamma-ray - detectors.

6.1.2 Energy calibration of organic scintillators

To interpret the energy deposition of particles scatters in organic scintillators, a gamma-ray source of known mono-energetic energy is required to calibrate each detector. Hence, a ^{137}Cs source is used to calibrate each detector using its mono-energetic 662 keV gamma ray. The Compton edge energy (CE) is calculated as

$$CE = E_\gamma \left(1 - \frac{1}{1 + 2\frac{E_\gamma}{m_e c^2}} \right), \tag{6.1}$$

where E_γ is the initial energy (662 keV) of the emitted gamma-ray and $m_e c^2$ is the rest mass of an electron (511 keV). Thus, a Compton edge of 478 keV is used to calibrate the light output of each detector, assuming zero energy deposition does not result in a pulse. Multi-energy emitters, such as ^{60}Co, lead to multiple CEs and a more complex calibration.

An ideal pulse integral distribution exhibits a sharp drop-off after a peak at the Compton edge. Realistically, this sharp edge is distorted by detector energy resolution (in this case, > 15%), leading the true location of the Compton edge to occur at a light output greater than the measured 'edge'.

6.2 Experiments to be conducted

The following measurements will be carried out:

Exp. 4.1: CeBr3 pulse height spectrum for Cs137, Co60, and Cf252.

Exp. 4.2: Organic scintillator pulse height spectrum for Cs137, Co60, Cf252, and PuBe.

6.2.1 Important Precautions

The following precautions need to be followed at all times to ensure the safety of the experimenters and equipment and to create high quality results.

1. The detectors have two cables: A BNC connector for the signal and a SHV connector for high voltage supply (HV). Note the visual difference between the connectors! Do not apply high voltage unless both cables are connected. Do not disconnect any cables when HV is on (can cause discharges that damage the electronics).
2. **When changing detectors or cables, always make sure that the high voltage switch is on OFF and that the display shows 0.0 kV!**
3. You will be measuring small radioactive sources. They are sealed and not dangerous to handle if they remain mechanically intact. This means - do not drop the source, do not scratch the source, do not rub your finger in the source, and leave the source always visible on the experiment table. If in doubt, stop and ask for help.

6.3 Required setup

The detectors are depicted in Figure 6.3. The high voltage unit and the digitizer for signal processing are shown in Figure 6.4. You may ask a attending radiation protection expert to hand you one of the sources for measurement (as shown in Figure 6.5).

Check if the following requirements are met for this experiment. If they are not available, please speak with your lab instructor.

Figure 6.3: **Left:** Scionix CeBr3 detector. The bottom houses the crystal, the top houses a crystal. The whole detector is encased in aluminium for light tightness and mechanical protection. **Right:** Organic scintillator. The top part is a Hamamatsu H3178-51 PMT, the bottom is a light-tight plastic hollow cylinder that contains a plastic scintillator cylinder of 1cm height and diameter. Be careful handling these detectors, the PMTs are delicate and the crystals can easily crack!

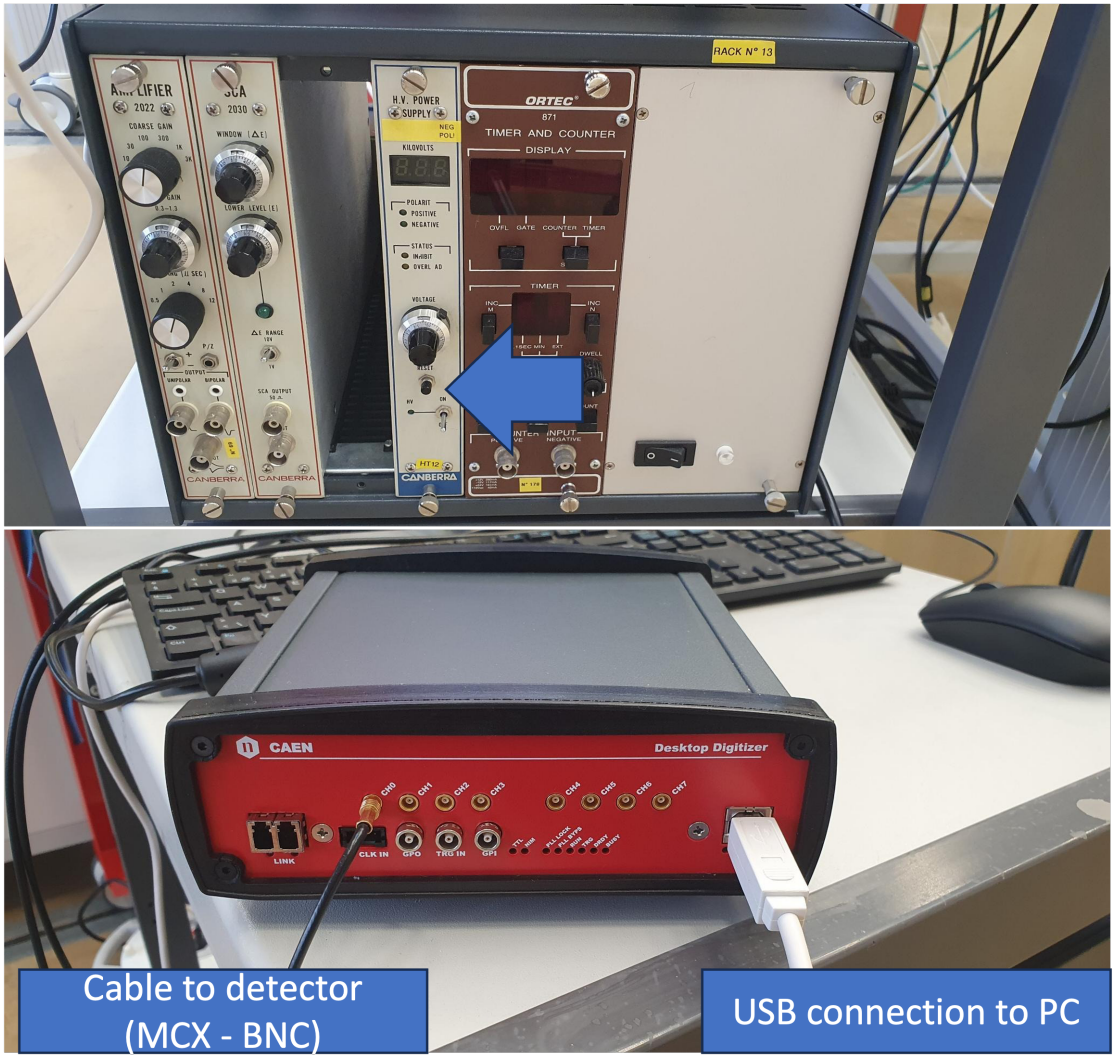

Figure 6.4: **Top:** High voltage unit in Rack 13. Note the negative polarity sticker, the PMTs for both detectors need negative polarity HV! **Bottom:** CAEN DT5730S 500-MHz desktop digitizer. The unit recevies the detector's signal output via MCX input in one of the channels, and sends the digitized data to a PC via USB.

Figure 6.5: **Left:** Co60 and Cs137 sources to be used for the experiment. **Right:** Californium source that can be used for a neutron/gamma pulse shape discrimination experiment.

1. Left side of the CARROUSEL facility is free.
2. CeBr3 scintillator and plastic scintillator (Figure 6.3).
3. CAEN digitzer and high voltage unit (Figure 6.4).
4. PC and COMPASS acquisition software.

6.4 Example of experiment with a detector

The procedure for an experiment to acquire the pulse height spectrum can look like this:

1. Choose a detector and source combination, set both on the table.
2. Verify that the high voltage is set to 'OFF'.
3. Use SHV/SHV and BNC/MCX cables to connect the HV output to the HV connector and the BNC signal output to the MCX channel on the digitizer.
4. Turn on the digitzer, a O/I switch is found on its back side.
5. Log on to the PC, make sure the digitizer is connected via the white USB cable to the PC.
6. Open the COMPASS software, the quick start icon is on the desktop.
7. In COMPASS, click on 'Load Project' to open a project folder ("CAEN measurements")
8. Once the board is recognized, you will be able to start the measurement (green play button on second COMPASS window).
9. Turn on the HV (switch to 'ON') and turn the knob until the display shows the desired voltage. **For CeBr3, do not go above 800V. For the plastic scintillator, do not go above 1200V.**
10. Open the digital waveform inspector and the energy histograms.
11. To save a spectrum, use the 'Save Spectrum' button.
12. For fast neutron measurements (Cf252, PuBe): In COMPASS, you can set pulse shape integration parameters (called short gate and long gate, see Figure 6.6) that can then be displayed in a PSD plot (button 'New PSD plot'). Tune the settings such that you can observe a distinct cluster forming, indicating neutron detection.

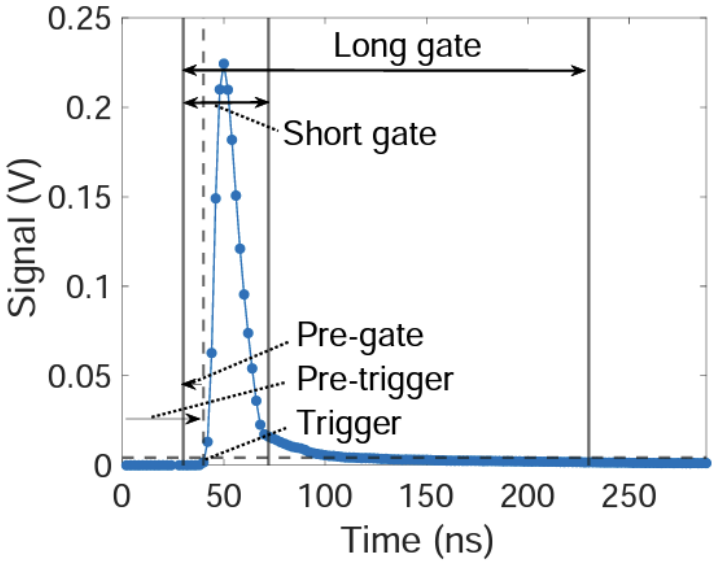

Figure 6.6: CAEN settings for a pulse.

6.5 Expected results

1. HV and COMPASS settings for each detector acquisition.
2. Pulse height spectra for each detector (organic vs. CeBr3), optimally in one plot with calibrated energy axis, for all sources (Cs137, Co60, Cf252, PuBe).
3. Discussion on the physics of gamma ray interaction, and how the pulse height spectra reflect that. Discuss what you see in the different spectra and what information they contain. What particles does a spontaneous fission source emit? Why is the pulse height shape the way it is?
4. A short report detailing gamma ray interactions with matter, scintillation, the experimental setup, results obtained, and discussion.
5. Pulse shape discrimination from the Cf252 and PuBe measurements, showing fast neutron detection. Compare the PSD plots of a neutron-emitting source to the Cs137 PSD plots to demonstrate that Cs137 does not emit neutrons.

7 Simulations with MCNP

7.1 Introduction

The goal of this "experiment" is to become familiar with the MCNP code, which is the reference in terms of neutron transport simulation. A simple problem is considered where the propagation of thermal neutrons through a body of water and graphite is investigated. The simulation results will be compared to reference values of the literature.

7.2 Theory

7.2.1 Monte Carlo simulations with MCNP

The Monte Carlo method does not solve any explicit equation, but rather obtains the desired answers by simulating individual particles and recording some aspects (tallies) of their average behaviour. It directly considers all the possible reactions taking place as the particles travel in the medium using probability distributions. This is essentially accomplished by using a set of random numbers and cumulative reaction probabilities derived from the cross-section data. The process consists of following each of many particles from a source until its death in some terminal category (fission, absorption, escape, etc). A typical trajectory of a neutron diffusing in a given medium is depicted in Fig. 7.1

MCNP [10] is a general purpose, continuous energy, generalized-geometry, time-dependent, coupled neutron/photon/electron Monte Carlo code. It can be used in several transport modes: neutron only, photon only, electron only, combined neutron/photon (where photons are produced as a result of neutron interaction), neutron/photon/electron, photon/electron or electron/photon. The neutron energy region covered is from 10^{-11} MeV to 20 MeV, and photon and electron energy from 1 keV to 1000 MeV. The code also includes the capability of calculating the effective multiplication factor (k_{eff}) for a system containing fissile material. In the current simulation, the neutron-only mode will be considered.

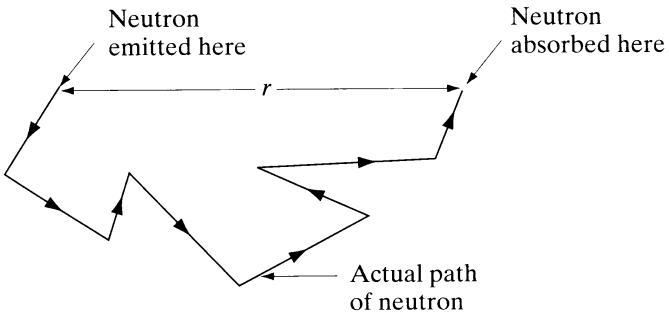

Figure 7.1: Trajectory of a neutron diffusing in a medium.

7.2.2 General instructions for preparing MCNP input

The execution of the code involves the creation of an input, which contains the following information:

1. Complete geometry specification of the problem,
2. Description of materials and the corresponding data set,
3. Definition of a neutron source,
4. Desired answers using appropriate tallies,
5. A variance reduction technique for efficient running of the problem (but this is beyond the scope of this lab).

The input deck starts with a title of the problem in a single line. Lines starting with 'c' in the first column are considered as comment and discarded by MCNP. The input-deck for MCNP can then be divided into three main blocks.

Cell instructions (several cells are required to define the whole geometry)
Blank line (to indicate that all the cells have been defined)
Surface instructions (one or more surfaces are required to describe a cell)
Blank line (to indicate that all the surfaces have been defined)
Data instructions (include instructions for cross-sections, mode, nps, sdef, tally and interactive plot)

The format of the MCNP input-deck is very strict and the blank lines (number and locations should be carefully checked). The error messages are self-explanatory unless something went wrong with the blank lines. The contents of each block are described as follows:

Block-I: Cell Instruction

The format for cell definition is:

	1	1	-1.0	2	-3	imp:n=1
				.....		
Entry	1	2	3	4		5

1 = cell number,
2 = material number,
3 = material density (in g/cm^3 if the sign is negative, or as number density x 10^{-24} if the sign is positive)
4 = a set of surfaces defining the geometry (e.g. if 2 and 3 stand for spheres of smaller and larger radius, then the above combination means the region within spheres 2 and 3),
5 = Importance of this cell volume is 1, for neutron transport.

Note: if 2^{nd} entry is zero, it is considered as a void region and the code does not consider any interaction in that cell. If the outermost region is defined as void or a region with imp:n=0, then the particle entering this region is considered lost and a new history must be selected.

Block-II: Surface instructions

For definition of different surfaces, see Table 3.1 on page 3-14 of the short extract of the MCNP manual [11].

	so	100
Entry	1	2

1 = denotes sphere centred around the origin (0.0 0.0 0.0),
2 = radius of the sphere

Block-III: Data instructions

a) Cross-section data specifications:

	m1	1001.60c	2	8016.60c	1
Entry	1	2	3	4	5

1 = material identification number,
2 = the general form is ZZZAAA.nnx, where Z, A, nn and X denote the charge number, mass number, data file identification and class of data, respectively. For example, 60c denotes ENDFB-VI data and C stands for continuous data,
3 = no. of hydrogen atoms per molecule of water,
4 and 5 = same as items 2 and 3 for oxygen

Note: It is important to include the S(α , β) thermal scattering instruction for moderators (see

page 2-53 of the MCNP manual [10]). For example, for water and graphite, this is denoted by lwtr.01t and grph.01t, respectively.

b) Mode:

mode n (specifies particle type for transport, neutron in this case)

c) nps 2E+5 (specifies limit for the termination of neutron histories)

d) SDEF instructions: These specify how the neutron source is to be defined. The following two examples would provide two different specifications:

sdef pos=0. 0. 0. Erg=0.025E-6 par=1 wgt=1 (for a fixed energy)
sdef pos=0. 0. 0. Erg=D1 par=1 wgt=1 (for energy distribution D1)

e) Tally specifications: The various parameters of interest are finally calculated via a so-called *tally*, or a tally in conjunction with an appropriate multiplier instruction. Thus, for example, the following instructions are used in the current studies:

F4:n 21 22 23 24 ..... provides average neutron fluxes in cells
F14:n 21 22 23 24 ..... provides average neutron absorption in cells
FM14:n (0.0883 1 -2) (arguments are material number density, material No. and ID for total absorption reaction, respectively)

7.2.3 General instructions for running MCNP

An executable resident on a Linux machine will be used for the simulations. Its location will be in the PATH variable of the Linux machine used during the lab. In order to run/plot a MCNP input, the following commands are needed:

mcnp i=*input_name*
runs neutron transport calculations using the file called *input_name* as input. It will provide a generic output file as *input_name.o* and a metafile *input_name.m* containing the tally information.

mcnp i=*input_name ip*
will open a GUI which allows checking the problem's geometry (errors are highlighted in red).

nano file_name displays the contents of the "file_name" for editing.

7.3 Neutron diffusion in homogeneous medium

The general steady-state diffusion equation in a multiplying or a non-multiplying medium is given by:

$$D\nabla^2\phi(r) - \Sigma_a\phi(r) + S = 0 \tag{7.1}$$

The source term S describes the fission term or an independent source, which does not depend upon the neutron flux. In the present (simulated) experiment, we consider the diffusion of neutrons from a point source placed at the centre of an infinite non-multiplying medium. In the entire medium, except at the centre, the source term S is zero, and the corresponding steady-state equation can be rewritten as:

$$D\nabla^2\phi(r) - \Sigma_a\phi(r) = 0 \tag{7.2}$$

For a point source in an infinite medium, spherical symmetry can be assumed. If the source is placed at the origin of the spherical coordinate system, the source -free diffusion equation can be written as:

$$\frac{d^2\phi(r)}{dr^2} + \frac{2}{r}\frac{d\phi(r)}{dr} - \frac{1}{L^2}\phi(r) = 0 \tag{7.3}$$

The general solution of Eq. 7.3, for the condition that the neutron flux is finite everywhere except at the origin, is given by:

$$\phi(r) = S\frac{e^{-r/L}}{4\pi Dr} \tag{7.4}$$

where L and D denote the diffusion length and the diffusion coefficient, respectively. Thus, the neutron absorption rate dA (or the number of neutrons that are absorbed per second), at a distance between r and r+dr from the source, is given by Equation 7.5 where $L^2 = D/\Sigma_a$:

$$dA = \Sigma_a\phi(r)dV = \Sigma S\frac{e^{-r/L}}{4\pi Dr}4\pi r^2 dr = \frac{S}{L^2}re^{-r/L}dr \tag{7.5}$$

It follows that the probability of neutron absorption per second between r and r+dr is given by:

$$p(r)dr = \frac{1}{L^2}re^{-r/L} \tag{7.6}$$

Therefore, the average of the square of the distance from the source to the location where a neutron is absorbed can be calculated from Equation 7.7:

$$r^2 = \int_0^\infty r^2 p(r) dr = \frac{1}{L^2} \int_0^\infty r^3 e^{-r/L} dr = 6L^2 \tag{7.7}$$

Eq. 7.7 states that the square of the diffusion length, L^2, is equal to one-sixth the average of the square of the crow-flight distance that a neutron travels from the starting point to where it is finally absorbed (see Fig. 7.1). It follows that the greater the value of L, the further neutrons move away from the source before getting absorbed, i.e. the more diffusive and less absorptive the medium is.

From Eq. 7.4, it is evident that in a hypothetical experiment, with a purely thermal neutron source at the centre of a large moderator tank (leakage being small), the spatial distribution of the response of a thermal activation detector (or an ionisation chamber employing a target sensitive to thermal neutrons) would be proportional to the corresponding thermal neutron flux and hence can be expressed by:

$$D_{res}(r) = K \frac{e^{-\frac{r}{L}}}{r} \tag{7.8}$$

or

$$ln(D_{res}(r)r) = ln(K) - \frac{r}{L} \tag{7.9}$$

It is evident from Equation 7.4 and 7.8 that, if the natural logarithm of the neutron flux (or detector response) multiplied by r, is plotted against r, then the negative slope of these distributions will give $1/L$. It would be a simple measurement but, in practice, it is not feasible to get a point thermal-neutron source. However, one can easily simulate such an experiment using the Monte Carlo method. Thereby, both neutron-flux and detector-response distributions can be determined from the simulation of neutron transport in a given medium and then, employing either Eq. 7.4 and 7.8, the diffusion length can be obtained.

Furthermore, if the average macroscopic neutron absorption is determined separately from the Monte Carlo calculation using an absorption tally, then the diffusion coefficient can be obtained from the definition of L^2. Alternately, the diffusion coefficient can be determined independently of L^2 as shown in Equation 7.10 and 7.11:

$$ln(\phi(r)r) = ln(S \frac{e^{-r/L}}{4\pi D}) \tag{7.10}$$

or

$$ln(\phi(r)r) = ln(\frac{S}{4\pi D}) - \frac{r}{L} \tag{7.11}$$

With the neutron flux from the Monte Carlo simulation usually being expressed per source neutron, the value of S will be unity. Thus, the intercept of the $ln(\phi(r).r)-$vs.$-r$ line (see Eq. 7.11) would yield the diffusion coefficient.

7.4 Experiment description

The goal of this "experiment" is to model the propagation of thermal neutrons through a sphere of water and graphite. The following "experimental" determinations will be carried out:

Exp. 7.1: Diffusion length
Exp. 7.2: Macroscopic absorption cross-section
Exp. 7.3: Diffusion coefficient from diffusion length
Exp. 7.4: Diffusion coefficient from flux distribution

7.4.1 Important precautions

The following precautions need to be followed at all times to ensure the safety of the experimenters and the equipment and to create high quality results.

1. The size of the moderator geometry must be chosen with care, such that the neutrons leaking out of the assembly do not significantly affect the shape of the neutron distribution.

2. For the various flux and detector response distributions, the number of neutron histories should be chosen such that the corresponding 1σ error is below 1%, especially for the regions in which the exponential fitting has to be carried out.

3. Preferably, volume tallies should be selected for simulation, in order to have better flux and detector response values.

7.5 Settings

For the simulation, the moderator materials considered are water and graphite, each in spherical geometry. A point neutron source is placed at the centre of the system with a thermal Maxwellian energy distribution corresponding to 20°C, emitting neutrons isotropically. In order to have an efficient tallying of the neutron flux/absorption rate at several locations at the same time, F4/F14 tallies with 44 concentric spherical volumes, each having a thickness of 1 cm for water and 3 cm for graphite are placed starting from the centre. The concentric volumes used for flux and response tallies are presented in Fig. 7.2.

The F4 tally will be employed directly to determine the neutron flux distribution at different

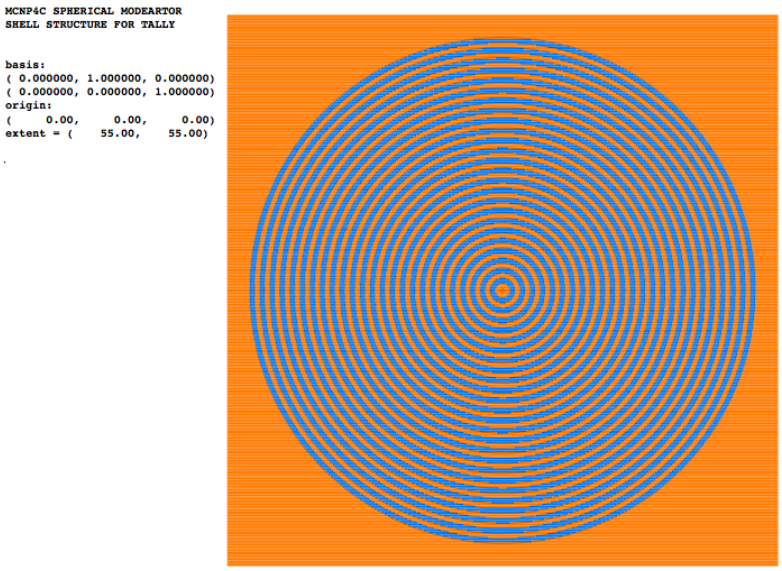

Figure 7.2: Concentric shells for neutron flux and detector response calculations.

positions. Similarly, the net absorption in each moderator shell would be determined separately by using the F14 tally along with an FM card specifying the proper number density and absorption cross-section identifier of each moderator type. The average macroscopic absorption cross-section can then be determined from its basic definition by dividing the net absorption by the corresponding integral flux in the various shells.

An incomplete input model for water will be provided and modified. Then it will be employed as the basis for implementing the input needed for the simulation with graphite as moderator.

7.6 Measurement steps

1. Become familiar with the Monte Carlo input/output and operation by modelling two concentric spheres of radii 10 and 50cm. The region between both spheres is filled up with water at room temperature. Assume a monenergetic point source (1eV) at the sphere centre and compute for flux and absorption cross section in the water. Report on the effect of the number of considered neutrons (or histories) on the flux and cross sections.

2. Open the incomplete Monte Carlo input for water moderator.

3. Make sure that the tallies correspond to each of the defined shell volumes.

4. Incorporate the integral flux tally for all the radial positions.

5. Incorporate the total absorption tally for all the radial positions.
6. Perform neutron transport calculations to get statistical errors on neutron flux, as well as detector response, below 1% in the region of interest.
7. Set up a similar spherical model for graphite of appropriate dimensions (depending upon its material properties) and carry out the corresponding simulations.
8. Extract the relevant data from the MCNP output for further processing.
9. Plot *ln(flux.r)*-vs.-*r* to determine the diffusion length.
10. Determine the average macroscopic absorption cross-section for each moderator, from the average neutron fluxes and the net neutron absorption values in the tally regions.
11. Determine the diffusion coefficient for each different moderator by using the corresponding values of diffusion length and average macroscopic absorption cross-section.
12. Determine the diffusion coefficient from the intercept of the flux distribution obtained under item 9.

7.7 Data analysis

For information, typical reported values for diffusion length and other parameters are summarized in Table 7.1 for the two moderators considered.

Table 7.1: Thermal neutron diffusion parameters of common moderators at 20°C [5, 6]

Moderator	Density (g/cm^3)	$\overline{D}$ (cm)	$\overline{\Sigma_a}$ (cm^{-1})	Diffusion length L (cm)
H_2O	1.0	0.16	1.97E-2	2.65
Graphite	1.60	0.84	2.40E-4	59

7.8 Expected results

1. Report on the different neutron behaviour diffusing in water and graphite.
2. Identification of the principal sources of errors for the simulated diffusion length.
3. A short note on the important conclusions.

8 Approach to critical

8.1 Introduction

In order to understand the process of achieving a critical configuration with a reactor, it is important to define basic terms such as the start-up neutron source, the subcritical multiplication, the effective multiplication factor and the reactivity.

In a nuclear reactor, apart from the neutron production via fission reactions, neutrons are also produced as a result of certain other nuclear reactions and these are usually referred to as source neutrons. These neutrons provide useful information during shutdown and start-up sequences, using neutron-sensitive monitors placed in and around the reactor. Since changes in the neutron population reflect on the state of the reactor, it is important to verify that there is sufficient neutron flux (also when the reactor is shutdown), which can be detected by an appropriate choice of neutron detectors. The source neutrons needed for the purpose can be “intrinsic” and/or “external”. A brief introduction is given below about the nature of such sources.

8.2 Theory

8.2.1 Intrinsic neutron source

Several heavy nuclides present in the reactor undergo spontaneous fission leading to the release of neutrons. A list of isotopes along with their specific neutron yields is given in Table 8.1.

Also, some of the heavier isotopes of uranium and plutonium emit alpha particles and, when boron is present in the fuel, these can interact with ^{11}B (80.1% of natural boron) to produce neutrons from the following reaction:

$$^{11}_{5}\mathrm{B} + ^{4}_{2}\mathrm{He} \rightarrow ^{14}_{7}\mathrm{N} + ^{1}_{0}\mathrm{n} \tag{8.1}$$

Table 8.1: Spontaneous fission neutron sources.

Nuclide	Half-life of spontaneous fission source[years]	Decay constant[s^{-1}]	Neutron production[n/s/g]
^{232}Th	1.00E+18	2.196E-26	1.20E-04
^{233}U	1.00E+15	2.196E-23	1.25E-01
^{235}U	1.80E+17	1.22E-25	7.57E-04
^{238}U	8.00E+15	2.75E-24	1.86E-02
^{239}Pu	5.50E+15	3.99E-24	3.21E-02
^{240}Pu	1.20E+11	1.83E-19	1.47E+03
^{252}Cf	66	3.33E-10	3.02E+12

Neutrons may also be produced by the following gamma interaction with deuterium.

$$^{2}_{1}\mathrm{H} + \gamma \rightarrow {}^{1}_{1}\mathrm{H} + {}^{1}_{0}\mathrm{n} \tag{8.2}$$

There are abundant high energy photons that are produced from the fission products, and their intensity is governed by the operating power level and the duration of the reactor operation. The atom % of deuterium in the water ranges from 0.015% for a light water reactor to 99.8% for a heavy water reactor. Since the neutron emission is essentially due to the production of gamma rays, the source strength for such a source depends on the operational and shutdown history of the reactor.

8.2.2 External neutron source

Since the neutron source strength due to intrinsic sources is quite small in low-power reactors, it becomes essential to use an external neutron source to bring the reactor to critical in a reasonable period of time. All experimental reactors have provision for introduction of an external neutron source into the reactor, with the sole objective of being able to quantify the shutdown levels properly with the help of neutron-sensitive monitors. The external neutron source is usually withdrawn back into its containment outside the reactor, once criticality has been achieved.

Among the standard external sources, ^{252}Cf (spontaneous-fission source) is an important one. It emits about 3.0E+12 n/sec per gram of the nuclide. However, it is quite expensive and also has certain other drawbacks, viz. a relatively short half-life and the emission of high energy gamma radiation. Several commercial neutron sources are based on the (α, n) reaction with beryllium as given in Equation 8.3:

$$^{9}_{4}\mathrm{Be} + {}^{4}_{2}\mathrm{He} \rightarrow {}^{12}_{6}\mathrm{C} + {}^{1}_{0}\mathrm{n} \tag{8.3}$$

These sources consist of metallic beryllium uniformly mixed with alpha emitter such as ^{210}Po, ^{226}Ra, ^{238}Pu and ^{241}Am. Another commonly available neutron source is based on the (γ, n) reaction given in Equation 8.4.

$$^{9}_{4}\mathrm{Be} + \gamma \rightarrow {}^{8}_{4}\mathrm{Be} + {}^{1}_{0}\mathrm{n} \tag{8.4}$$

The gamma radiation is usually obtained from a radioisotope such as ^{124}Sb (which can be produced in a reactor from neutron capture in ^{123}Sb). Unlike sources based on (α, n) reaction, photon-based sources do not need to be uniformly mixed. In fact, some designs employ a gamma source contained in a capsule, which is surrounded by a sleeve of beryllium.

8.2.3 Subcritical multiplication

When a neutron source is placed in a block of moderating material such as graphite, there will be a steady-state neutron flux (or density) distribution, which will depend upon the strength of the neutron source, the absorption of neutrons in the graphite and the neutron leakage. When a fissile material is added to the moderator, there will be an increase in the neutron flux at any given point in the assembly. This will depend upon the kind and amount of fissile material added, as also the geometrical arrangement used for the materials.

The multiplication M, of a subcritical fissile assembly of the above type, is defined as the ratio between the thermal neutron flux due to both the primary source and fission, and that due to the primary source alone. If a neutron detector placed in the assembly is assumed to measure, in the presence of a neutron source, a count rate (*cps*) proportional to the neutron flux, then the neutron multiplication M of the system is given by:

$$M = \frac{\textbf{cps with fuel}}{\textbf{cps without fuel}} = \frac{I_{wf}}{/\,I_{nf}} \tag{8.5}$$

where I_{wf} and I_{nf} denote neutron flux (or detector response) with and without the fissile material, respectively.

8.2.4 Effective multiplication factor

In reactor experiments, the spatial and energy distributions of greatest significance are those characteristics of the critical reactor, in which the effective multiplication factor, k or k_{eff} (defined as the ratio of the number of neutrons in one generation to that in the preceding generation), is unity.

In the case of a subcritical assembly with a neutron source, the distributions are more complex. However, in any case, the subcritical multiplication M can be related to the assembly's k value,

which is less than 1. Thus, S source neutrons result in kS, k^2S, k^3S ... neutrons in the 1^{st}, 2^{nd}, 3^{rd} ... generations, respectively. Hence, the M value for the assembly is given by Equation 8.6:

$$M = \frac{S(1 + k + k^2 + k^3 + k^4...)}{S} = \frac{1}{1-k} \tag{8.6}$$

There are certain practical difficulties to obtain an accurate value of k from a multiplication experiment, e.g. difficulties in distributing the source in the "normal mode" and in measuring the neutron count rates throughout the assembly, particularly when the measurements are required for a series of subcritical states.

Instead, one adopts an empirical approach, the count rate, $C_{wf}(k)$ of a neutron detector placed in or near the assembly being taken as a relative measure of the neutron population and being determined as a function of the corresponding k value. The multiplication M, as observed by such a detector, is then given by Equation 8.7:

$$M = \frac{C_{wf}(k)}{C_{nf}} \tag{8.7}$$

where C_{wf} and C_{nf} correspond to the count rates with and without the fissile material, respectively.

8.2.5 Reactivity

For completeness, one needs to recall that the concept of a critical configuration can also be defined in terms of reactivity (ρ), defined by Equation 8.8:

$$\rho = \frac{\delta k}{k_{eff}} = \frac{k_{eff} - 1}{k_{eff}} \tag{8.8}$$

Clearly, the reactivity is zero for a critical reactor, negative for a subcritical assembly and positive for a supercritical reactor. It is common to express reactivity in pcm units (1 pcm = 10^{-5}). For example, the maximum possible positive reactivity in CROCUS is +200 pcm, i.e. ρ = 0.002.

8.2.6 Approach-to-critical experiment

As indicated earlier, there are certain difficulties in relating M_{obs} to the true subcritical multiplication M. These arise from the sensitivity of the spatial and energy distributions of the neutron flux to k_{eff}, source location and assembly geometry. This means that the observed multiplication will depend on the position of the detector, its energy response and details of

the experimental conditions. It is known, however, that for approximately $k > 0.95$ and depending on the system, the neutron spectrum remains nearly constant and the flux increases almost proportionately throughout the reactor as k is increased.

Despite its drawbacks as a method to measure k, the multiplication experiment is performed routinely in the context of the safe loading, or "approach to critical", of any given multiplying assembly being brought to critical for the first time. Usually, an approach to critical is achieved by loading fuel material in small steps. It is, however, possible to demonstrate the basic principles by increasing the k-value of a subcritical reactor in relation to a change in the moderator level or the withdrawal of a control rod. In an approach-to-critical experiment, the basic relations employed are those of Equations 8.6 and 8.7 formulated into Equation 8.9:

$$M_{obs} = \frac{C_{wf}(k)}{C_{nf}} = \frac{1}{1-k} \tag{8.9}$$

From the definition of k, it is evident that, for $k < 1$, the number of fissions, and hence neutron flux decreases from one generation to the next, the chain reaction being subcritical. In an approach-to-critical experiment, i.e. for achieving $k = 1$, the value of k needs to be changed slowly from a low value, while tracking the response of the detector which is proportional to the factor M_{obs} of Eq. 8.9. By plotting $1/M_{obs}$, or $1/C_{wf}(k)$ (C_{nf} being constant), against the amount of fuel loaded and extrapolating the value to achieve the loading corresponding to $1/M_{obs} = 1/C_{wf}(k) = 0$, one gets the critical configuration. Clearly, as mentioned, one may be employing a different means of varying k, such as change in moderator level or control rod position. The basic procedural steps, however, are similar

An approach-to-critical experiment needs to be done extremely carefully, ensuring that, under any circumstances, criticality is not reached inadvertently. Such a situation could possibly arise because the slope of the plots obtained during an approach-to-critical experiment can have different shapes depending upon the choice of the location of the detector. As illustration, representative results are discussed for an Argonaut multiplication assembly, a cut-away view of which is shown in Fig. 8.1.

Figure 8.2 shows the results of a representative approach-to-critical experiment, carried out using BF_3 detectors, the inverse count rates having being plotted for three different BF_3 detector positions. While an ideal curve would be a linear one, it can be seen that plot No. 1 & 3 are particularly "dangerous" for extrapolating to the critical mass unless one has carried out measurements with small loading steps till at least about 1.5 kg of U^{235} (in this particular example). Plot No. 2, which reflects the neutron flux at a location closer to the fissile material, in comparison to the other locations, gives a significantly better description for extrapolation from a loading onwards of about 1.0 kg U^{235}.

A typical, "well-behaved" inverse-counts plot is shown in Fig. 8.3, the prediction of the critical loading here being seen to be relatively reliable, although small-step measurements, even in

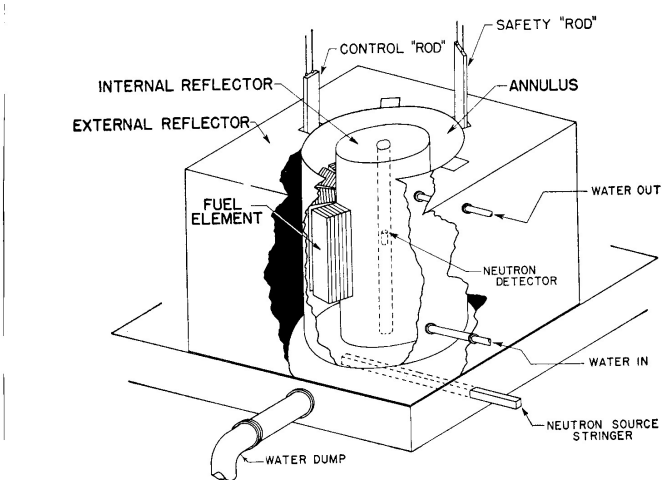

Figure 8.1: Schematic view of the Argonaut multiplication assembly.

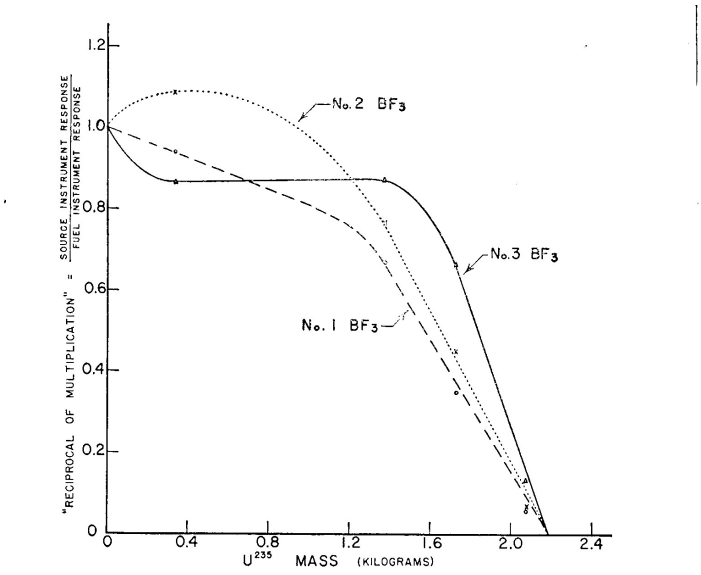

Figure 8.2: An approach-to-critical experiment with the Argonaut multiplication assembly using BF3 detectors; 1) detector located at top of the central hole; 2) detector outside the reflector on the fuel side; 3) detector about 120 cm above the central hole.

this case, remain essential till quite near to the end. An often used prescription for calculating the next ”loading step” during an approach to critical is to implement no more than about one-third of the increment predicted (to zero inverse counts) at any given stage [12].

When a nuclear reactor is built, one needs more than just the critical mass of fissile material. For a power reactor, the excess reactivity is required to compensate for burnup effects and ensure a certain cycle length of steady-state operation for the loaded fuel. Even in the case of a zero-power reactor such as CROCUS, some slight excess reactivity is needed in order to be able to increase the neutron flux, i.e. establish different low-power values. In all case, the

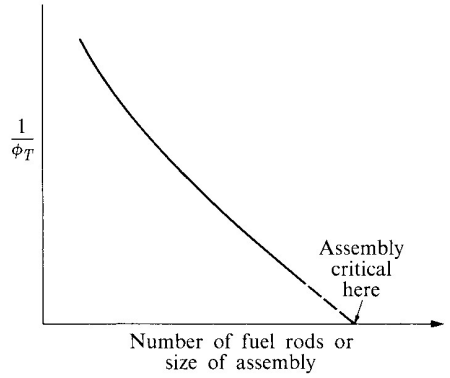

Figure 8.3: A "well-behaved" inverse counts plot during an approach-to-critical experiment.

excess reactivity has to be compensated, and this is usually done by introducing absorbing material in the form of control or regulating rods.

8.3 Experiment description

In the CROCUS facility (see Appendix C giving a description), there are two types of approach-to-critical experiments which are possible. The increase of the moderator (water) level, without any use of the control rods, is clearly one possible means of varying the k_{eff} value. The other possibility is to have, at the start of the experiment, at least one of the control rods fully inserted and the moderator level at a specific height. The k_{eff} variation of the reactor can then be carried out in terms of small-step withdrawals of the inserted control rod, in order to extrapolate to zero inverse-counts for the critical control-rod position.

In the present context, the approach to critical for CROCUS reactor will be carried out by varying the water level.

8.3.1 Important Precautions

The following precautions need to be followed at all times to ensure the safety of the experimenters and the equipment and to create high quality results.

1. Each intended change in reactivity should be carefully evaluated and communicated to the reactor operator.
2. The change in water level is to be carried out only by the reactor operator.
3. Following a water level change, sufficient time (about 10 minutes) should be allowed for the flux to stabilize, before carrying out the data acquisition.
4. The inverse-counts-vs.-water-level plot should be acquired "on-line", in order to properly

assess the next increment in water level.

8.4 Required setup

In addition to the zero-power CROCUS reactor itself, a fission chamber and an ionization chamber, constituting part of the reactor safety chain and having fixed preamplifier and amplifier settings, will be used to perform the approach-to-critical experiment.

8.5 Operational settings

1. Fission chamber

Tennelec counter and timer model is used with the following settings:

- Multiplier =0.01 sec or 0.01 min
- Discriminator=0.2
- Time of counting can be selected using the jumpers N and M.

The fission chamber can also be connected to a Multichannel Scale Counter (MCS) connected to a PC in the control room allowing to record the counts as a function of the time.

2. Ionization chamber

Ionization current can be read directly from the display; the scale is changed automatically between 10E-10 and 10E-4 A.

8.6 Measurement steps

1. Switch on the power supplies of all the associated electronic units and verify the specified settings. Switch on the PC, if needed, for data processing or for using the MCS acquisition system connected to the fission chamber.
2. Make sure that the CROCUS reactor has an initial water level such that the configuration is subcritical (k_{eff} ~0.96); this is done by the reactor operator.
3. Make sure the start-up Pu(α, n)Be neutron source is under the core before starting the measurements.
4. Switch on the data acquisition for the fission chambers for a definite period of time. For a given measurement point, the data acquisition is initiated after a waiting time of ~10 min following the change in water level (to ensure stabilization of the delayed neutron

precursors). It is necessary to have sufficient counting statistics for each measurement point (assuming a Poisson distribution). A compromise between accuracy and measurement duration has to be found. Several series of measurements can also be used. Read the ionization current directly on the instrument.

5. Increase the water level in steps of ~10 mm and repeat the above measurements.
6. Finally, verify that the reactor is critical assuming the predicted water level. Consider the need of the source at that instant.

8.7 Data analysis

1. The initial water-level height for starting the experiment is 900 mm.
2. The water-level increment in height is 10 mm in the first step.
3. Reactivity per mm change in the water level is about 4 pcm.
4. Physical locations and specifications of the fission and ionization chambers are given below:

Table 8.2: Information for data processing

Description	Ionisation chamber	Fission chamber
Location from core centre (X,Y,Z), [cm]	8.6/-36.5/35.5	35.8/8.7/19.7
Active deposit / [wt%]	B^{10} / 92%	U^{235} / 93%
External Ø of inner electrode, [mm]	25	28
External Ø of outer electrode, [mm]	36	31
Active length, [cm]	35.5	9.4

8.8 Expected results

1. Plot a graph of the water level vs. the inverse counts of each detector.
2. Find the water level corresponding to the critical height by suitably extrapolating the inverse-counts-vs.-water-level plot to zero value.
3. Qualitative explanation of the behaviour of the inverse-counts plots and assessment of the suitability of each detector and its location for realistic prediction of the critical height.
4. Identification of the sources of error.
5. A short note with the important conclusions.

9 Neutron Noise

In this experiment, we will measure the prompt neutron decay constant α in the CROCUS reactor using the so-called neutron noise method. We first introduce some fundamental aspects of reactor kinetics and then discuss the neutron noise techniques. The concepts are then applied to an experiment. The CROCUS experimental reactor is made critical, and the statistical distribution of the neutron population in the reactor is characterized using Frequency domain analysis of a combined counting signal from a detector array. From this, important parameters of the reactor such as the decay constant are inferred.

9.1 Introduction

The goal of this experiment is to gain insight into the statistical distribution of signals measured in reactor physics and to learn how to use them to determine some kinetic properties of a nuclear reactor.

9.2 Reactivity and reactor kinetics

Safety and good operation of a reactor require knowing and controlling the average time behavior of the neutron population. The neutrons' time behavior is predicted using reactor kinetics equations. These equations express the neutron population as a function of the neutronic and thermal-hydraulic parameters characteristic of the reactor. Among these parameters, the reactivity ρ, which is the ratio of average neutron production to neutron absorption plus leakage, plays a central role in reactor control.

In a zero-power reactor, thermal effects are negligible because of the low power. The time dependence of the neutron population is typically described by the so-called point kinetics equations – a set of coupled differential equations derived from the time-dependent Boltzmann transport equations and several assumptions. Some of the assumptions are, for example, a point-like and therefore homogeneous space (thus the name), isotropic scatter and fission,

and others that are similar to those used to derive the diffusion equation. The equations for the neutron population $n(t)$ and i precursor populations c_i (usually grouped arbitrarily into 6 groups):

$$\frac{dn(t)}{dt} = \left(\rho(t) - \beta_{\text{eff}}\right)/\Lambda n(t) + \sum_i \lambda_i c_i + S$$

$$\frac{dc_i(t)}{dt} = \beta_i/\Lambda n(t) - \lambda_i c_i \quad \text{for } i = 1,\ldots,6$$

The solution for the time-dependent neutron population behavior $n(t)$ is, as for any linear time-invariant system, a sum of exponential terms $N(t) = \sum_j A_j e^{\omega_j t}$ whose ω_j are solutions of the characteristic equation of the system, in nuclear engineering also called the "in-hour equation":

$$\rho = \Lambda\omega + \sum_i \frac{\beta_i \omega}{\omega + \lambda_i}$$

The time behavior of the reactor, therefore, depends on:

- The reactivity ρ
- The generation time Λ, which is the average time between the birth of a neutron and a fission event it may cause
- The delayed neutrons which are usually gathered in six groups "i" and characterized by their delayed neutron fractions β_i and decay constants λ_i, and the effective total delayed neutron fraction β_{eff}
- The so-called the prompt neutron decay constant, the coefficient in front of the neutron population $(\rho - \beta_{\text{eff}})/\Lambda = \alpha$

These quantities are also referred to as the kinetic parameters of a reactor, as they fully define the time-dependent behavior in the absence of thermal feedback.

As illustrated above, the determination of ρ, $\beta = \sum \beta_i$, and Λ is of critical importance for reactor design and ultimately safety. The parameters can be inferred experimentally by inducing a transient in the reactor (e.g., moving an absorber rod) and recording the evolution of the neutron population. Such dynamic experiments, however, require active perturbation of the reactor. Another method, called the noise method, consists of measuring the microscopic fluctuations of the neutron population in a macroscopically stable reactor. This method is far less intrusive and is the subject of this experiment.

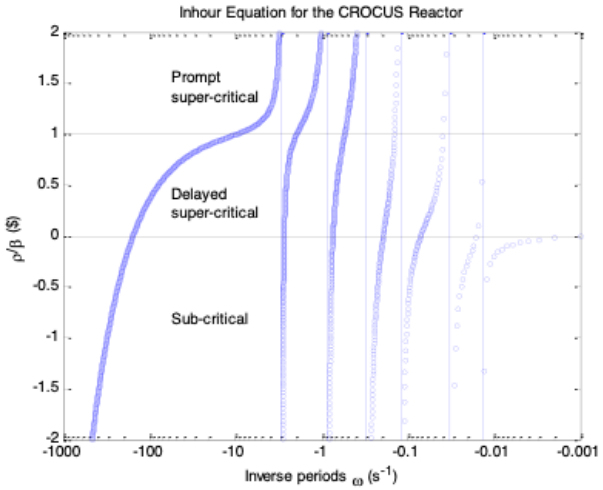

Figure 9.1: Plot of the In-hour equation to quantify the decay constants of the neutron population following the insertion of a reactivity ρ.

Noise measurements in a nuclear reactor

Noise commonly refers to the phenomenon of the temporal fluctuation of a given measure around its mean value. The measurement and investigation of said noise are called noise analysis. In a stationary reactor, the power P predicted by a deterministic calculation is a scalar:

$$P_0 = \sum_f \Phi E_f V$$

with the inputs of macroscopic fission cross-section Σ_f and the reactor volume V convoluted with the calculated flux Φ and the energy released per fission E_f. A measurement, however, will reveal a non-static noisy behavior. A noisy measurement in physics often refers to an observation where the true expected physical response is concealed by random fluctuations. Noise as a kinetics measurement method thus has to deal with the dichotomy of containing both useful and unwanted noise. The origin of noise in a detector's signal can be of the following kind (non-exhaustive list):

- Thermal noise caused by random motion of particles at a certain temperature, described by the Nyquist formula.
- Pressure or temperature variations and the resulting mechanical vibrations.
- 1/f noise, or flicker noise, appearing mostly in direct current applications due to e.g. conductor impurities, usually following a normal distribution.
- Interference, i.e. the change or cancellation of a signal caused by other electronic

systems such as WiFi.

- Spontaneous processes, such as radioactive decay, that exhibit a natural fluctuation around the mean.

In radiation detection measurements, for example in the case of a single photon decay sample, the resulting fluctuations in radiation flux and thus detector signal originate from the constant independent decay probability of the isotope. If other noise sources can be neglected or are filtered out, the resulting time intervals between subsequent signals follow a Poisson distribution. Noise analysis allows here to predict the uncertainty of one measurement by assuming the underlying statistical model. Deviations from Poisson distributed values can then indicate added noise or correlation sources.

In a neutron-multiplying medium such as a nuclear reactor or a fissile sample, the measured statistical behavior is modified due to events generating several particles at the same time, such as (n,xn) reactions and fission (generating up to 10 neutrons). This altered statistical behavior can be exploited by means of noise analysis, yielding the kinetic parameters of a given system.

As an illustration, Fig. 2 shows a neutron fission chain in blue. The chain has fission (f), captures (c), and detection (d) events. The detection time is shown on the upper time scale. Using these times it is possible to plot a histogram of time differences between the detections. In this example, the time differences $T_b - T_a$, $T_c - T_a$, and $T_c - T_b$ would be added to a histogram. Extrapolating to a large amount of detections, we might intuit that the probability to detect neutrons from the same fission chain will decrease in time due to the certain probability of the chain dying out over time, and due to the overlap of random, other fission chains causing detections. This will, therefore, result in a histogram of exponential shape.

This method is the Rossi-α method and is often used in practice. The histogram of time difference is of the form:

$$f(T) = A + Be^{\alpha T}$$

where $\alpha = (\rho - \beta)/\Lambda$ is the prompt decay constant and T is the time difference between two detections.

This method, however, requires exact time stamping of each detected event and the calculation of memory-intensive time difference histograms.

Another way to characterize the statistical behavior of the detected neutrons is to plot the frequency behavior of the detector by taking the Fourier transform of the time series, for instance the current measured in a detector.

This method is the so-called Power Spectral Density (PSD) method, and its theoretical expres-

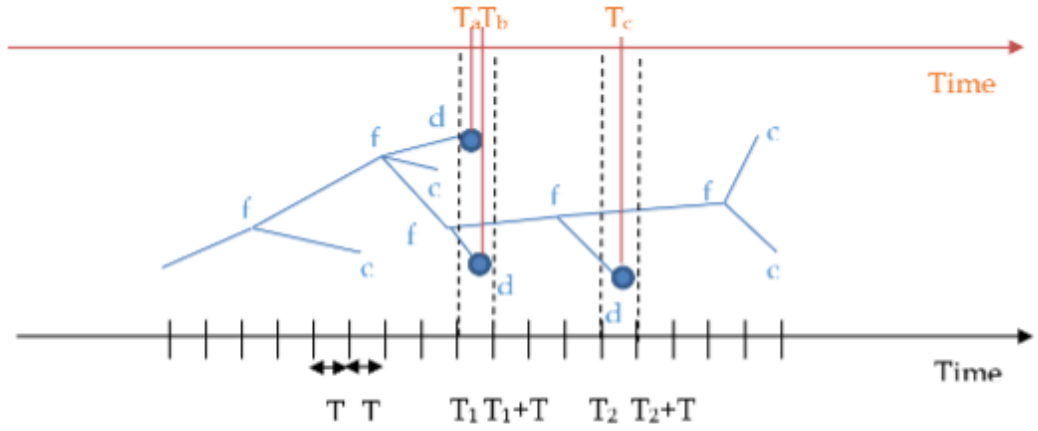

Figure 9.2: Example of neutron chains with fission, capture, and detection events.

sion for a single detector is the Fourier transform of the Rossi-α equation:

$$\mathrm{PSD}(f) = \int_{-\infty}^{\infty} e^{-i\omega T}\left(A + Be^{\alpha T}\right) dT = \frac{D}{1+(\omega/\alpha)^2} + C \quad (1)$$

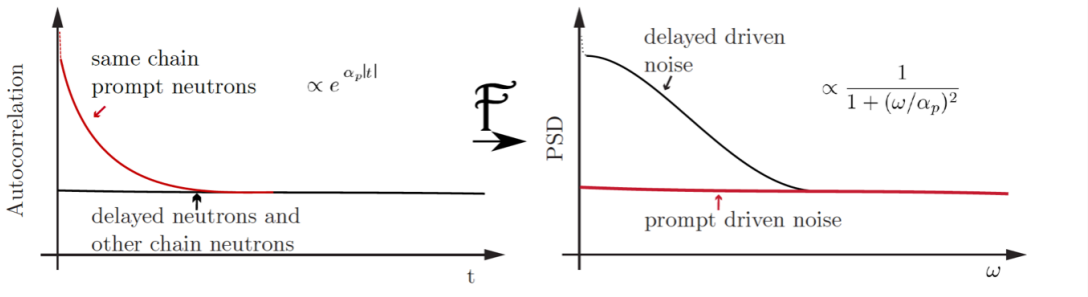

Figure 9.3: Illustration of the Rossi-α histogram vs. its Fourier transform – the power spectral density of the nuclear reactor. In the time domain, a prompt fission chain decays away with an exponential shape (with constant α), whilst in the frequency domain the shape is that of the Fourier transform of an exponential decay: A Lorentzian bell curve.

Experiment description

Characterize the statistical distribution of the neutrons in the reactor using the power spectral density and infer parameters of the reactor such as the decay constant $\alpha = (\rho - \beta)/\Lambda$.

Required setup

In the experiment, the CROCUS reactor is made critical with a power of 50 mW. The instrumentation consists of the SAFFRON detector array (see Figure 9.4). The detectors are connected to Silicon Photomultipliers (SiPM) inside a temperature controlled enclosure. The signals are then read into a PC that operates a set of CAEN digitizer baords that manage all 150 channels.

Measurement steps

Experiment in CROCUS

- Make CROCUS critical with a power of 50 mW without the start-up neutron source (assisted by the operator).
- Power up the instrumentation and set parameters according to the settings given in the previous section. The measurement will need to be conducted by the assistant.
- Test the detectors by observing the signal during start-up of the reactor using the oscilloscope.

Acquisition dry-run

- With a sample set of data provided by the assistant, check if all channels of SAFFRON are detecting neutrons.

Acquisition

- Once the reactor is stable, begin an acquisition for about 60 min.

Preparation of fit routines

- During the measurement, prepare the scripts (in Python on the PCs provided, or on your personal computer in the language you prefer) to calculate and fit the PSD or Rossi-alpha curves in order to derive the decay constant value α and its uncertainty.

Post-processing of the data

- When the acquisition is finished, copy the data onto any amount of computers that will attempt the fitting.
- Fit the data and observe the difference the fitting range has on the result. Do you need to fit all of the data (i.e., from 0 Hz to few kHz)? Or can we constrain it to a 'region of interest'?

The Monte Carlo reference for α with Serpent 2 and the JEFF 3.3 nuclear data library is $160.6\,s^{-1}$.

Things to consider

- How would the PSD curves change if the reactivity was lower (i.e., in sub-critical states)?
- Could you extract more characteristics of the reactor from the curves than just α assuming that you know the fission rate in the reactor?

References

1. M. M. R. Williams, *Random Processes in Nuclear Reactors*, Pergamon Press Oxford New York Toronto Sydney, 1974.
2. "Genie 2000 manual." *https://www3.nd.edu/ wzech/Genie 2000 Operations Manual.pdf*

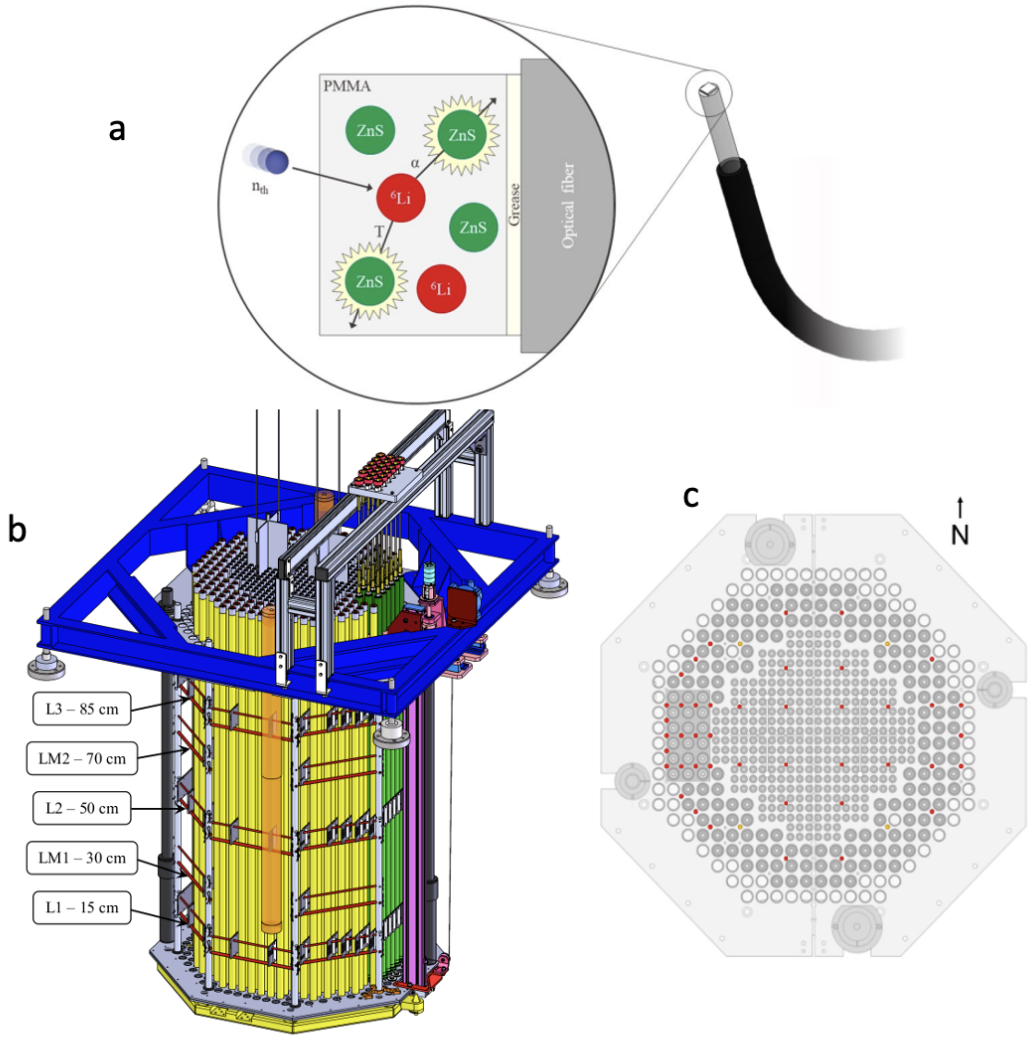

Figure 9.4: **a:** MiMi detector principle. The tip consists if a Li doped ZnS scintillator coupled to an optical fiber. The optical fiber carries the scintillation light to a SiPM detector outside of the reactor. **b:** The SAFFRON detector array. About 150 MiMi detectors are dispersed in the core on 5 main levels. **c:** The red dots along the core cross section indicate MiMi detector locations of the main floors L1, L2 and L3.

10 Neutron flux measurements in CROCUS

10.1 Introduction

An integral measurement of the neutron flux can be carried out either directly using a neutron detector such as a fission chamber or a BF3 counter, or indirectly by applying a foil activation technique. In the latter case, neutron capture (or another nuclear reaction) leads to activation of a specific irradiated sample and, following the irradiation, the resulting radionuclide's activity can be measured using a radiation detector. The induced activity is an integral parameter and depends upon the energy dependence of the neutron flux (i.e. on the neutron spectrum), as also of the given activation cross-section. Effectively, the activity measurement corresponds to the determination of an integral of the given neutron reaction rate over energy and the irradiation time.

Since neutron absorption cross-sections are usually higher at low energies, activation detectors are commonly employed for the measurement of slow neutrons. The neutron mean free path (average neutron interaction distance in a given medium) for such reactions is very small at low energies, so that the material thickness for activation studies needs to be small for avoiding any significant perturbation of the neutron flux at the given location, as well as the self-shielding effect within the sample itself. The most commonly employed types of activation detectors are thin foils or small-diameter wires. If several detectors are irradiated simultaneously, then there must be sufficient spacing between them in order to avoid shadowing effects, i.e. a reduction of the neutron flux incident on a given sample due the presence of other detectors.

Activation measurements can also provide useful information on the neutron energy spectrum. Thus, for example, at a given location in a fast reactor, one could use an appropriate set of threshold reactions (i.e. activation reactions with finite cross-sections only above a certain characteristic, minimal "threshold" value). By irradiating the corresponding activation detectors at the given location and measuring their activities, integral data are generated which, in turn, can be analyzed using a suitable "spectrum unfolding" algorithm.

This experiment introduces students to flux measurements using activation techniques. Stu-

dents will activate gold foils in CROCUS and measure the foils radioactivity to estimate the reactor's neutron flux.

10.2 Theory

10.2.1 Neutron activation

When a thin foil is irradiated in a constant neutron flux, the rate of formation of the new radioactive species, in its general form, is given by:

Formation rate = Production rate – Decay rate – Destruction rate by absorption

Mathematically, one may write Equation 10.1 where N_0, N_a, and λ denote the number of target atoms in the foil, the number of atoms of the radionuclide and its decay constant, respectively, while σ_a, σ_c and ϕ stand for the microscopic cross-section for the activation reaction, the neutron cross-section for absorption (usually capture) in the radionuclide and the average neutron flux over the foil surface, respectively. N_0 can be calculated from $N_A m/M$, where N_A, m and M represent Avogadro's Number, the mass of the foil and the molecular weight of the foil material. The upper energy integration limit represents the maximum energy E_m, beyond which the neutron flux is zero.

$$\frac{dN_a}{dt} = N_0 \int_0^E \sigma_a(E)\phi(E)dE - \lambda N_a - N_a \int_0^E \sigma_c(E)\phi(E)dE \tag{10.1}$$

To a first approximation, under low flux conditions, the last term is very small, and hence Equation 10.1 gets simplified to Equation 10.2, where R denotes the integral reaction rate in the foil leading to the formation of atoms of the radionuclide.

$$\frac{dN_a}{dt} = N_0 \int_0^E \sigma_a(E)\phi(E)dE - \lambda N_a = R - \lambda N_a \tag{10.2}$$

The solution of Equation 10.2, with the initial condition $N_a = 0$, at time $t = 0$, is given by Equation 10.3.

$$N_a(t) = \frac{R}{\lambda}(1 - e^{-\lambda t}) \tag{10.3}$$

The foil activity, defined as the number of disintegrations per unit time, thus builds up with time and approaches its asymptotic value (the so-called saturation value) for infinitely long irradiation duration. The induced activity for a time of irradiation t_0 can thus be written as Equation 10.4, where $A_s(= R)$ stands for saturation activity, i.e., the maximum activity that can be produced in a given sample for a given flux and activation reaction.

$$A(t_0) = \lambda N_a(t_0) = R(1 - e^{-\lambda t_0}) = A_s(1 - e^{-\lambda t_0}) \tag{10.4}$$

The build-up of activity as a function of time is shown in Figure 10.1.

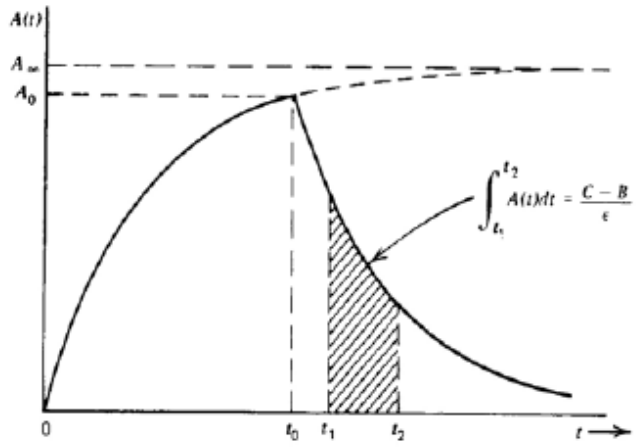

Figure 10.1: The build-up of activity during an irradiation of duration t0, followed by its decay; the shaded area indicates the total activity during a time of measurement between time t1 and t2.

In practice, one irradiates samples for a finite time to achieve a measurable activity, taking into consideration the decay time and the neutron flux [1]. The activity A_m, measured between time t_1 and t_2, of a sample irradiated for a duration t_0 (all times are considered from the start of the irradiation, $t = 0$) can be written as follows:

$$A_m = A_s(1 - e^{-\lambda t_0}) \int_{t_1}^{t_2} e^{-\lambda(t-t_0)} dt = \frac{A_s(1 - e^{-\lambda t_0})e^{\lambda t_0}(e^{-\lambda t_1} - e^{-\lambda t_2})}{\lambda} \tag{10.5}$$

Or

$$A_m = \frac{A_s(1 - e^{-\lambda t_0})e^{-\lambda(t_1-t_0)}(1 - e^{-\lambda(t_2-t_1)})}{\lambda} = \frac{A_s(1 - e^{-\lambda t_0})e^{-\lambda t_w}(1 - e^{-\lambda t_c})}{\lambda} \tag{10.6}$$

where t_w and t_c represent the waiting time between the end of the irradiation and the start of counting, and the counting duration, respectively.

In case the activity is measured using a gamma detector, and if C and B denote the total counts under the photo-peak and the corresponding background counts for the same time of measurement, then the saturation activity can be expressed as:

$$A_s = \frac{A_m \lambda}{(1-e^{-\lambda t_0})e^{\lambda t_0}(e^{-\lambda t_1} - e^{-\lambda t_2})} = \frac{(C-B)\lambda}{\epsilon_{de}\epsilon_{ep}\epsilon_{pm}(1-e^{-\lambda t_0})e^{\lambda t_w}(1-e^{-\lambda t_c})} \tag{10.7}$$

where ϵ_p , ϵ_{de} and ϵ_{pm} denote the photon emission probability of the radionuclide, the photo-peak efficiency of the detector and the photon non-absorption probability, respectively.

With measured values for C and B, and assuming the parameters ϵ_p , ϵ_{de} and ϵ_{pm} to be known, the saturation activity of the irradiated sample can be determined from Equation 10.7. Table 10.1 gives a list of commonly used activation detectors for slow neutrons.

Table 10.1: Materials used as slow neutron activation detectors.

Element	Isotope (Abundance in Percent)	Thermal Activation Microscopic Cross Section (in 10^{-28} m^2)	Induced Activity	Half-Life
Manganese	^{55}Mn (100)	13.2 ± 0.1	^{56}Mn	2.58 h
Cobalt	^{59}Co(100)	16.9 ± 1.5	^{60m}Co	10.4 min
		20.2 ± 1.9	^{60}Co	5.28 y
Copper	^{63}Cu(69.1)	4.41 ± 0.20	^{64}Cu	12.87 h
	^{65}Cu(30.9)	1.8 ± 0.4	^{66}Cu	5.14 min
Silver	^{107}Ag(51.35)	45 ± 4	^{108}Ag	2.3 min
	^{109}Ag(48.65)	3.2 ± 0.4	^{110m}Ag	253 d
Indium	^{113}In(4.23)	56 ± 12	^{114m_1}In	49 d
		2.0 ± 0.6	^{114}In	72 s
	^{115}In(95.77)	160 ± 2	^{116m_1}In	54.12 min
		42 ± 1	^{116}In	14.1 s
Dysprosium	^{164}Dy(28.18)	2000 ± 200	^{165m}Dy	1.3 min
		800 ± 100	^{165}Dy	140 min
Gold	^{197}Au (100)	98.5 ± 0.4	^{198}Au	2.695 d

In the case of a fast reactor, as mentioned in the introduction, activation measurements can provide useful information on the neutron energy spectrum, if one uses an appropriate set of threshold reactions (i.e. activation reactions with finite cross- sections only above a certain characteristic, minimal threshold value). Table 10.2 provides a list of such activation detectors, along with the corresponding threshold neutron-energy values.

10.2.2 Effective cross-section and integral flux

The present experiment involves the use of thin gold foils (100% ^{197}Au), as activation detectors, for measuring the neutron flux in the CROCUS reactor. In this case, apart from the thermal neutron capture in ^{197}Au (σ_c = 98 barn, at 0.025 eV), a significant activity results from the first capture resonance (σ_c = 3.0E+5 barn, at 1.9 eV). Thus, self-shielding effects due to the finite

Table 10.2: Materials used as threshold activation detectors.

Material	Reactions of Interest	Isotopic Abundance (at %)	Half-Life	γ Energy (MeV)	γ Abundance (%)	Threshold (MeV)
F	^{19}F(n, 2n)^{18}F	100.0	109.7 min	0.511^{+}	194°	11.6
Mg	^{24}Mg(n, p)^{24}Na	78.7	15.0 h	1.368	100	6.0
Al	^{27}Al(n, α)^{24}Na	100.0	15.0 h	1.368	100	4.9
Al	^{27}Al(n, p)^{27}Mg	100.0	9.46 min	0.84–1.01	100	3.8
Fe	^{56}Fe(n, p)^{56}Mn	91.7	2.56 h	0.84	99	4.9
Co	^{59}Co(n, α)^{56}Mn	100.0	2.56 h	0.84	99	5.2
Ni	^{58}Ni(n, 2n)^{57}Ni	67.9	36.0 h	1.37	86	13.0
Ni	^{58}Ni(n, p)^{58}Co	67.9	71.6 d	0.81	99	1.9
Cu	^{63}Cu(n, 2n)^{62}Cu	69.1	9.8 min	0.511^{+}	195°	11.9
Cu	^{65}Cu(n, 2n)^{64}Cu	30.9	12.7 h	0.511^{+}	37.8°	11.9
Zn	^{64}Zn(n, p)^{64}Cu	48.8	12.7 h	0.511^{+}	37.8°	2.0
In	^{115}In(n, n′)^{115m}In	95.7	4.50 h	0.335	48	0.5
I	^{127}I(n, 2n)^{126}I	100.0	13.0 d	0.667	33	9.3
Au	^{197}Au(n, 2n)^{196}Au	100.0	6.18 d	0.33–0.35	25–94	8.6
Li	^{7}Li(n, αn′)t	92.58	12.3 y	0–0.019$^{\times}$	100$^{\times}$	3.8

thickness of the Au foils used can be significant, and an appropriate effective cross-section for the ^{197}Au (n,γ) reaction needs to be estimated, in order that the corresponding integral flux value can be determined from a given measurement of the saturation activity of the produced radionuclide (^{198}Au).

In terms of energy dependent neutron flux and microscopic cross-section, the induced saturation activity per atom of an irradiated foil can be written as:

$$\frac{A_s}{N_0} = \int_0^{E_{max}} \phi(E)\sigma(E)dE = \frac{\int_0^{E_{max}} \phi(E)\sigma(E)dE}{\int_0^{E_{max}} \phi(E)dE} \int_0^{E_{max}} \phi(E)dE = \overline{\sigma_{av}} \int_0^{E_{max}} \phi(E)dE \qquad (10.8)$$

In the above equation, the left hand-side is an experimentally determined quantity, and one can determine either the integral flux, knowing the average cross-section over the neutron spectrum, or the average cross-section if the integral flux is provided. In the present case, an effective average cross-section for the ^{197}Au (n,γ) reaction has been estimated for the neutron energy spectrum at the measurement positions in CROCUS. This has been done via the BOXER code, modelling of the experimental situation, i.e. for the case of Au foils of 17.8 mm diameter

and 10 μm thickness, as to be used currently. The thus estimated average cross-section value is 40.6 barn ±3%.

10.2.3 Cadmium ratio for a given reaction rate

It is useful to have the neutron flux expressed in two energy groups under consideration of thermal reactor neutronics. From the experimental viewpoint, related information can be generated by using activation detectors in conjunction with a covering material which absorbs thermal neutrons strongly. Cadmium is an ideal material in this context, as indicated in Fig. 10.2, showing the total neutron cross-section of Au and Cd. (The scattering cross-section being fairly constant and small in each case, the curves essentially represent the absorption, i.e. (n,γ) cross-sections.)

It can be seen that the large thermal capture cross-section of Cd, though close to 1/v at very low energies, peaks to about 7200 barns at 0.176 eV, before dropping sharply to very low values at higher energies. Clearly then, Cd could be employed for "filtering out" the thermal neutrons from a given neutron spectrum, since these would be strongly absorbed by the Cd and the epithermal neutrons would pass through without significant interaction. Thus, the neutron-induced activity in a material such as Au - with significantly high cross-sections at both thermal and epithermal (i.e. resonance) energies - could be separated into the corresponding components by simultaneously irradiating two types of foils of the material, viz. bare and Cd-covered. The saturation activity of the former foil type would correspond to the total absorption rate, while that of the latter would represent the epithermal component, i.e. the absorption rate of neutrons above the "Cd cut-off".

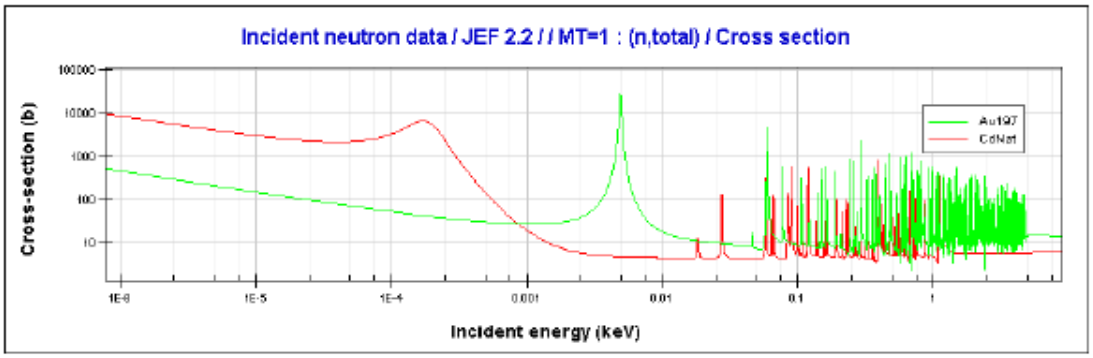

Figure 10.2: Total neutron cross-sections of Au and Cd vs. energy.

In accordance with the above, the cadmium ratio of a certain reaction rate in a given neutron spectrum is defined as the saturation activity of a bare foil of the activation material to that of a cadmium-covered foil of the same material, i.e. [13]:

$$R_{cd} = \frac{A_s^b}{A_s^{Cd}} \tag{10.9}$$

where the superscripts b and Cd denote the bare and Cd-covered foil, respectively.

The above equation can be written as:

$$R_{cd} = \frac{A_s^{sub-Cd} + A_s^{epi-Cd}}{A_s^{epi-Cd}} \tag{10.10}$$

Or

$$R_{cd} - 1 = \frac{A_s^{sub-Cd}}{A_s^{epi-Cd}} \tag{10.11}$$

where the superscripts *sub-Cd* and *epi-Cd* denote the reaction rate components below and above the Cd cut-off energy, respectively. The Cd ratio minus one may thus be regarded as a measure of the importance of the thermal neutron activation, relative to the epithermal.

It may be noted from Figure 10.2 that, in the case of the ^{197}Au (n,γ) reaction, the main contribution to the epithermal activation will be that of the large low-energy resonance i.e. will occur in the range $0.4 \leq E \leq 2$ eV. Clearly, measurements with Cd-covered foils provide information related to the resonance integral of the reaction in question.

10.2.4 Reactor power calibration

The reactor power can be determined on the basis of the neutron flux measurement at a certain location in the reactor, if an appropriate calibration factor is available for the necessary conversion. The latter can be deduced, for example, via a neutronics modelling of the reactor, in which the flux at the given location is related to the total rate of fissions occurring in the reactor.

In the present experiment, several Au foils are to be irradiated along the central axis of the CROCUS reactor, so that the saturation activity per atom can be determined from the counting of the 411.8 keV ^{198}Au gamma rays using a calibrated HP(Ge) system. By substituting the average cross-section value of 40.6b in Equation 10.8, one can then obtain values for the integral flux at the corresponding locations, allowing one to determine the maximum flux in CROCUS. This, in turn, can be converted to the reactor power, using the calibration factor provided.

10.3 Experiment description

In order to save time, a single irradiation will be carried out in CROCUS, so that both reactor power and the Cd ratio (characterizing the neutron spectrum) can be measured in a single

experimental run. Thus, five Au foils are to be irradiated along the central axis of the reactor such that the four foils located at 0 (reactor centre), ±10 and +20 cm are bare foils, while the fifth foil located at -20 cm is covered with Cd. The flux distribution of the bare foils will be used for power calibration, while the flux values from the Cd-covered and bare foils at ±20 cm (in conjunction with the asymmetry factor provided in Section 10.7) will give the Cd ratio. Effectively, the following measurements will be carried out:

- Experiment 1: Integral neutron flux
- Experiment 2: Cadmium ratio
- Experiment 3: Reactor power calibration

10.3.1 Important Precautions

The following precautions need to be followed at all times to ensure the safety of the experimenters and the equipment and to create high quality results.

1. For fixing the Au foils in position, do not apply scotch tape directly on them. Instead, the Au foils should first be covered with a thin plastic foil (use the provided machine to do it) and then with scotch tape. An additional, long piece of scotch tape covering all the foils is used to block their positions. Verify that the Au foils cannot move.
2. The detector-to-foil distance, i.e. the counting geometry, should be held fixed throughout the measurements.
3. The foils should be handled gently with a forceps. Do not touch the files with bare hands.
4. At the end, place the used foils in a plastic box, indicating the date on the cover.

10.4 Required setup

- CROCUS reactor
- 5 thin Au foils (10 micron thickness and 17.8 mm diameter)
- Cylindrical Cd-cover box
- Calibrated HP(Ge) system (see Experiment 3)

10.5 Operational settings

1. The 5 thin Au foils will be fixed on a plastic rod, such that they can be positioned at 0, ±100, and ±200 mm from the core centre. The foil at -200 mm will be covered with Cd.

2. The reactor will be operated at a power of about 12 W, and the irradiation carried out for a period of approximately 30 minutes.

3. The foils will be counted using the calibrated HP(Ge) system, connected to a digital spectral analyser (DSA-1000) controlled by a PC.

10.6 Measurement steps

1. Irradiation of the Au foils, with and without the Cd cover, will be carried outthe pre-selected positions along the central axis.

2. The calibrated HP(Ge) system will be used, under the appropriate operating conditions (see Experiment 3), for the gamma counting of the irradiated foils.

10.7 Data analysis

1. The reference calibration factor, relating the maximum value of the integral flux in CROCUS to the reactor power, is 3.95E-8 W.cm^{-2}s^{-1}.

2. As mentioned, the cadmium ratio is to be determined via measurements at the two positions +20 cm (bare Au foil) and -20 cm (Cd-covered foil). It is known, from separate measurements, that there is a certain axial flux asymmetry in CROCUS, the ratio of the flux at -20 cm to that at +20 cm being 1.048. This needs to be applied as a correction factor.

3. The values for gamma emission probability and photon non-absorption probability in the foil are as follows [14]:

   ϵ_{ep} = 0.954
   ϵ_{np} = 0.988

4. For the gamma-ray energy to be counted (411.8 keV), the photo-peak efficiency for the two available detector systems are (derived from Experiment 3):

Table 10.3: Photo-peak efficiency for the two available detector systems

Detector ID No.	Distance between detector and sample (mm)	Photo-peak Efficiency
S/N:11044024	20	3.57E-2
	50	1.55E-2
S/N:06041239	20	4.01E-2
	50	1.62E-2

10.8 Expected results

1. Integral flux values
2. Cadmium ratio for the ^{197}Au (n,γ) reaction
3. Power of the reactor
4. Identification of the sources of errors
5. A short note on the important conclusions

11 Reactor Period Measurements

11.1 Theory

11.1.1 General

For a reactor, with an effective multiplication factor k_{eff}, or simply k, the reactivity ρ is defined by Equation 11.1:

$$\rho = \frac{k-1}{k} \tag{11.1}$$

For a critical system (k_{eff}=1), the reactivity is zero. If the reactor is subcritical ($k < 1$), its reactivity is negative. If it is supercritical ($k > 1$), the reactivity is positive and the neutron flux will increase exponentially, i.e. the reactor will have a positive stable period (see Section 11.1.3).

11.1.2 Reactivity worth in CROCUS

CROCUS is primarily controlled via the water level. An equivalent experiment of control rod worth determination is to determine the water level worth, i.e., determining the reactivity for a given super-critical water level.

In this experiment, the water level reactivity of the CROCUS reactor will be calibrated via application of the inhour equation, which relates the step change in reactivity in a given reactor to the corresponding stable period (see next section). The reactivity worth values obtained for different water levels being calibrated will then be compared to the theoretical prediction.

11.1.3 Stable reactor period

Hypothetical case of a system *without* delayed neutrons

Applying the so-called point reactor model to the hypothetical case of a reactor in which all the neutrons are considered born as prompt neutrons, the rate of increase of the neutron population is given by Equation 11.2:

$$p(t) = p(0)exp\Big[\frac{(k_{eff}-1)}{l}t\Big] \tag{11.2}$$

where $P(0)$, k_{eff} and l represent the neutron population at $t = 0$, the effective infinite multiplication factor and the prompt neutron lifetime, respectively. The latter is effectively a measure of the time between the birth of a neutron and its disappearance in face of absorption and leakage.

Eq. 11.2 may be written as Equation 11.3, where $\tau = l/(k_{eff}-1)$, stands for the reactor period and can be interpreted as the time resulting in the e-fold increase in reactor power or flux.

$$N_F(t) = N_F(0)e^{\frac{t}{T}}\, p(t) = p(0)e^{\frac{t}{\tau}} \tag{11.3}$$

A typical value for the prompt neutron lifetime in a thermal reactor is 10^{-3} sec. Thus, in the hypothetical case with all neutrons assumed to be prompt, an increase of k_{eff} from 1.000 to say 1.005 would result in a reactor period of just $\tau = 0.001/0.005 = 0.2$ sec, i.e. the reactor power would increase by $e^{1/0.2} = e^5 = 148$ every second, a clearly uncontrollable scenario. In reality, due to the presence of delayed neutrons, the rate of power increase is much slower.

Reactor with delayed neutrons

For the real case of a reactor with delayed neutrons – usually considered in six groups with group-specific values for the decay constant (λ_i) and the delayed-neutron fraction (β_i) – the point-kinetics equations are Equations 11.4 and 11.5, where P is the neutron population, C_i is the precursor concentration for group i, and one has used the definition of reactivity, $\rho = (k_{eff}-1)/k_{eff}$, and the prompt neutron generation time, $\Lambda = l/k_{eff}$.

$$\frac{dP}{dt} = \frac{\rho(t) - \beta}{\Lambda} P(t) + \sum_{i=1}^{6} \left[\lambda_i C_i(t) \right] \tag{11.4}$$

and:

$$\frac{dC_i}{dt} + \lambda_i C_i(t) = \frac{\beta_i}{L} P(t) \tag{11.5}$$

The solution of the above system of coupled, linear differential equations for the case of a step change in reactivity ρ leads to an evolution of the neutron population of the type described in Equation 11.6, where the B_j are constants and the ω_j are given by the roots of the so-called Reactivity (or Inhour) equation shown in Equation 11.7.

$$\frac{P(t)}{P(0)} = \sum_{j=1}^{j=7} B_j e^{w_j t} \tag{11.6}$$

$$\rho = \Lambda\overline{\omega} + \sum_{i=1}^{6} \frac{\beta_i \overline{\omega}}{\overline{\omega} + \lambda_i} \tag{11.7}$$

Fig. 11.1 is a schematic depicting the graphical solution of Eq. 11.7, for both positive and negative ρ values are. It is seen that, for the case of a positive step change in reactivity, there is just a single ω value which is positive (ω_1), all other roots being negative and thus corresponding to terms in Eq. 11.6 which die away. The stable (positive) period for the neutron population, or flux, is thus $T = 1/\omega_1$. For the case of a negative step change in reactivity, all the seven roots of Eq. 11.10 are seen to be negative. Here, since the terms in Eq. 11.6 associated with the larger ω values die away quicker, the stable (negative) period is also simply $T = 1/\omega_1$.

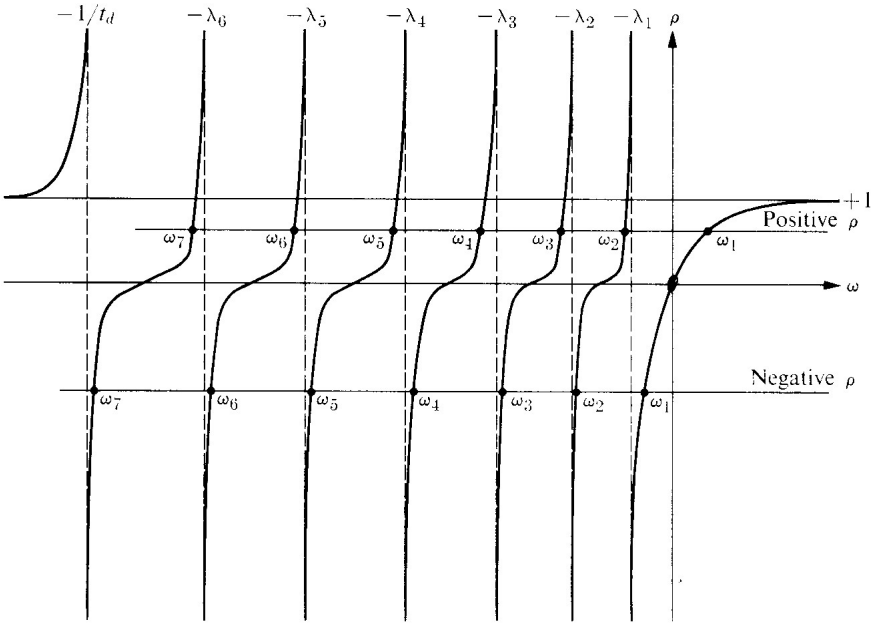

Figure 11.1: Schematic of the reactivity equation showing the seven roots for positive and negative reactivity.

Fig. 11.2 illustrates the evolution of the neutron flux, following a 0.001 step increase of reactivity in a ^{235}U fuelled thermal reactor [5]. The "transient region" at the beginning corresponds to the die-away of the six terms of Eq. 11.6 which have negative ω values. It can be shown that the coefficients B_j associated with these terms are also negative, the vanishing of negative terms being the explanation why the transient region corresponds to an initial rapid increase of the flux. The slower stable rate of flux increase thereafter corresponds to the stable reactor period, $T = 1/\omega_1$.

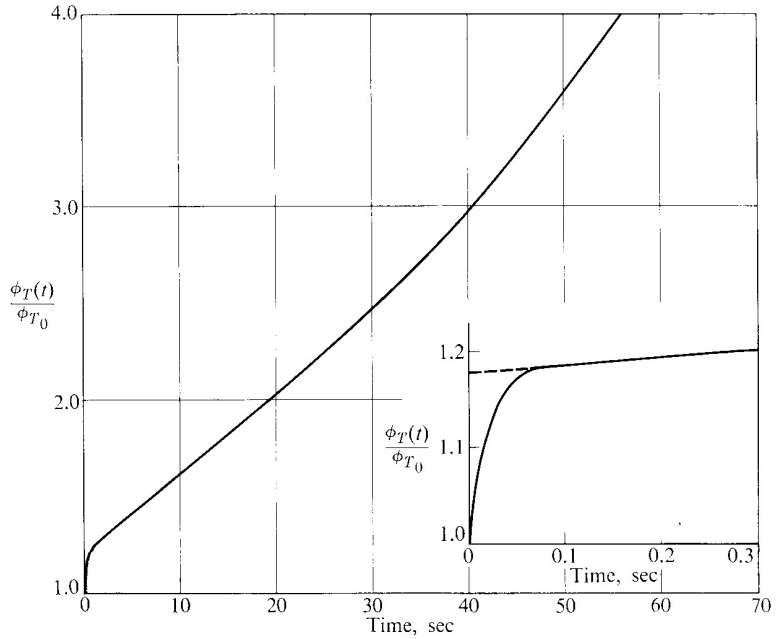

Figure 11.2: Time behaviour of thermal neutron flux in infinite ^{235}U fuelled, H_2O moderated thermal reactor following step reactivity insertion of 0.001.

Clearly, in the present measurements of the stable period corresponding to a given water level in CROCUS, it will be necessary to use an appropriate range of the time-dependent data for deducing ω_1, i.e. to ensure that the initial data points corresponding to the transient region have been exempted from the exponential fitting. This is especially important as the water level increase takes a few seconds, i.e., the reactivity introduction is not a 'step'. The ρ value (or worth) can then be obtained by substituting the deduced ω_1 value into the Reactivity Equation (Eq. 11.7), along with the provided "kinetics parameters (Λ, λ_I, β_i) for the CROCUS reactor.

11.2 Experiments to be conducted

The following measurements will be carried out:

Exp. 11.1: Water level reactivity calibration via period measurement

11.2.1 Important Precautions

The following precautions need to be followed at all times to ensure the safety of the experimenters and the equipment and to create high quality results.

1. Start the data acquisition program at the same time as the change of water level.

2. The initial transient region has to be assessed carefully and remove prior to the fitting.

11.3 Required setup

The following components are required for this experiment. Check to see if they are available. If they are not available, please speak with your lab instructor.

1. The CROCUS reactor, critical at low power with partial insertion of the control rod to be calibrated.
2. DSA-1000 (multi-channel data acquisition system).
3. PC and MATLAB based routine, available in the control room.

Note: The reactor experiments are conducted with two groups in parallel. Two independent data acquisition systems are provided and each one is connected to a different fission chamber.

11.4 Operational settings

- Fission Chamber Nos. 1 and 2, DSA-1000 data acquisition systems from CANBERRA used in MCS[1] mode and computers for recording the flux as a function of time
- In the DSA-1000, the "Gamma Acquisition Analysis" (GENIE-2000) software is used. The following has to be done:
  - Start the GENIE-2000 program and then, launch the needed configuration: Open-source → Select DET#01 → (count vs time window appears)
  - Open in MCA tab → Adjust → MCS

There, the "dwell time" can be adjusted. This corresponds to the time interval per channel for data acquisition. There are 8192 channels in the DSA-1000. The total counting time has to be set such that this is sufficient to record, in an adequate manner, the increase of power consecutive to the withdrawal of the control rod.

11.5 Measurement steps

1. The operator stabilizes the reactor at very low power (about 50 mW). The water level for critical state is about 953.1 mm. Suddenly increase the water level to 960 mm and start the data acquisition with the operation fission chambers of CROCUS.

[1] Multichannel scaling

2. Make sure the acquisition system is ready with a dwell time chosen for recording the power increase in an appropriate manner. (An estimate of the expected reactor period can be made on the basis of Table 11.1 and Fig. 11.3).

3. Acquire the fission chamber counts rates per dwell-time channel for a sufficient period of time (usually over 2 decades of change in power, typically in the power range 0.1 W to 10 W).

4. Perform several measurements of this type up to 1000 mm of water. Each reactor transient is ended at around 10 W power by lowering the power level to its initial level via a rapid reduction of the water level by the operator.

5. Stop the acquisition system and save the measurement in the *.TKA format (ASCII). Keep a record of the water level and the dwell time.

6. For each water level variation, determine the stable period of the reactor and the corresponding reactivity, using the inhour equation and the kinetic parameters of the CROCUS reactor given in Table 11.1.

11.6 Data analysis

1. Fit the exponential rise with your program of choice to determine ω_1.

2. Compare the graph of the measured values of reactivity vs. water level with the data of Figure 11.3.

Important information:

- The power level range for measurements is in the range of 0.1 to ~10 Watt.
- The reactivity worth of 40 mm of water (beyond critical water level) is equal to +200 pcm, the maximal allowed and possible positive reactivity in CROCUS.
- It is seen, from Table 11.1, that the total delayed neutron fraction (β) for CROCUS is about 0.75%, i.e. considerably higher than 0.65%, the value for a purely ^{235}U-fuelled system. This is largely due to the fact that there is a significant contribution of fast fissions in ^{238}U, for which the delayed neutron fraction is as high as about 2%. The other contributing factor to the relatively large β-value of CROCUS is that delayed neutrons have a significantly lower average energy (~0.4 MeV) than prompt neutrons (~2 MeV). In a high-leakage core, such as CROCUS, there is consequently a preferentially higher leakage of prompt neutrons.
- Clearly, the Reactivity Equation (Eq. 11.7) can be used for calculating the stable reactor period ($T = 1/\omega_1$) for any reactivity introduced into a given reactor, on the basis of its kinetics parameters (Λ, β_i, λ_i).

- Fig. 11.3 provides, in graphical form, calculated results for the reactor period corresponding to a wide range of positive reactivity values (ρ) introduced into CROCUS. It is clear to see that the period becomes dangerously short as ρ approaches the delayed neutron fraction (β) of 0.75%, i.e. as ρ approaches the value of 1 dollar (the unit for reactivity, relative to the delayed neutron fraction).
- Prompt criticality ($\rho \geq \beta$) is a "forbidden" state for a reactor. As mentioned earlier, and as indicated in Fig. 11.3, the maximum permitted positive reactivity for CROCUS is 200pcm = $2{\cdot}10^{-3}$ = (0.002/0.0075)\$ = 27cents.

Table 11.1: Kinetics parameters for the CROCUS reactor. The table lists the mean values of the different calculated results reported in [7].

Λ = 5.93E-05 s		
Delayed neutron group	β_i	λ_i [s^{-1}]
1	2.43E-04	1.29E-02
2	1.45E-03	3.14E-02
3	1.35E-03	1.19E-01
4	2.96E-03	3.16E-01
5	1.10E-03	1.197
6	3.47E-04	3.495
Total	7.46E-03	-

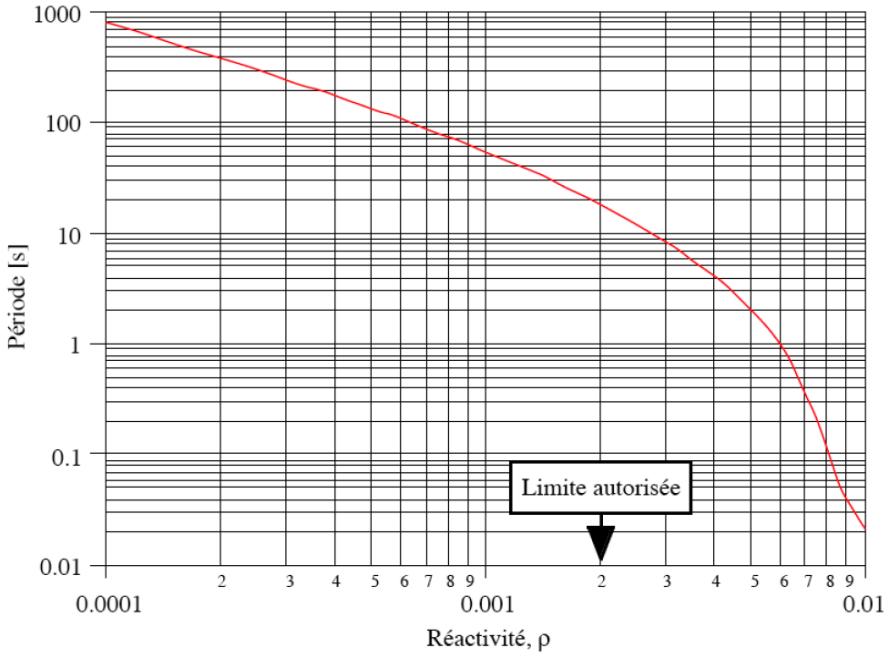

Figure 11.3: Reactor period ($1/\omega_1$) vs. positive reactivity for the CROCUS reactor.

11.7 Expected results

1. Calculate, as a first approximation, the reactivity as a function of the inverse of the square of the water height, knowing that the dependence is linear (this hypothesis will be theoretically demonstrated and experimentally confirmed), that the reactivity for a water height of 1000 mm is 200 pcm, and that the critical state corresponds to 953.1 mm of water.

2. Calculate the ω_i solutions of the Inhour equation (11.7) for different water heights, using the β_i, λ_i, and Λ values given in Table 11.1. Identify the unique positive solution ω_+.

3. Calculate the coefficients B_i of equation (11.6), knowing that they are expressed as follows:

$$B_i = \frac{\Lambda + \sum_{j=1}^{12} \frac{\beta_j}{\omega_i + \lambda j}}{\Lambda + \sum_{j=1}^{12} \frac{\beta_j \lambda j}{(\omega_i + \lambda j)^2}} \tag{11.8}$$

4. Graphically represent the time evolution of the population in general (11.6) and considering only the positive root ω_+:

$$\frac{N(t)}{N_0} = B_+ exp(\omega_+ t) \tag{11.9}$$

5. Calculate the time at which the ratio between the detailed solution (11.6) and the simplified solution (11.9) is less than one percent. Graphically represent the reactivity as a function of this time.

12 Gamma-ray absolute activity determination by coincidence measurements

12.1 Introduction

This experiment illustrates coincident radiation emissions during radioisotope decay. Typical gamma-ray spectroscopy coincidence set-ups are used to determine the absolute activity of a radioisotope source.

12.2 Theory

Radioisotopes generally emit multiple radiations almost simultaneously, i.e. with time differences smaller than the resolving time of standard spectroscopy detectors and electronics. For example, beta decay emits an electron often followed by gamma rays resulting from the de-excitation of the daughter nucleus. A common case is that of the Co-60 radioisotope whose simplified decay scheme is illustrated in Figure 12.1

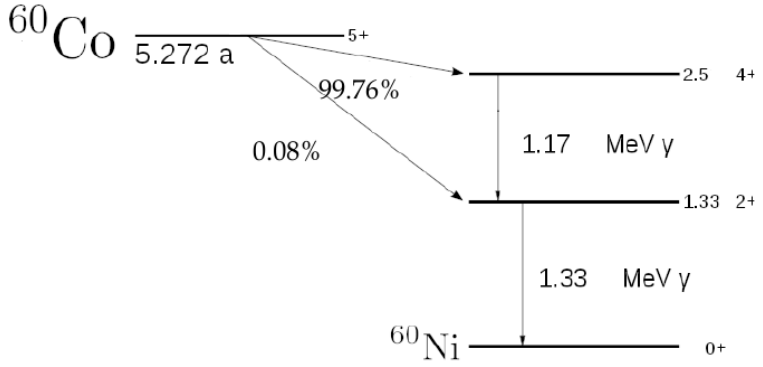

Figure 12.1: Decay scheme of a ^{60}Co source with two gamma rays represented.

Most of the time the Co-60 decay occurs by beta emission to the 2.507 MeV excited state of Ni-60. Subsequent decay to the ground state always occurs by emission of an 1173 keV gamma-ray to the 1.332 MeV level, followed almost simultaneously by emission of an 1332

keV gamma ray to the ground state.

12.2.1 Measurement with one detector

The Co-60 gamma-ray spectrum (number of gamma-rays as a function of their energy), measured for example with a detector made of a sodium iodide crystal doped with thallium NaI(Tl), exhibits two photo-peaks (also named full-energy peaks) with energies corresponding to the two gamma-rays γ_1 = 1173 keV and γ_2 = 1332 keV. These full-energy peaks result from interactions in which the gamma-ray-rays γ_1 and γ_2 deposit separately their full energy in the crystal (mainly by photo-electric interactions or Compton interactions followed by photo-electric interactions). It is, however, possible that the two gamma-rays deposit almost simultaneously all their energies in the detector. This result in a so-called sum peak whose energy is 1173+1332 = 2505 keV. This sum peak is a proof of the coincident nature of the two gamma-rays.

The average count-rate in the two full-energy peaks (once the background is subtracted) can be approximated as Equation 12.1, where N_0 is the activity of the Co-60 source (number of decay per seconds), γ_i is the probability of emitting the corresponding gamma-ray per Co-60 decay, Ω is the solid angle under which the source sees the detector (Detector area/4π*(distance detector-source)^2) and ϵ_i is the intrinsic peak efficiency; that is the probability for a gamma-ray of energy E_i entering the detector to deposit all its energy, i.e. to contribute to the full-energy peak.

$$N_1 \approx N_0 \gamma_1 \Omega \epsilon_1 \quad \text{and} \quad N_2 \approx N_0 \gamma_2 \Omega \epsilon_2 \tag{12.1}$$

The expression for the sum peak can be approximated with the same notations is given as Equation 12.2, in which N_0 is the number of decay per seconds, $(\gamma_1 \Omega \epsilon_1)$ expresses the probability of producing the gamma-ray "i" and that it deposit all its energy in the detector, and finally W(0) accounts for the angular correlation between the two gamma-rays "1" and "2".

$$N_{12} \approx N_0 (\gamma_1 \Omega \epsilon_1)(\gamma_2 \Omega \epsilon_2) W(0) \tag{12.2}$$

The term W(0) expresses that although γ_1 is isotropically emitted, the angle at which γ_2 is emitted will depend (though weakly) of the angle at which γ_1 has been emitted. When measuring the average distribution of γ_1 or γ_2 separately it does not play a role, but it does if the two gamma-rays of a same decay are detected together (as in the sum peak). It can be shown that the angular correlation distribution is of the form $W(\theta) = 1 + a_1 \cos^2(\theta) + a_2 \cos^4(\theta)$ where θ is the angle between the two gamma-rays. For them to be detected in the same detector $\theta = 0$ and W(0) = 1.167.

Note: The two gamma-rays stems from the same Co-60 decay and as such are generally named true coincidence. If the activity N_0 times the detection and processing time dt is large, the probability of having random coincidences, i.e. coincidences between two gamma-rays issued from two different decays that happen close in time, is not negligible. The probability to have a count in the sum peak during the time *dt* becomes Equation 12.3.

$$N_{12}dt \approx N_0 dt(\gamma_1\Omega\epsilon_1)(\gamma_2\Omega\epsilon_2)W(0) + N_0^2 dt^2(\gamma_1\Omega\epsilon_1)(\gamma_2\Omega\epsilon_2) \tag{12.3}$$

For the sake of clarity, we will however develop the mathematical framework assuming no random coincidences.

In normal conditions N_{12} is far less than N_1 or N_2 because the solid angle and the intrinsic efficiency are generally small. Practically with NaI detectors N12 becomes significant only when the source-detector distance is small (<couple of centimeters).

Using the formula for the full-energy peaks and the sum peak we can approximate the value of the Co-60 source activity as Equation 12.4.

$$N_0 \approx \frac{N_1 N_2}{N_{12}} W(0) \tag{12.4}$$

In the first measurement, we will set-up a NaI detector and a Co-60 source in order to measure the absolute activity of the source according the formula above and check its validity.

12.2.2 Measurement with two detectors

The same type of measurement can be performed with two detectors A and B and the Co-60 source. This time, however, we are interested in the coincident detection of γ_1 in detector A and γ_2 in B and vice versa. This cannot be seen in any of the gamma-ray spectrum and requires additional piece of equipment to count the coincident gamma-rays (see Section 12.4). However, mathematically, when considering a low intensity source, the expressions for the count rate in the full energy peaks of each detector and for the coincident rate are similar to that of the previous section.

$$\begin{gathered} N_{A1} \approx N_0\epsilon_1\Omega^A\epsilon_1^A, \quad N_{A2} \approx N_0\epsilon_2\Omega^A\epsilon_2^A, \quad N_{B1} \approx N_0\gamma_1\Omega^B\epsilon_1^B, \quad N_B2 \approx N_0\gamma_2\Omega^B\epsilon_2^B \\ N_{A1,B2} \approx N_0(\gamma_1\Omega^A\epsilon_1^A)(\gamma_2\Omega^B\epsilon_2^B)W(\theta) \quad \text{and} \quad N_{A2,B1} \approx N_0(\gamma_2\Omega^A\epsilon_2^A)(\gamma_1\Omega^B\epsilon_1^B)W(\theta) \end{gathered} \tag{12.5}$$

Note: As for the Measurement #1 we only considered here true coincidences, i.e. coincidence between two gamma-rays emitted during the same decay. If the activity N0 times the de-

tection/processing time dt is not negligible, then additional terms appear in the formula for $N_{A1,B2}$ and $NA2,B1$. In practice, however, there is an easy experimental way to estimate the random coincidences between gamma-rays of different decays and subtract them from the measured coincidences (see Sections 12.4.1 and 12.4.2). We will therefore continue to develop the theoretical framework assuming no random coincidences.

From these expressions we can construct similar ratio to that of the previous section to determine the source activity N0. As an example, using the sums of counts N_{A1}+N_{A2}, N_{B1}+N_{B2} and $N_{A1,B2}$ + $N_{A2,B1}$, and thus maximizing the measurement efficiency, we can write Equation 12.6.

$$N_0 \approx \frac{(N_{A1}+N_{A2})(N_{B1}+N_{B2})}{N_{A1,B2}+N_{A2,B1}} W(\theta) \frac{\gamma_1\gamma_2(\epsilon_1^A\epsilon_1^B+\epsilon_2^A\epsilon_2^B)}{(\gamma_1\epsilon_1^A+\gamma_2\epsilon_2^A)(\gamma_1\epsilon_1^B+\gamma_2\epsilon_2^B)} \tag{12.6}$$

For the Co-60 source $\gamma_1 \approx \gamma_2 \approx 1$, the expression can be simplified to Equation 12.7, where $R_A = \epsilon_1^A/\epsilon_2^A$ and $R_B = \epsilon_1^B/\epsilon_2^B$ are the relative efficiency of the two full-energy peaks for each detector and can be measured beforehand.

$$N_0 \approx \frac{(N_{A1}+N_{A2})(N_{B1}+N_{B2})}{N_{A1,B2}+N_{A2,B1}} W(\theta) \frac{R_A+R_B}{1+R_A+R_B+R_AR_B} \tag{12.7}$$

A typical set-up is to arrange the detectors back-to-back with the source in the middle, such that θ = 180 degrees and W(180) = 1.167. This is the basic set-up we will use in the second measurement. We could also repeat the experiment for different angle θ between the two detectors to measure the relative angular correlation distribution W(θ).

12.3 Experiment description

The following experiments will be carried out using the Z spectrometer. Provide summary for experiments here

- **Experiment 1:** Measure the absolute activity of a Co-60 source using a NaI detector using the full-energy and sum peaks.

- **Experiment 2:** Measure the absolute activity of the Co-60 source using the coincident gamma-rays detected by two NaI(Tl) detectors.

12.4 Required setup

The following setups are described for experiment 1 and 2.

12.4.1 Experiment 1 required setup

Two 3"x3"" NaI(Tl) detectors are positioned on each side of the ^{60}Co source #10353. Each detector is connected to an ORTEC photo-multiplier/pre-amplifier (PMT) which is powered by a low voltage and a 500 V high voltage provided by an ORTEC 556 unit. The signal is amplified and shaped by an Amplifier unit (AFT Research Amplifier Model 2025). The resulting signal is provided to a Multi-Channel Analyzer (MCA Multiport II from CANBERRA), which transmits the signal to the acquisition PC running the GENIE2000 software. The energy spectra of the gamma-ray detected in the NaI(Tl) detector is obtained on the PC. Two acquisition lines (one per detector) are available. For the first experiment, we will focus on one acquisition line; that corresponding to the top detector.

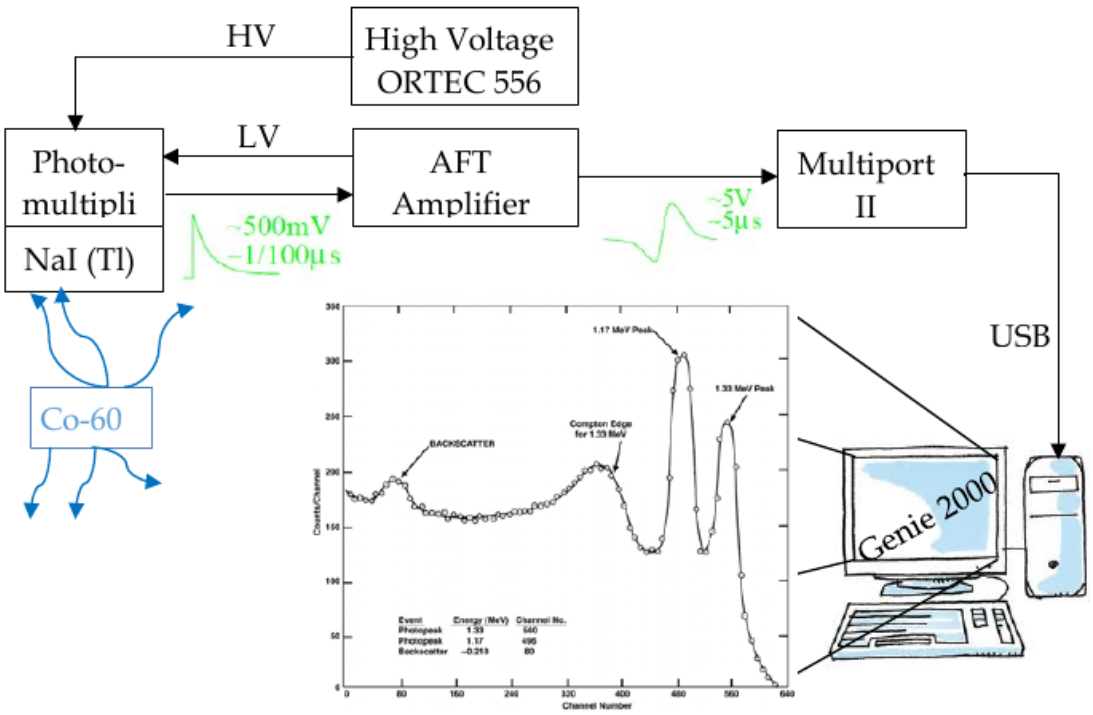

Figure 12.2: Block diagram of the experimental setup for measurement 1.

In this measurement you will acquire the pulse-height spectra of one detector, determine the count rates of the two full-energy peaks at 1173 keV and 1332 keV and of the sum peak at 2505 keV, and derive the absolute activity of the source according to equations of Section 12.2.1.

12.4.2 Experiment 2 measurement setup

Two main setups are used for this measurement. The first one is similar to that of Measurement #1 illustrated in Figure 12.2, i.e.

Detectors/PMT/Amplifier/Multiport-II/PHA spectra

However, it comprises two acquisition lines (one for each detector). In the second one the Multiport II and PC with Genie2000 are replaced with two Timing Single Channel Analyzer units, a coincident unit and three counters in order to determine the count rate in the two detectors and the coincident counts (see Figure 12.3).

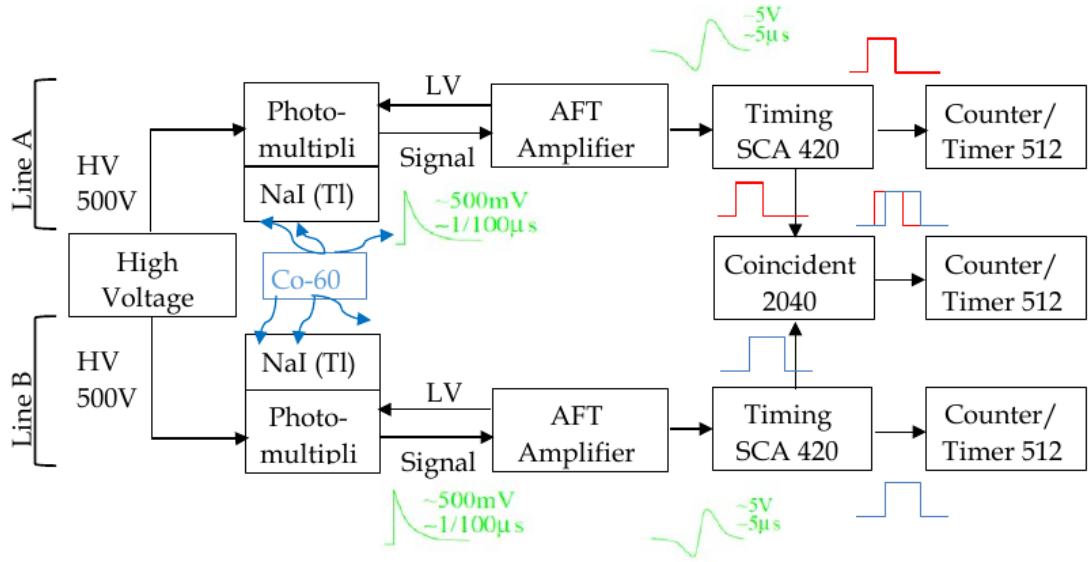

Figure 12.3: Coincidence measurement setup

The Timing SCA unit emits a short TTL pulse for each input signal whose amplitude, i.e. the energy of the detected radiation, is between E_0 and $E_0+\Delta E$. By setting E_0 and $E_0+\Delta E$ correctly we can trigger a TTL signal for each gamma-ray that deposits all its energy in the detector, i.e. that is part of the two full-energy peaks of the spectra acquired in Measurement #1. Counting the TTL pulses with the dual Counter/Timer CANBERRA 512 we obtain all radiations of the two photo-peaks, that is, with the notation of Section 12.2.2, $N_{A1}+N_{A2}$ and $N_{B1}+N_{B2}$ for the acquisition lines A and B, respectively. The output of the Timing SCA unit of each acquisition line is also fed to a coincident unit (CANBERRA 2040), which performs a logical AND on the two signals and deliver a TTL signal when the output of the timing units arrive simultaneously (i.e. within the resolving time of the coincident unit, which is adjustable). The ouput of the coincident unit is, with the notation of Section 12.2.2, related to the coincident gamma-rays $N_{A1,B2}+N_{A2,B1}$.

In practice, because the time for the signal to travel from the Photo-Multiplier Tube to the Coincident unit may vary between the acquisition lines A and B, a variable delay is available for the output of each Timing SCA unit. The delay corrections can be found by feeding the signal of a pulse generator (e.g. Research Pulser 841FP from CANBERRA) to the two Amplifiers instead of the signal from the detectors and PMT.

The delay has another practical function. As mentioned in Sections 12.2.1 and 12.2.2, if the activity times the time of detection/processing $N_0\ x\ dt$ is large enough the measured

coincidences account for true and random coincidences. Random coincidences happen between two gamma-rays of two separate decays. The activity of the source N_0 is constant during the measurement and separate decays are not correlated in time. In other words, the amount of random coincidences between two gamma-rays both detected and processed during the interval $[t_0, t_0 + dt]$ is equal to the amount of random coincidence between 1 gamma-ray detected and processed during $[t_0, t_0 + dt]$ and another one detected and processed during $[t_1, t_1 + dt]$. True coincidence, however, happen only when the gamma-rays are both detected and processed during the same interval $[t_0, t_0 + dt]$. By delaying one acquisition line by a sufficiently large value t_1 - t_0, it is therefore possible to only count the amount of random coincidences, which remain constant during the measurement.

The pulse generator can also be used to determine the upper and lower threshold of the Timing SCA units to set correct values for E_0 and $E_0 + \Delta E$. The measurement set-up of Figure 12.2, in which the two detectors and PMT are replaced with the pulse generator can be used to find the amplitude of the pulse generator that gives counts in the channels C_0 and C_1 delimitating the two full-energy peaks of the Co-60 energy spectra (see Figure 12.4). Once the amplitude are known, the setup of Figure 12.3 can be used with the same pulse generator and E_0 and $E_0+\Delta E$ adjusted to count the generated pulses.

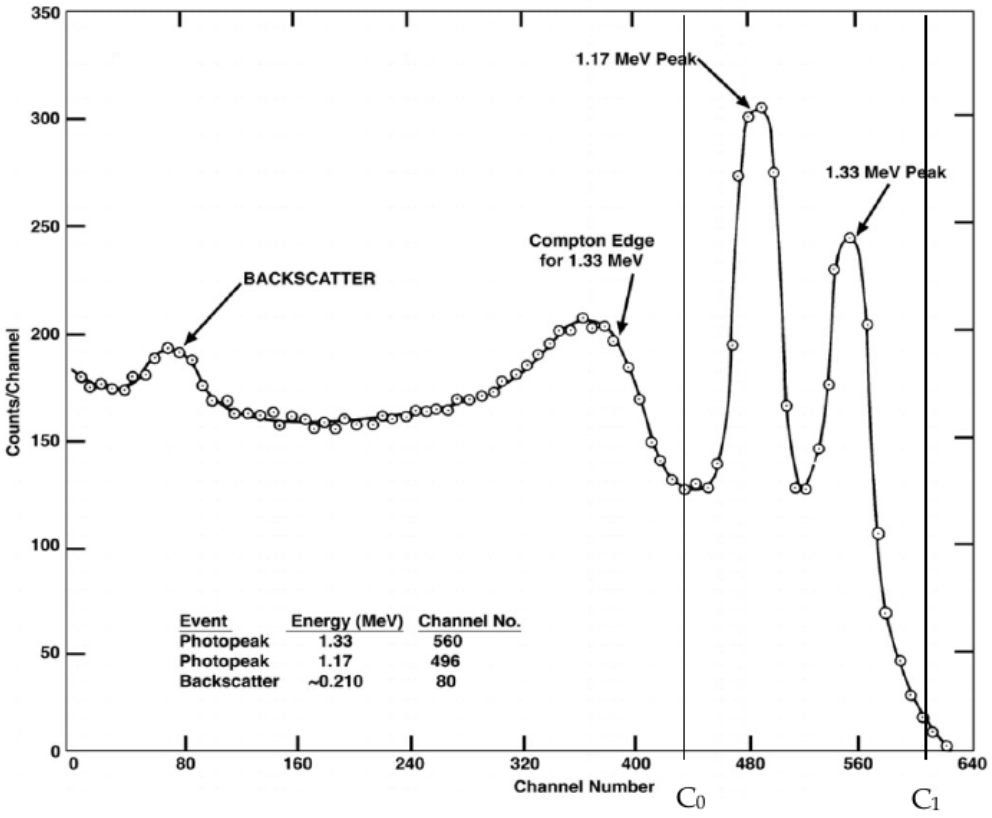

Figure 12.4: Channels of interest to set the lower and upper thresholds

12.5 Measurement steps

12.5.1 Experiment 1: Measure the absolute activity of a Co-60 source using a NaI detector using the full-energy and sum peaks

1. Adjust the position of the top detector as close to the source as possible (about 2-3 cm).
2. Place the Co-60 source on its support and insert the support in the lead shield using the measurement device ("EIN" and "PROBE EIN").
3. Make sure that the high voltage cable connects the HV input on each photomultiplier tube (PMT) base to the back panel of the high voltage supply ORTEC 556.
4. Make sure the HV supply are down; power up the NIM electronic crates and verify that the low voltage (LV) is provided by the Amplifier to the PMT.
5. Turn on the HV and set it to 500V
6. Check the signal (amplitude and time constant) at the output of the PMT with an oscilloscope.
7. Connect it to the Input of the Amplifier (AFT) and observe the bipolar output from the amplifier
8. Set the coarse and fine gains of the amplifier such that the pulse height is about 4-5V.
9. Feed the bipolar output of the amplifier to the top entry of the MULTIPORT II crate (MCA #1)
10. Acquire the gamma-ray spectra with GENIE2000 [15] such that you can identify the 2 full energy peaks and the sum peak.
    (a) Log on as LRSPC45 (same password)
    (b) Launch Genie 2000 (shortcut and manual [15] on the desktop)
    (c) Select the multichannel scaler Analyzer entry from the Multiport II named MCA1_16K (MCA #1 with 16384 channels)
    (d) Run the acquisition for 5-10 minutes and save it
11. Eventually perform an energy calibration
12. Determine the integral of each peak (e.g. in the menu Analyze/Execute Sequence/Peak Analysis with Reports or counting manually using the cursors on the plot). Reports spectra plot and area of the peak values.
13. Derive the total source activity according to equations in Section 12.2.1.
14. Is the activity comparable to that labelled on the source?

12.5.2 Experiment 2: Measure the absolute activity of the Co-60 source using the coincident gamma-rays detected by two NaI(Tl) detectors.

1. Preparation:
   - Adjust the position of the two detectors at 3-5 cm from the support of the source.
   - Check that the Co-60 source is located between the two detectors.
2. Determination of efficiency ratios and full-energy peaks channels:
3. Repeat Measurement #1 with the two detectors (use e.g. MCA1_8K detector in Genie 2000, i.e. MCA #1 with 8192 channels)
4. Determine the channel C_0 and C_1 of interest around the full-energy peaks, and measure the efficiency ratios $R_A = \epsilon_1^A/\epsilon_2^A$ and $R_B = \epsilon_1^B/\epsilon_2^B$ together with their uncertainties (the target uncertainty is about 1%).
5. Determination of the Timing SCA delay times, and lower and upper thresholds:
   - Replace the two detectors/PMTs by the pulse generator as the input of the two amplifiers.
   - Determine the amplitude A_0 and A_1 of the pulse to obtain counts in the channel C_0 and C_1 for each acquisition line.
   - Disconnect the MCA from the Amplifiers and replace them with the Timing SCA, Counters and Coincident Unit as shown in Figure 12.3.
   - Adjust the delay of the two Timing SCA units to synchronize the signals emitted by the pulse generator. You can for example use the oscilloscope to visualize the output of the two Timing SCA units.
   - Check that the count rates of the three Counters are the same and equal to the pulse generator rate 6 .
   - Adjust the lower threshold E_0 and the window ΔE to count pulse of amplitude A_0 and A_1 in each acquisition line.
6. Determination of the full-energy peak counts and coincident counts:
   - Run the acquisition to have an uncertainty of the order of 1% on each count
   - Delay the signal of one acquisition line by a value significantly larger than the resolving time of the coincident unit (the resolving time is adjustable in front of the coincident unit; a typical value is 220 ns).
   - Evaluate the random coincidence rate and its uncertainty
   - Correct the coincident rate and propagate the uncertainty
7. Results:
   - Derive the activity of the source N_0 and its uncertainty
   - Compare with the data provided by the manufacture

12.6 Expected results

- Determine the integral of each peak (e.g. in the menu Analyze/Execute Sequence/Peak Analysis with Reports or counting manually using the cursors on the plot). Reports spectra plot and area of the peak values.
- Derive the total source activity according to equations in Section 12.2.1.
- Is the activity comparable to that labelled on the source?
- Evaluate the random coincidence rate and its uncertainty
- Correct the coincident rate and propagate the uncertainty
- Derive the activity of the source N_0 and its uncertainty
- Compare with the data provided by the manufacture

13 Radioprotection measurements

13.1 Introduction

Radiation dose refers to the amount of energy deposited in matter and/or biological effects of radiation, and should not be confused with the unit of radioactive activity (becquerel, Bq). Exposure to a radioactive source will give a dose which is dependent on the activity, time of exposure, energy of the radiation emitted, distance from the source and shielding. A common quantity for dose used by nuclear engineers is the *equivalent dose* which is quantified by means of weighting factors. Dose is a measure of deposited dose, and therefore can never go down—removal of a radioactive source can only reduce the rate of increase of absorbed dose, never the total absorbed dose. The worldwide average background dose for a human being is about 3.5 mSv per year, mostly from cosmic radiation and natural isotopes in the earth. The largest single source of radiation exposure to the general public is naturally-occurring radon gas, which comprises approximately 55% of the annual background dose.

This lab introduces students to important theories and practices in radioprotection. Because nuclear engineers often work in radioactive environments, it is critical that students know how to measure dose and to evaluate if a given dose is significant or not. Additionally, students will learn how to use the most common detectors employed in radioprotection.

13.2 Theory

13.2.1 Absorbed dose

Absorbed dose is a measure of the energy deposited in a medium by ionizing radiation per unit mass. It is equal to the energy deposited per unit mass of medium, which may be measured as joules per kilogram and represented by the equivalent SI unit, gray (Gy), or the antiquated CGS units, rad. The absorbed dose depends not only on the incident radiation but also on the absorbing material: a soft X-ray beam may deposit four times higher dose in bone than in air, or none at all in a vacuum.

The radiation absorbed dose D is the mean energy imparted to matter of mass M:

$$D = \frac{dE}{dM} \qquad [\,1\ \ Gy = 1\ \ J/kg = 100\ \ rad\,] \tag{13.1}$$

13.2.2 Dose equivalent

The equivalent absorbed radiation dose (equivalent dose) is a computed average measure of the radiation absorbed by a fixed mass of biological tissue that attempts to account for the different biological damage potential of different types of ionizing radiation. The equivalent SI unit is sievert (Sv), or the antiquated CGS units, rem.

The radiation dose equivalent H is the product of the absorbed dose D and the quality factor wR (or Q) characterizing the damage associated with each type of radiation:

$$H = w_R D \qquad [\,1\ \ Sv = 1\ \ Gy \cdot \mathrm{w}_R = 100\ \ rem\,] \tag{13.2}$$

13.2.3 Effective dose

The effective dose in radiation protection and radiology is a measure of the cancer risk to a whole organism due to ionizing radiation delivered non-uniformly to part(s) of its body. It is not intended as a measure of deterministic or other effects of radiation. The equivalent SI unit is sievert (Sv).

The effective dose E is the equivalent dose H_T in organ or tissue T multiplied with a weight factor w T describing the sensitivity of the tissue to radiation:

$$E = \sum w_T H_T = \sum w_T \sum w_R D_{T,R} \tag{13.3}$$

13.2.4 Radiation effects on living tissue

The distinction between absorbed dose (gray, Gy) and dose equivalent (sievert, Sv) is based upon the biological effects of the weighting factor (denoted w_R or Q) and tissue/organ weighting factor (w_T) have been established, which compare the relative biological effects of various types of radiation and the susceptibility of different organs.

13.2.5 Radiation weighting factors

By definition, X-rays and gamma rays have a weighting factor of unity, such that 1 Gy = 1 Sv (for whole-body irradiation). Values of w_R (Q), see Table 13.1, are as high as 20 for alpha particles and neutrons, i.e. for the same absorbed dose in Gy, alpha particles are 20 times as biologically

potent as X or gamma rays.

Table 13.1: Conventional radiation quality factors to calculate equivalent doses.

RADIATION	ENERGY	WR (Q)
X-rays, gamma rays, electrons, positrons, muons		1
neutrons	<10 keV	5
	10 keV - 100 keV	10
	100 keV - 2 MeV	20
	2 MeV - 20 MeV	10
	>20 MeV	5
protons	>2 MeV	2
alpha particles, nuclear fission products, heavy nuclei		20

13.2.6 Organ dose weighting factors

By definition, the weighting factor for the whole body is 1, such that 1 Gy of radiation delivered to the whole body (i.e. an evenly distributed 1 J of energy deposited per 1 kg of body) is equal to 1 Sv (for photons with a radiation weighting factor of 1, see Tab. 13.1). Therefore, the weighting factors for each organ in the whole body must sum to 1 as the unit Gy is defined per kilogram and is therefore a local effect. As the table below shows, 1 Gy (taking the example of photons as the incident radiation) delivered to the gonads is equivalent to 0.08 Sv to the whole body—in this case, the actual energy deposited to the gonads, being small, would also be small.

Table 13.2: Conventional radiation quality factors to calculate equivalent doses.

	TISSUE WEIGHTING FAC TORS		
ORGANS	ICRP30(I36) 1979	ICRP60(I3) 1991	ICRP103(I6) 2008
Gonads	0.25	0.2	0.08
Red Bone Marrow	0.12	0.12	0.12
Colon	-	0.12	0.12
Lung	0.12	0.12	0.12
Stomach	-	0.12	0.12
Breasts	0.15	0.05	0.12
Bladder	-	0.05	0.04
Liver	-	0.05	0.04
Oesophagus	-	0.05	0.04
Thyroid	0.03	0.05	0.04
Skin	-	0.01	0.01
Bone surface	0.03	0.01	0.01
Salivary glands	-	-	0.01
Brain	-	-	0.01
Remainder of body	0.3	0.05	0.12

The goal of this experiment is to get familiar with different sources available in the laboratory and different dosimetric devices, such as neutron dosimeter, γ-dosimeter and surface contamination monitors. Different types of detectors will be used in the experiments to measure the γ and neutrons dose rate as well as the surface activity. The latter is important for determining the contamination which a material or a surface might have. The dose rate (Sv/h) and the surface contamination (Bq/cm^2) are two important parameters to be known in order to work safely and according to radioprotection regulations. Note that the regulation is country specific.

Knowing the dose rate of a source is of primary importance to respect the annual dose limits: (1) 1 mSv for public members and (2) 20 mSv for professionals using radiations (industry, nuclear industry, hospital, medical imagery centres, etc.).

13.3 Experiment description

The following measurements will be demonstrated:

- **Experiment 1:** Neutrons and gamma radiation detection as a function of the source distance
- **Experiment 2:** Moderation effect (polyethylene blocks) and neutron dose rate
- **Experiment 3:** Dose rate of different sources, measurement of surface contaminations, nuclide identification with portable equipment)
- **Experiment 4:** Analyse a background spectrum obtained with a HPGe system
- **Experiment 5:** Identify an unknown nuclide.
- **Experiment 6:** Check definition of exposure, effective dose, biological dose, Q-factor, Discuss the units.

13.3.1 Important Precautions

The following precautions need to be followed at all times to ensure the safety of the experimenters and the equipment and to create high quality results.

1. Do not stay within the safe where the Pu-Be source is located.
2. Use a personal dosimeter per person doing the experiment.
3. Check for hands contaminatin at the end of the experiment using the “hand/foot” monitor located in the lab corridor. Report any problem toa lab assistant.

13.4 Required setup

The following components are required for this experiment. Check to see if they are available. If they are not available, please speak with your lab instructor.

1. A Pu-Be source placed in a safe for safety and security reasons. The source is placed at the end of a metallic railing system allowing moving easily different detectors placed on a platform. The distance to the source is directly measured on a digital display, see Figure 13.1.
2. Acquisition equipment: neutron Berthold dosimeter. Geiger-Müller sensor for ambient dose rate measurement (probe connected to LB 112 unit).
3. Power supply NIM rack with He_3 or BF_3 ionisation detector, pre-amplifier, amplifier, SCA and scaler. This equipment is to be used for Exp. 13.2.

Different low activity sources included minerals. LB 124 Berthold surface contamination detector and Exploranium dosimeter (with nuclide identification capability) to measure and quantify the sources and the possible surface contamination, see Figure 13.2 and Figure 13.3.

Figure 13.1: Experimental setup for the neutron and gamma detection.

Figure 13.2: Images of the dosimetric equipment to be used.

Figure 13.3: Example of samples to be measured.

13.5 Operational settings

For the neutron and gamma detection experimental part:

- The amplifier settings for the He-3 or BF3 ionisation detectors should be preferentially used in such manner that the dominant peak corresponds to a voltage of 4 to 5 volts in each case. It is advised to re-check the settings for each detector with the help of the oscilloscope.
- High tensions for the He-3 and BF3 detectors are 1.1 kV and 1.65 kV, respectively.

For the characterisation of radioactive sources and radioprotection measurements:

- Follow the instruction of the lab assistant.

13.6 Measurement steps

13.6.1 Experiments 1 and 2: neutron and gamma detection experimental part:

1. Place one of the ionisation detectors, neutron Berthold dosimeter, Geiger-Müller sensor (probe connected to LB 112 unit) and install it on the platform of the metallic railing system in the safe; be sure that the detectors are correctly placed and connected.
2. Switch on the power supply, set the appropriate voltage and all the associated electronic units, adjust the settings and verify the characteristics of the signal using the oscilloscope. The coarse and fine gains must be adjusted to get appropriate pulse heights.
3. Take dose and count rate measurements at four different distances from the Pu-Be source using the railing system to change the distance.
4. Fix detectors and measuring sensors at distance of 0.5 m from the Pu-Be source. Take dose and count rate measurements without and with polyethylene blocks in order to observe the polyethylene effect on neutron moderation. Compare dose and count rates from all detectors and sensors.
5. Use appropriate measuring equipment while adjusting the experimental setup to ensure the safety and radioprotection standards.

13.6.2 Experiments 3: For the characterisation of radioactive sources and radioprotection measurements:

1. Choose appropriate measuring equipment in order to determine type of radiation, dose rate, and radionuclides present in the radioactive source.

2. Use a different type of shielding material to observe if the radioactive sources are pure radiation emitters.
3. Take dose/count rates, spectrum measurements to identify appropriate radionuclide/-s present in the radioactive source, state a dose rate and determine precautions and suitable shielding material.
4. Use tables of radionuclides, decays schemes, GENIE-2000 software from Canberra, etc. for your identification and characterisation of radioactive sources.

13.7 Data analysis

- Analysis of the polyethylene effect on neutron moderation.
- Explanation of differences between gamma, and neutron detection.
- Evaluation of the measuring capabilities of different equipment used in radioprotection.
- Analysis of the unknown radioactive sources.
- Analysis of the background spectrum (provided by the lab assistant)

13.8 Expected results

- γ-dose rate and neutron dose rate as a function of the distance to the source
- Dose rate as a function of polyethylene thickness; discuss the measured curve.
- Proper usage of surface contamination monitor.
- Identification of significant peaks of the background spectrum.
- Identification of the radiation type, dose rate and radionuclides present in the unknown radioactive sources and discussion of the suitable shielding materials.
- Understanding of the basic terminology in radioprotection.

A Statistical analysis and error prediction

Characterization of Data

Radioactive decay, as well as the detection of radiation via its interaction with matter, are random processes. Consequently, any measurement involving radiation is subject to some degree of fluctuations. These inherent, or so-called statistical, fluctuations are unavoidable and represent a source of imprecision or error on the quantity being measured. In order to understand the errors associated with a given measurement, some standard terms are defined below.

Let us assume that N measurements of the same physical quantity have been carried out and the corresponding values are x_1, x_2, x_3, x_4 ..... x_N. Let us further assume that a single typical value x_i from this set can only assume an integer value. The data represent, for example, the number of counts obtained with a radiation counter over a given interval of time. The two elementary properties of this data set are the **Sum**, Σ, and the **Experimental Mean**, $\overline{x_e}$:

$$\Sigma = \sum_{i=1}^{i=N} x_i \tag{A.1}$$

$$\overline{x_e} \equiv \Sigma / N \tag{A.2}$$

It is often convenient to represent a data set by a frequency distribution F(x), as defined below:

F(x) = number of occurrences of value x / number of measurements

The distribution as per definition is automatically normalized, i.e.

$$\sum_{i=0}^{\infty} F(x) = 1 \tag{A.3}$$

The mean value of the distribution being its first moment can be written as:

$$\overline{x_e} = \sum_{i=0}^{\infty} xF(x) \tag{A.4}$$

However, there is another important term, called the sample variance, which quantifies the magnitude of internal fluctuations in the data set. It is defined through a residual of any data point from the mean of the distribution, given by:

$$d_i \equiv x_i - \bar{x}_e \tag{A.5}$$

There will be equal contributions of positive and negative residuals so that:

$$\sum_{i=1}^{N} d_i = 0 \tag{A.6}$$

However, if we take the square of each residual and perform the sum as above, then we will get a positive result.

It must be kept in mind that in reality we are interested in finding the departure from the true mean and not the experimental mean value, i.e. the deviation from the true mean can be written as:

$$\epsilon_i \equiv x_i - \bar{x} \tag{A.7}$$

where $\bar{x}$ stands for the true mean value, usually not known. The sample variance, which is a measure of internal scatter in the data, is then defined as:

$$s^2 \equiv \bar{\epsilon}^2 = \frac{1}{N}\sum_{i=1}^{N}(x_i - \bar{x})^2 \tag{A.8}$$

Since the true mean is not known, the above definition presents a real difficulty in getting the value of the variance. It is however found that an alternative expression presented below is valid where true mean is replaced by the experimental mean value, which is simple to obtain from the measured values.

$$s^2 = \frac{1}{N-1}\sum_{i=1}^{N}(x_i - \bar{x}_e)^2 \tag{A.9}$$

The sum of squared residuals in the above equation is divided by N-1, rather than by N as in A.8, a distinction that is only significant when N is small. For a large data set, therefore, the sample variance can be thought of as the mean squared value of either the residuals or the deviations. The variance can also be expressed via the distribution function as:

$$s^2 = \sum_{x=0}^{\infty} (x - \bar{x})^2 F(x) = \overline{x^2} - (\bar{x})^2 \tag{A.10}$$

The R.H.S parameters can be determined from the experimental values.

In order to have greater insight on the precision of the measurements, it is necessary to perform a statistical analysis of the data by employing statistical models.

Statistical Models

Under certain conditions, the distribution arising from the repetition of a measurement can be predicted. For example, for a binary process (two mutually exclusive events), where the measurement is either a success or a failure and the probability of success remains fairy constant, the distribution can be interpreted as a Binomial, Poisson or Gaussian distribution, depending upon the conditions.

The Binomial Distribution

This is the most general statistical model and widely applicable to all situations with constant probability of success 'p'. It is unfortunately cumbersome to apply to radioactive decay because of the large number of nuclei and only rarely used in nuclear applications. The distribution for x number of successes with n trials, each with a success probability p, is given by:

$$P(x) = \frac{n!}{x!(n-x)!} p^x (1-p)^{n-x} \tag{A.11}$$

where P(x) is the predicted probability distribution function and is defined for integer values of x and n as shown in Figure A.1.

The distribution assumes that the events are a) dichotomous, b) mutually exclusive, c) independent and d) random. The following are the important properties of the Binomial distribution:

The distribution is normalized, i.e. the total probability is unity:

$$\sum_{x=0}^{n} P(x) = 1 \tag{A.12}$$

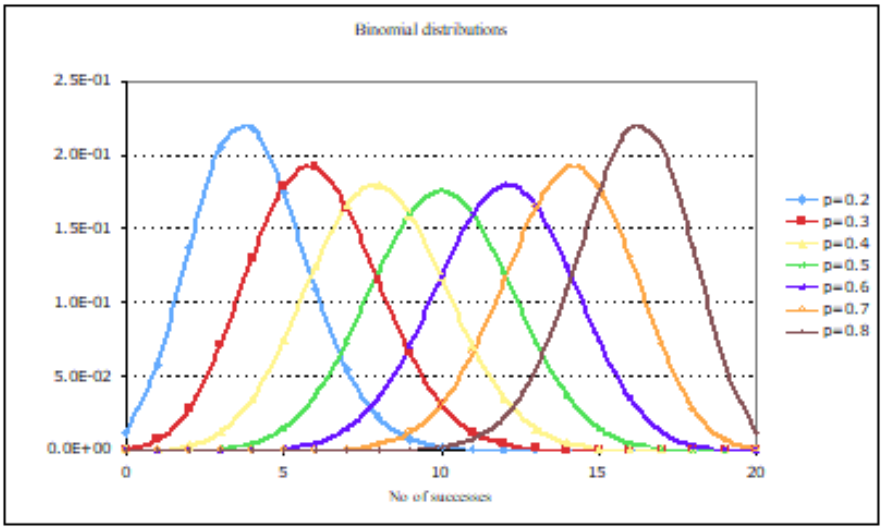

Figure A.1: Example of Binomial distributions

The average value for the distribution is given by:

$$\bar{x} = \sum_{x=0}^{n} xP(x) = pn \tag{A.13}$$

Similarly, the variance of the distribution is given by:

$$\sum_{x=0}^{n} (x-\bar{x})^2 P(x) = np(1-p) = \bar{x}(1-p) \tag{A.14}$$

Thus, we have an expression that provides an immediate prediction of the magnitude of inherent data fluctuation associated with the Binomial distribution in terms of the basic parameters of the distribution, n and p.

The Poisson Distribution

In certain applications such as radioactivity measurements or particle beam transmission experiments, binary processes can be characterised by a constant and small probability. Under these conditions, the binomial distribution reduces to the Poisson distribution, which is given by:

$$P(x) = \frac{(pn)^x e^{-pn}}{x!} = \frac{(\bar{x}^x e^{-\bar{x}})}{x!} \tag{A.15}$$

where pn = $\bar{x}$

It is evident from the last equation that the Poisson distribution, unlike the Binomial distribution, depends upon a single parameter, viz. the product of n and p. The distributions for some average values are depicted in Figure A.2.

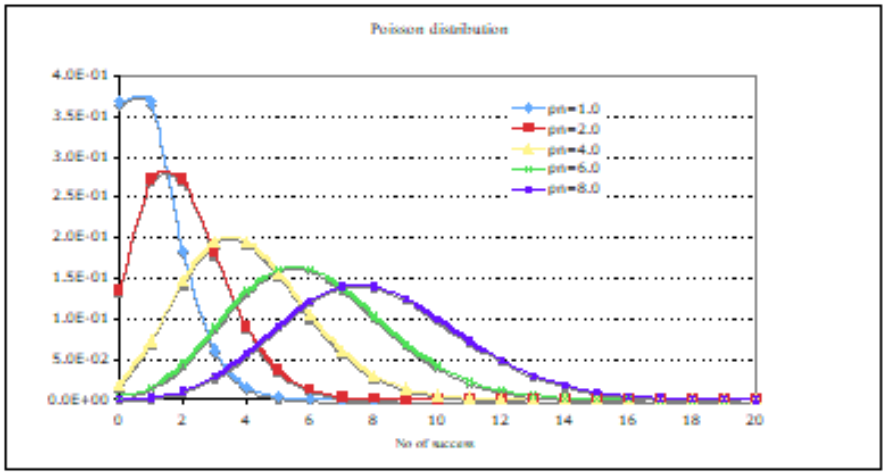

Figure A.2: Example of Poisson distributions

Some of the properties of the Poisson distribution follow directly, e.g.

The distribution is normalized:

$$\sum_{x=0}^{n} P(x) = 1 \tag{A.16}$$

the average value for the distribution is given by:

$$\bar{x} = \sum_{x=0}^{n} xP(x) = pn \tag{A.17}$$

and finally the variance is given by:

$$\sigma^2 \equiv \sum_{x=0}^{n} (x-\bar{x})^2 P(x) = np = \bar{x} \tag{A.18}$$

so that the predicted standard deviation is given by:

$$\sigma = \sqrt{\bar{x}} \tag{A.19}$$

Thus, we see that the predicted standard deviation of a Poisson distribution is simply the square root of the mean value of the distribution it characterises. It may be recalled that the same results would be obtained for the Binomial distribution for p«1 (see A.14), which is already assumed in the formulation of the Poisson distribution.

The Gaussian or Normal Distribution

The Poisson distribution is a simplification of the Binomial distribution in the limit p«1. If, in addition, the mean value of the distribution is large (>20), an additional simplification of the Binomial distribution results, leading to the Gaussian, or Normal, distribution, given by:

$$P(x) = \frac{1}{\sqrt{2\pi\bar{x}}}\exp\left(-\frac{(x-\bar{x})^2}{2\bar{x}}\right) \tag{A.20}$$

This is again a point-wise distribution function defined only for integer values of x. It shares the earlier mentioned properties with its parent, the Poisson distribution.

The distribution is normalized:

$$\sum_{x=0}^{n} P(x) = 1 \tag{A.21}$$

the average value of the distribution is given by:

$$\bar{x} = \sum_{x=0}^{n} xP(x) = pn \tag{A.22}$$

and finally the variance is given by:

$$\sigma^2 = \sum_{x=0}^{n} (x-\bar{x})^2 P(x) = np = \bar{x} \tag{A.23}$$

so that the predicted standard deviation is given by:

$$\sigma = \sqrt{\bar{x}} \tag{A.24}$$

A typical distribution for a given average value is presented in Figure A.3.

Two important characteristics of the Gaussian distribution are a) it is symmetric about the

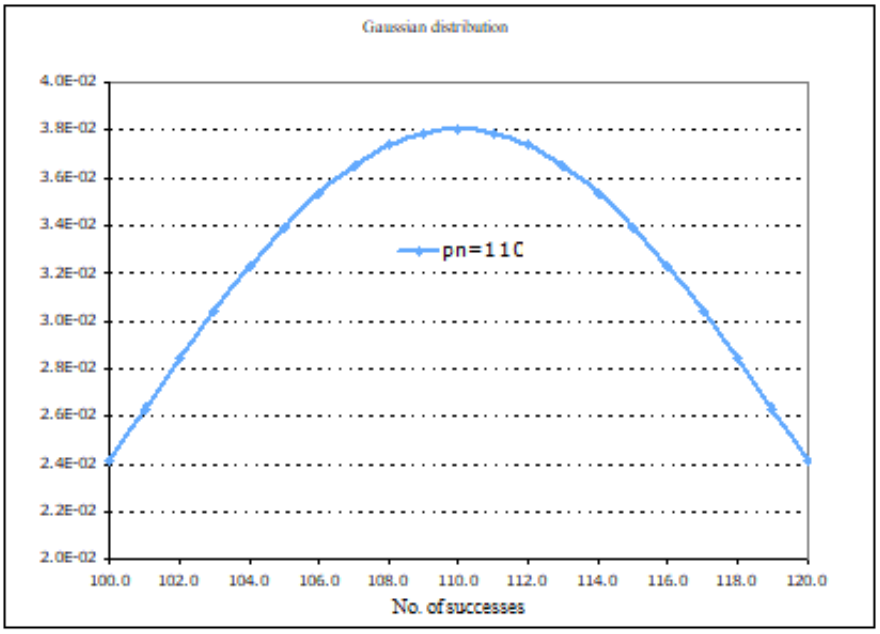

Figure A.3: Example of Gaussian distribution

mean value, and b) the mean value being large, P(x) is a slowly varying function. In terms of the standard deviation, this can be rewritten as:

$$G(\epsilon) = \sqrt{\frac{2}{\pi \bar{x}}} e^{-\frac{\epsilon^2}{2\bar{x}}} \tag{A.25}$$

Furthermore, if is expressed in units of σ ($t^2 = \epsilon^2/\bar{x} = \epsilon^2/\sigma^2$), then the above equation in its most general form becomes:

$$G(t) = \sqrt{\frac{2}{\pi}} e^{-\frac{t^2}{2}} \tag{A.26}$$

From the above, one finds that, corresponding to values of "t" of 1, 2 and 3, one has probabilities of occurrence of 68.3, 95.5 and 99.7%, respectively. Thus, for example, the Gaussian distribution predicts that 68.3% of the time, the measured x value will be confined within a single sigma value around the mean value.

The following important aspects of statistical models should be kept in mind, viz. a) they allow one to ascertain if a set of multiple measurements of the same physical quantity conforms to the fluctuations predicted by the model, and b) they enable an error to be assigned to a single measurement, i.e. even in the absence of several measurements (see below).

Single measurement and standard deviation

If the single measurement belongs to either a Poisson or Gaussian statistical distribution, then, by considering the single value to be the mean value, the variance of a set of measurements of which that single measurement forms a part would be equal to the mean value itself. The corresponding standard deviation is thus the square root of the mean value. We therefore conclude that

Standard deviation = $\sqrt{s^2} = \sigma = \sqrt{x}$

is the best estimate of the deviation from the true mean, which is taken to be the value of the single measurement.

Error Propagation

In most of applications, it is also important to consider other parameters contributing to error apart from the counting statistics. More often, the data obtained need to be processed by additional steps such as addition, subtraction, multiplication and other functional manipulations, in order to arrive at the specific parameter of interest. The numerical values arising from these steps will be distributed in a way that is dependent on both the original distribution and the types of operations carried out.

Let us imagine that a particular measurement follows a Gaussian distribution. Now, if the same measurement is repeated while doubling the measurement time, or by increasing the detector efficiency by a certain factor, the question arises as to whether the new distribution would also be Gaussian. From Eqs. A.25 and A.26, it is quite evident that the new distribution would be the same, whereas the average value and the variance would be different. It is found that operations such as multiplying or dividing the data by a constant, combining two Gaussian-distributed variables through addition, subtraction or multiplication, etc., all produce data which retain the basic Gaussian distribution characteristics. While the mean of the derived distribution can be simply predicted from the mean values of the original distributions, the standard deviation values are not so very obvious.

The standard deviation on a quantity u(x, y ,z,...) can be derived from the standard deviation of each independent variable denoted by σ_x, σ_y, σ_z ..., using the standard error propagation formula given by:

$$\sigma_u^2 = \left(\frac{\partial u}{\partial x}\right)^2 \sigma_x^2 + \left(\frac{\partial u}{\partial y}\right)^2 \sigma_y^2 + \left(\frac{\partial u}{\partial z}\right)^2 \sigma_z^2 + \ldots \tag{A.27}$$

The use of Eq. A.27 is illustrated below for some simple cases.

Sums or differences of counts

Let us define: u = x + y or u = x - y

Then application of Eq. A.27 yields:

$$\sigma_u^2 = (1)^2\sigma_x^2 + (\pm 1)^2\sigma_y^2 \tag{A.28}$$

or

$$\sigma_u = \sqrt{(\sigma_x^2 + \sigma_y^2)} \tag{A.29}$$

This is normally referred to as combining the errors in quadrature sum.

Multiplication or division by a constant

For the functions u = Ax and v = x/B, the corresponding standard deviations, using Eq. A.27, would be given by:

$$\sigma_u^2 = A^2\sigma_x^2 \quad \text{and} \quad \sigma_v^2 = \sigma_x^2/B^2 \tag{A.30}$$

However, in each case, the fractional (or relative) standard deviation (σ_u/u or σ_v/v) would be given simply by σ_x alone.

Multiplication of counts:

For the case u = xy:

$$\sigma_u^2 = y^2\sigma_x^2 + x^2\sigma_y^2 \tag{A.31}$$

Dividing each side by $u^2 = x^2y^2$, we get:

$$\left(\frac{\sigma_u^2}{u}\right)^2 = \left(\frac{\sigma_x^2}{x}\right)^2 + \left(\frac{\sigma_y^2}{y}\right)^2 \tag{A.32}$$

Similarly, if u = x/y, the square of the fractional variance would be given by the same Eq. A.32. Thus, for either u = xy or u = x/y, the fractional errors in x and y combine in quadrature sum to give the fractional error in u.

Mean value of multiple independent counts

Imagine N repeated counts are taken, each for the same period of time. Then, their sum and variance, as derived from the formulas of error propagation, are given by:

$$\Sigma = x_1 + x_2 + x_3 ..... + x_N \tag{A.33}$$

and

$$\sigma_\Sigma^2 = \sigma_{x_1}^2 + \sigma_{x_2}^2 + \sigma_{x_3}^2 + ... + \sigma_{x_N}^2 = x_1 + x_2 + x_3 ..... + x_N = \Sigma \tag{A.34}$$

or $\sigma_\Sigma = \sqrt{\Sigma}$, i.e. the standard deviation for the sum is the same as that for a single measurement performed over the entire duration of all the independent measurements. The mean value of all these measurements would be given by:

$$\bar{x} = \frac{\Sigma}{N} \tag{A.35}$$

Thus, the error associated with the mean value is given by:

$$\sigma_{\bar{x}} = \frac{\sigma_\Sigma}{N} = \frac{\sqrt{\Sigma}}{N} = \frac{\sqrt{N\bar{x}}}{N} = \sqrt{\frac{\bar{x}}{N}} \tag{A.36}$$

The above states that the mean value based on N independent counts will have an expected error that is smaller by a factor $\sqrt{N}$ compared with any single measurement on which the mean is based. A general conclusion, is that if we wish to improve the statistical precision of a given measurement by a factor of 2, we must count for four times the initial counting time.

B Radiation protection considerations

Radiation Exposure and Dose

For personnel working with radiation, e.g. at a hospital or in a laboratory, it is mandatory to respect established prescriptions. In Switzerland, it is mandatory to know and follow strictly the official radioprotection rules “Ordonnance sur la radioprotection, ORaP, 22 juin 2004”. This document specifies in detail the procedures that need to be followed when working in a radiation environment or in the presence of radioactive material. It the context of the current laboratory work, it is required to use a calibrated portable dosimeter (usually one dosimeter per one group conducting a specific experiment) to measure the total dose received during the course of the day. It is essential to respect the prescribed limit of 1 mSv per year, for people non-professionally exposed to radiation.

The following agencies continually release precise information related to the biological effects of radiation, as also to prescriptions for its usage:

a) International Commission of Radiological Units (ICRU),
b) International Commission of Radiological Protection (ICRP),
c) US National Commission on Radiation Protection (NCRP).

Exposure

In order to help understand the health effects of radiation on human beings, it is important to introduce certain concepts, as also the units employed for quantifying the amount of radiation and its effects. Two terms one uses in the latter context are exposure and dose. Radiation exposure is measured in terms of the electronic charge created in unit mass of air as a result of the interaction of the radiation, i.e. ionisation of the constituents of air. In other words, the exposure X is given by:

$X = dQ/dm$

where dQ and dm stand for the amount of charge produced in air of mass dm. The SI unit of exposure is C/kg.
The historical unit of radiation exposure is the roentgen (written as R), defined as the exposure that results in the generation of one electrostatic unit of charge (2.08×10^9 ion pairs) per 0.001293g (1 cm^3 at STP) of air. The above-mentioned two units of exposure are related by:

1 R = 2.58×10^{-4} C/kg

Absorbed Dose

The exposure unit is not directly linked to the physical phenomena of interest in considering radiation effects, although it is often of interest in radiation dosimetry. Changes in physical properties and/or the induction of chemical reactions are found to depend more directly on the energy absorbed in a given medium. If, instead of air, one needs to consider another material, e.g. human tissue, then clearly both exposure and the energy absorbed per unit mass would depend on the medium's properties, as also on the type and energy spectrum of the incident radiation.

The historical unit for the absorbed dose has been the rad, defined as 100 ergs/g. This has been replaced by the SI unit, the gray (Gy), defined as 1 J/kg. The two units are related to each other by:

1 Gy = 100 rad

It has been found that the absorbed dose in air and water (which is a close approximation for human tissue) is about the same, for a given exposure to gamma radiation. This follows from the similarity of the average atomic number in the two cases.

Biological Dose

A given amount of absorbed dose, i.e. measured in gray, can have different biological effects on living organisms, depending on the type and energy of the interacting radiation. This may be attributed to the fact that the manner in which the energy is deposited along the path of the radiation can differ considerably. Thus, for example, a particle of high Linear Energy Transfer (LET), such as a heavily charged ion, can cause much greater biological damage, for a given amount of energy absorbed, than low-LET particles such as electrons. This leads to defining biological (or equivalent) dose H, as the absorbed dose D multiplied by the "quality factor" Q of the radiation involved, i.e.

$H = D \cdot Q$

The current unit for biological dose is the sievert (Sv). Historically, it was the rem, with 1 Sv = 100 rem. The quality factor (which converts gray to sievert) is a measure of the biological

effects of the given radiation, relative to that of 200 keV X-rays.

For fast electrons, X-rays and gamma rays of different energies, one finds that Q=1, whereas for heavy charged particles it is much greater. For neutrons as well, Q > 1 and depends considerably on the neutron energy (which determines the cross-sections for the different secondary-particle producing reaction rates). The quality factors for different radiation types are given in Tab. B.1.

Table B.1: Quality factor for different types of radiation.

Radiation type	Energy (MeV)	Quality factor
Electrons and photons	All energies	1
Apha, multiple-charged particles, and fission fragments	All energies	20
Protons	>2 MeV	5
Neutrons	< 10 keV	5
	10 to 100 keV	10
	>100 keV to 2 MeV	20
	>2 to 20 MeV	10

Radiation dose limits

The principle of ALARA (As Low As Reasonably Achievable) is the central philosophy of radiation protection and safety. The official prescriptions for biological dose limits in Switzerland are summarised below:

For professionals working with radiations: 20 mSv/y
For the general public: 1 mSv/y

Instruments currently employed in our laboratory for dose measurements

- The experiments are conducted in a controlled area equipped with fixed gamma dosimeters for monitoring the radiation levels. In each room, an alarm will be audible if the

dose rate exceeds 1 mSv/h.

- It is very important to avoid any inhalation or ingestion of radioactivity. It is forbidden to eat and/or drink in the controlled area. In the rare eventuality of a surface contamination, a shower is available in the locker room.
- For controlling the dose, each group of students will receive, at the beginning of the experimental day, a portable dosimeter. This instrument has to be worn by one of the persons while working in the controlled zone. During breaks or at lunch time, the dosimeter must be deposed at the entrance station. The log-book entry must be made while taking and depositing a dosimeter. The dose registered has to be written in the log-book at the end of the day.
- In case of any unknown situation or accident while manipulating a source, or a radioactive liquid, immediately alert the laboratory staff for assistance. The general emergency numbers are listed on the emergency sheet in Figure B.1
- The laboratory is fully equipped with diverse instruments available to measure dose levels (see Tab. B.2).
- Finally, it is useful to recall that radioactivity exists in nature and we are continuously exposed to radiation. Primary contributions come from sources in the earth (radon gas and also food) and from outer space, in the form or cosmic rays. In the context of laboratory experiments, the natural sources of radiation result in "background" counts, and these usually need to be accounted for by measuring the background contribution separately.
- In addition to the natural sources, there exists a large list of artificial or man-made sources responsible for the overall radiation level to which a person can be exposed:
  - Smoke detectors
  - Self-luminous dials and signs
  - Global radioactive contamination due to historical nuclear weapons testing
  - Radiation techniques in medicine
  - Emissions of radioactivity from burning fossil fuels, e.g. from coal-fired power plants
  - Normal operation of facilities used for nuclear power generation and scientific research
  - Nuclear power station or nuclear fuel reprocessing accidents (though these are very rare)
- The average "natural" radiation dose level is around 0.1 μSv/h in Switzerland (meaning 1 μSv per working day).

Figure B.1: Emergency sheet

Table B.2: Details of the various dosimeters used for measurement of doses received by personnel.

No.	Type of dosimeter	Model No.	Range of measurement	Location
1.	X-Ray/Gamma	RADOS-50S	1-10 μSv	Entrance
2.	Gamma dose rate meter	Berthold BF-2338-1	0-10^3 μSv/h	Counting room
3.	Neutron dose rate meter	Berthold LB 123	-	CROCUS hall

C Description of the CROCUS reactor

Reactor type and specifications

CROCUS is a light water moderated reactor and, for ease of operation, is limited to a maximum fission power of 100 watts. It is a cylindrical reactor with two distinct concentric fuel zones. The inner zone consists of uranium oxide fuel rods with an enrichment of 1.806%, arranged in a square lattice with a pitch of 1.837 cm. The outer zone consists of uranium metal rods, with an enrichment of 0.947% and a square lattice pitch of 2.917 cm. There are 336 fuel rods in the central zone, and the outer region may contain either 172 or 176 fuel rods. The reactor core is located in a tank of 132.4 cm diameter, filled with demineralized light water such that there is water surrounding each fuel rod for providing the desired moderation of fission neutrons and a sufficient thickness of water around the outer region to act as reflector. Figure C.1 presents a top view of the reactor, with some of the principal components clearly visible.

The principal specifications of the two different types of CROCUS fuel rods are summarized in Table C.1. Each fuel rod consists of pellets, stacked inside aluminium clad with the surrounding gap filled with inert helium gas. The fuel rods are held in a vertical position with the help of top and bottom grids, each containing a 0.5 cm layer of cadmium to absorb the neutrons leaking axially from the reactor.

Shut-down of the CROCUS reactor can be achieved via two independent types of mechanisms. The first involves the rapid insertion (in the inner fuel region) of two cross-shaped safety rods containing cadmium. The second mechanism is the rapid opening of four valves, which causes the water level in the tank to drop rapidly. Each of the six separate shut-down units – the two safety rods and the four valves (which cause the water to exit rapidly into four separate chambers) – is sufficient on its own to bring the reactor to a safe sub-critical state.

Fine control of the CROCUS reactor is achieved either by adjusting the water level in the core or by means of two control rods, each containing B_4C pellets, located diagonally opposite each other at the edge of the core.

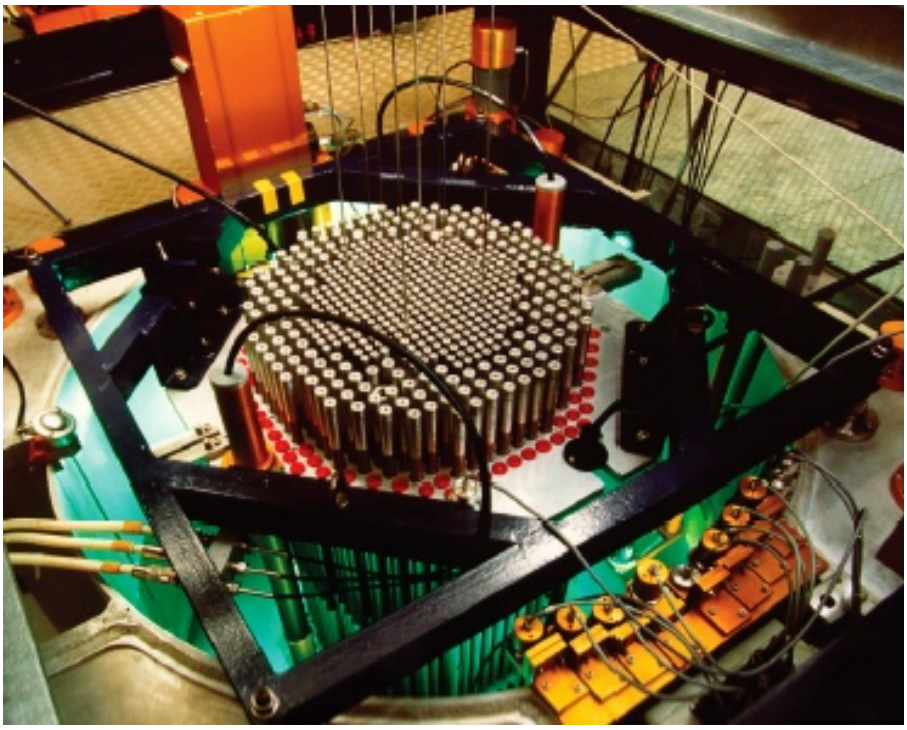

Figure C.1: Top view of the CROCUS reactor, showing the cylindrical water tank, the two types of fuel rods in the inner and outer core regions, as well as neutron detectors forming part of the reactor instrumentation. The two safety rods (cadmium crosses) are fully inserted into the core in this picture.

Table C.1: Specifications of the CROCUS fuel rods.

Description	Inner zone	Outer zone
Fuel	UO_2	U-metal
Density (g/cm^3)	10.556	18.677
Fuel radius (cm)	0.526	0.850
Fuel height (cm)	100.0	100.0
Inner radius of aluminium clad (cm)	0.545	0.8675
Thickness of clad (cm)	0.085	0.100
Pitch of fuel (cm)	1.837	2.917

Criticality conditions

Corresponding to the two fine-control mechanisms, there are two different ways in which the CROCUS reactor can be made critical. In the first case, the water level is increased slowly to reduce the axial neutron leakage from the core. In the second case, the water level is kept fixed and the position of one of the two fine control rods is adjusted to achieve criticality, the

withdrawal of a control rod from the core corresponding to a reduction of neutron absorptions. In the current laboratory context, the first method will be used to in the “approach-to-critical” experiment, while rod withdrawal will be applied in the control rod calibration experiment.

Finally, it needs to be mentioned that four neutron detectors (2 fission chambers and 2 BF_3 counters) are located at the edge of the CROCUS core, in the water reflector region, for providing all necessary information regarding the state of the reactor – sub-critical (monitored using a neutron source) or critical (flux level, reactor period, etc.).

D Data Analysis References

Solving In-hour Equation and plotting the neutron population time dependence in MATLAB

```
%Initialization
clear all; close all; clc;

% Delayed neutron data for CROCUS
l = [ 0.01336; 0.03259; 0.1211; 0.30604; 0.86235; 2.89645];
b = [ 0.00024; 0.0013; 0.00125; 0.00279; 0.00128; 0.00051];
beta = sum(b);

% Generation time (in seconds)
L = 45E-06;

% Reactivity and plot initialization
Rea_dollars = [ -2 -1 -0.1 -0.01 0.01]; % Reactivities in dollars
t = 0:0.1:500; t = t(:);                % Time vector for plot
nr = length(Rea_dollars);
nt = length(t);
N = zeros(nt,nr);                       % Neutron population
Lab = cell(nr,1);                       % Label for plot

for n = 1:nr
    % Reactivity
    rdollars = Rea_dollars(n);  % In dollars, i.e. per unit of beta
    r = rdollars*beta;

    % Solving In-hour equation
    syms s;
    [w, Orders, A] = poles(...
        ( L + b(1)/(l(1)+s) + b(2)/(l(2)+s) + ...
        b(3)/(l(3)+s) + b(4)/(l(4)+s) + ...
        b(5)/(l(5)+s) + b(6)/(l(6)+s) ) / ...
        ( -r + L*s + b(1)*s/(l(1)+s) + ...
        b(2)*s/(l(2)+s) + b(3)*s/(l(3)+s) + b(4)*s/(l(4)+s) + ...
        b(5)*s/(l(5)+s) + b(6)*s/(l(6)+s)));
    nw = length(w);

    % Neutron population time behavior
    P = exp(repmat(w',nt,1).*repmat(t,1,nw))*A;
    N(:,n) = P;

    % Parameters for plot
```

```
41      Lab{n} = ['\rho/\beta = ', sprintf('%1.2f $',rdollars)];
42  end
43
44  %Plot Neutron population behavior for different reactivity values
45  plot(t,N,'-','LineWidth',1);
46  xlabel('Time (s)');
47  ylabel('Normalized neutron population');
48  title(['Evolution of the neutron population - ',...
49      '\beta = ', sprintf('%1.0f pcm ', beta*1e5),...
50      'and \Lambda = ', sprintf('%1.2g s',L)]);
51  legend(Lab);
```

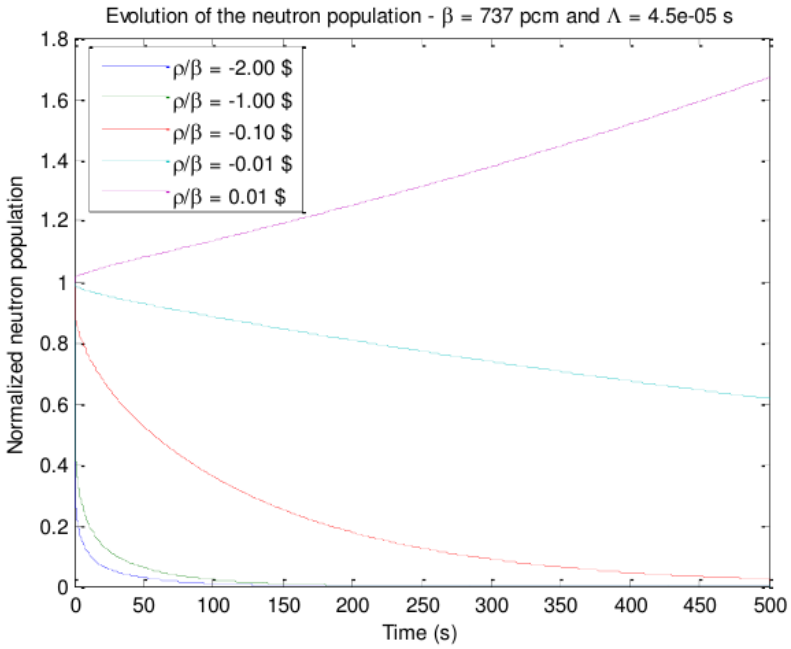

Figure D.1: Curve fitting tool in MATLAB

Fitting data in MATLAB using cftool

This appendix illustrates how to import ascii data in MATLAB R2013/2014 and fit them with cftool.

- Ascii data in column format can be imported using the "Import Data" command of MATLAB (Home/Import Data in the Ribbon) or using for example "load" on the MATLAB command line
- Define the weight "w" from the uncertainty "s" on each points using the equation $w = 1/s^2$
- Launch cftool from the MATLAB command line and select data and the equation to fit (using the Custom Equation if none of the choices are satisfactory).

- Results of the fit are indicated with the confidence interval on the left. Residues of the fit can be plotted as well.

The figure D.2 shows an example for an exponential fit using the cftool GUI. More help can be obtained from MATLAB searching for "Interactive Curve and Surface Fitting" in the help menu.

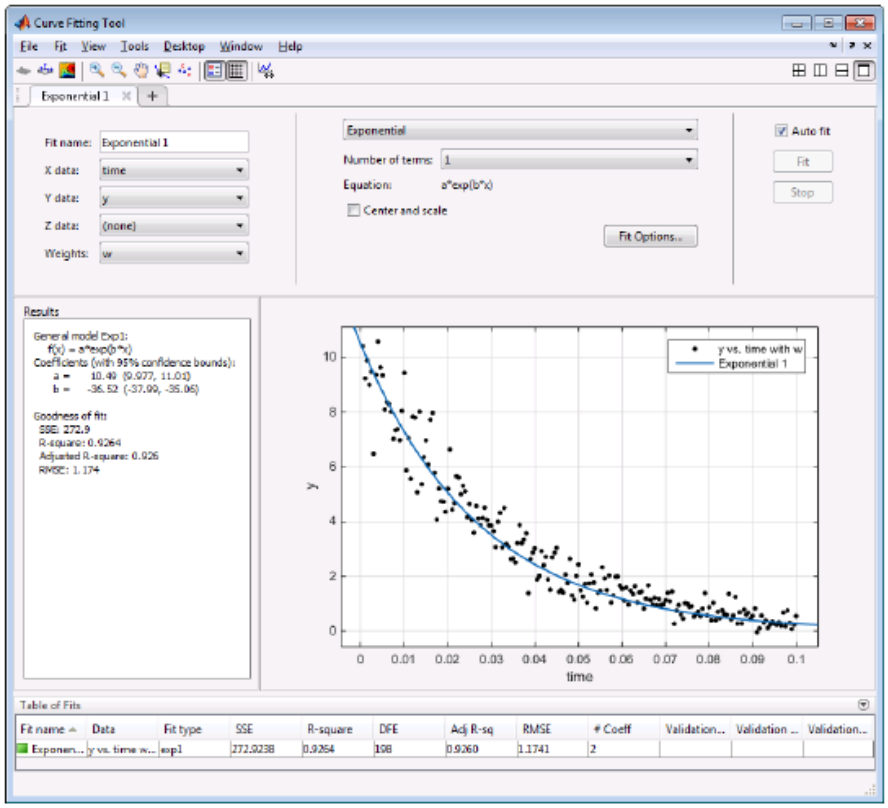

Figure D.2: Curve fitting tool in MATLAB

Fitting data in Excel using the add-in Solver

Non Linear Curve Fitting (Example)

The Solver Add-in in Microsoft Excel can be useful and utilized to solve many types of problems, including fitting non linear curves to data. In order to get access to it, go to the « Manage Add-ins » section of the options page and check the « Solver Add-in » box. This will result in an extra icon appearing in the analysis section of the Data ribbon as shown in Figure D.3.

The screen shot in Fig. D.3 shows how the data can be laid out. The columns « **X** » and « **Y** » contain the data collected from an experiment; « **X** » being the set value and « **Y** » the response of the system, and we want to fit a four parameter logistic function which has the following formula:

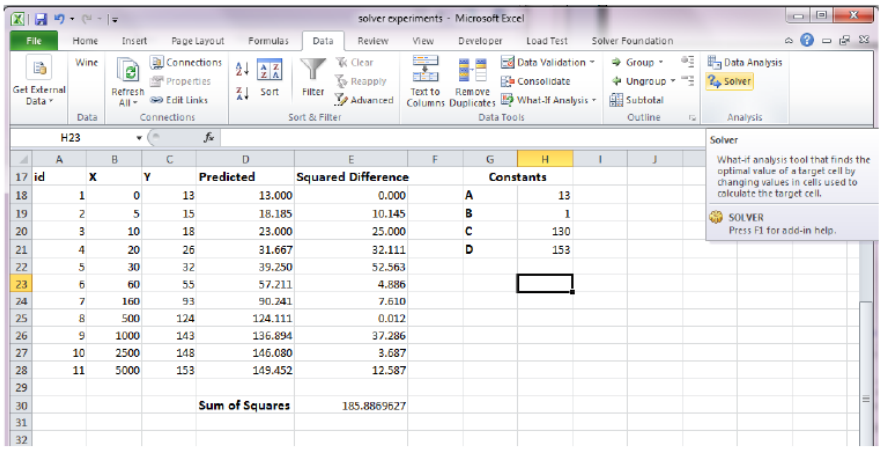

	A	B	C	D	E	F	G	H
17	id	X	Y	Predicted	Squared Difference		Constants	
18	1	0	13	13.000	0.000		A	13
19	2	5	15	18.185	10.145		B	1
20	3	10	18	23.000	25.000		C	130
21	4	20	26	31.667	32.111		D	153
22	5	30	32	39.250	52.563			
23	6	60	55	57.211	4.886			
24	7	160	93	90.241	7.610			
25	8	500	124	124.111	0.012			
26	9	1000	143	136.894	37.286			
27	10	2500	148	146.080	3.687			
28	11	5000	153	149.452	12.587			
29								
30				Sum of Squares	185.8869627			
31								
32								

Figure D.3: Screen shot of the excel spread sheet with the non linear curve fitting example

$$y = D + \frac{(A-D)}{1+(\frac{x}{c})^B}$$

The graphic representation of the data is shown in Fig. D.4.

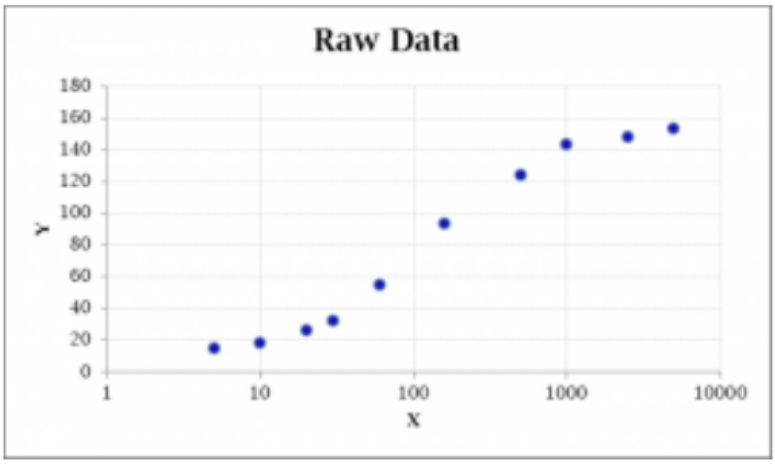

Figure D.4: Graphic representation of the non linear curve fitting example data

The « Predicted » column contains the result of the above equation for each **X** value using the four constants listed on the right of the sheet shown in Fig. D.3, and the cell **D18** contains the following formula:

=$H$21+(($H$18-$H$21)/(1+(B18/$H$20)^$H$19))

To decide if the « Predicted » data is close to the experimental values, a function is needed to measure how well the prediction is matching the data. The standard method is to calculate the difference between predictions and experimental values, and then, square it. The sum of these

squares will then be zero, if the predicted values are in an exact match to the experimental values and it will get larger as the predictions are further away. To do this, the next column « Squared Difference » is the difference between the experimental **Y** value and the predicted value squared. Thus, in the cell **E18** is the following formula

=(C18-D18)^2

These results for each data point are summed up and shown at the bottom of the data, « Sum of Squares », **E30**.

Initially, the values for the four constants are setup using knowledge of the function which is being fitted : **A** will be around the minimum point of the line, with **D** being the maximum. **B** is the slope of the middle part of the curve and **C** is the point of inflection, or the point where the curve changes direction. Using the experimental data, it is possible to guess the four parameters.

It is always best to enter some educated guesses as starting values otherwise the solver can get stuck and give unexpected results.

Now the solver can be initiated, the objective is to minimize the sum of squares value defined above, as we want this to be as small as possible meaning that the predicted values will be as close as possible from the experimental data. The four constants need to be selected in the « By Changing Variable cells » as the solver is going to adjust these by minimization of the sum of squares, see Fig. D.5.

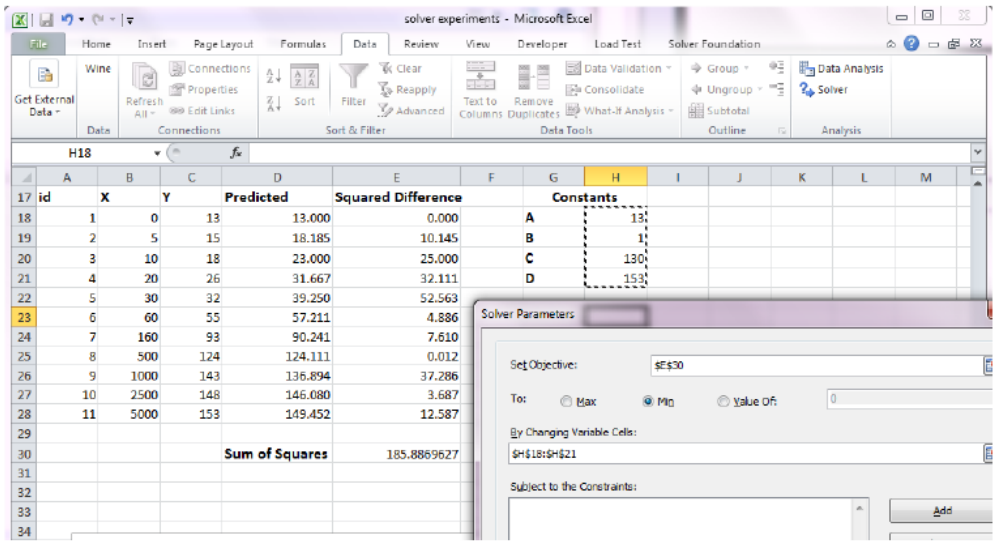

Figure D.5: Minimization of the sum of squares in Solver Parameters Tab

Press solve and the four constants will be overwritten with the solver results. The results in our case are: A=11.345, B=1.127, C=130.285, D=153.936 and the final fitted line is shown in Fig.

D.6.

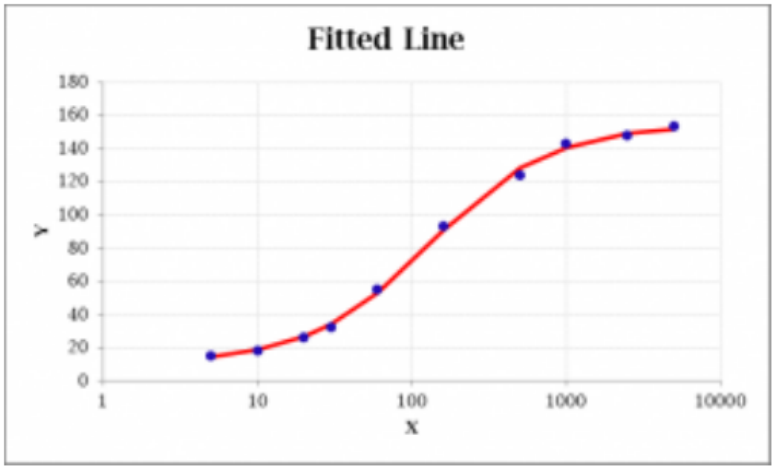

Figure D.6: Fitted line to the non linear curve fitting example data

Uncertainty bars for a data chart in Excel

Once you created your preliminary chart, to add uncertainty bars:

1. Double-click on one of your data points (or data bars)
2. A menu named "Format Data Series" will pop up, select either the "X Error Bars" or the "Y Error Bars" depending on which (or both) parameter has the uncertainty.
3. Usually, the error bar has is both positive and negative, so select that as the display option.
4. If you calculated the standard deviation or standard error for you data, use the "Custom" option and enter the grids that contain the data for your "Error amount". Otherwise choose the "Error amount" option that suits your data the best.
5. If you have more than one series of data, repeat steps 1-4 for that series as well. (Simply double-click on one of the data points for that series)

Finding the uncertainty in the slope of a line (Excel's LINEST Function)

Frequently we find a physical quantity as the slope of a graph. However, we don't have any way to evaluate the uncertainty in the slope we obtained. Fortunately, Excel has a worksheet function LINEST which extends the results of the TRENDLINE function to give the uncertainty in the slope. The syntax of this function is: LINEST(*known_Y_ values, known_X_values, Constant, Statistics)*.

If *Constant* is TRUE, LINEST calculates the intercept. Otherwise, the intercept is set to $y = 0$. If Statistics is TRUE, LINEST returns regression statistics.

LINEST returns several values and thus is an example of an array function. To use an array function we must:

(1) Select an output range,

(2) Press CTRL+SHIFT+ENTER to complete the entry. LINEST returns an array that is two columns wide and three rows long with values as follows:

Slope	Intercept
Standard error (se) of the slope	Standard error (se) of the intercept
R2	Standard error (se) in y

The spreadsheet below shows a set of data. We will show you how to use LINEST to find the uncertainty in the calculated slope.

	A	B	C	D
1	X	Y		
2	1	2.34		
3	2.4	3.78		
4	5.5	11.2		
5	7.2	14.1		
6				
7				
8	m	1.998815	-0.19023	b
9	se slope	0.153543	0.723652	se b
10	R2	0.988336	0.75295	se y
11				

(1) Open a new Excel worksheet. Enter the text in A1:B5.

(2) Select B8:C10, type the formula =LINEST(B2:B5,A2:A5,TRUE,TRUE) and press CTRL+SHIFT+ENTER to complete the entry.

(3) Notice that the slope is determined to be 2.0 ± 0.2

E Summary of Important Statistical Distributions

Several probability distributions are used routinely in several scientific fields. A very good summary is provided on line [16] or in textbook [17] Among the main distributions we found the uniform, Gaussian (or normal), Log-normal, Binomial and Poisson distributions. A small summary of these distributions is provided below.

Uniform distribution

- Probability density function f(x) = 1/n between a and b, zero otherwise.

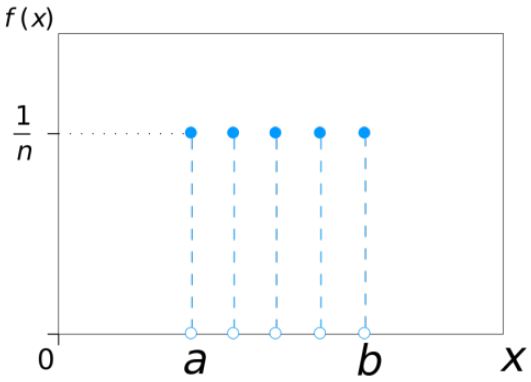

- A known, finite number of outcomes equally likely to happen

Normal distribution (Gaussian distribution)

- Probability density function f(x) = $\frac{1}{\sigma\sqrt{2\pi}} e^{-\frac{(x-\mu)^2}{2\sigma^2}}$
- Fully characterized by its average μ and standard deviation σ.
- Normal distributions are extremely important in statistics and are often used in the natural and social sciences for real-valued random variables whose distributions are not known.

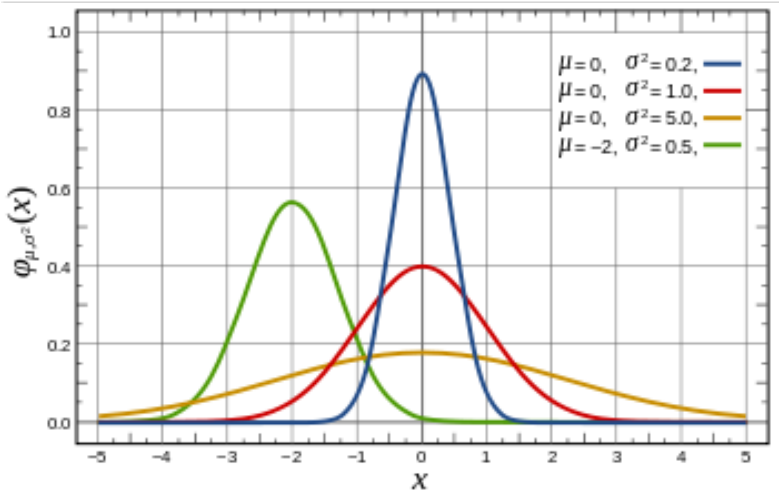

- The normal distribution is immensely useful because of the central limit theorem, which states that, under mild conditions, the mean of many random variables independently drawn from the same distribution is distributed approximately normally, irrespective of the form of the original distribution

Log-normal

- Probability density function f(x) = $\frac{1}{x\sqrt{2\pi}\sigma} e^{-\frac{(\ln x-\mu)^2}{2\sigma^2}}$

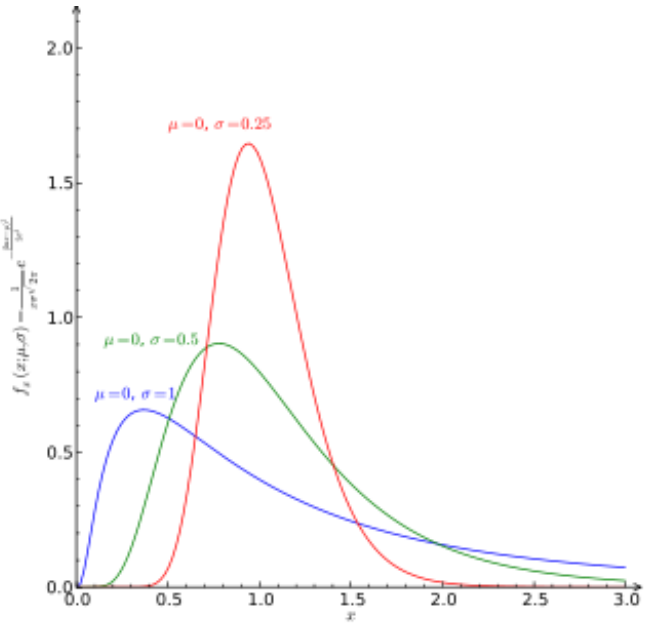

- Fully characterized by its average μ and standard deviation σ.

- A variable might be modeled as log-normal if it can be thought of as the multiplicative product of many independent random variables each of which is positive.

Binomial

- Probability density function f(k) = $\binom{n}{k} p^k (1-p)^{n-k}$

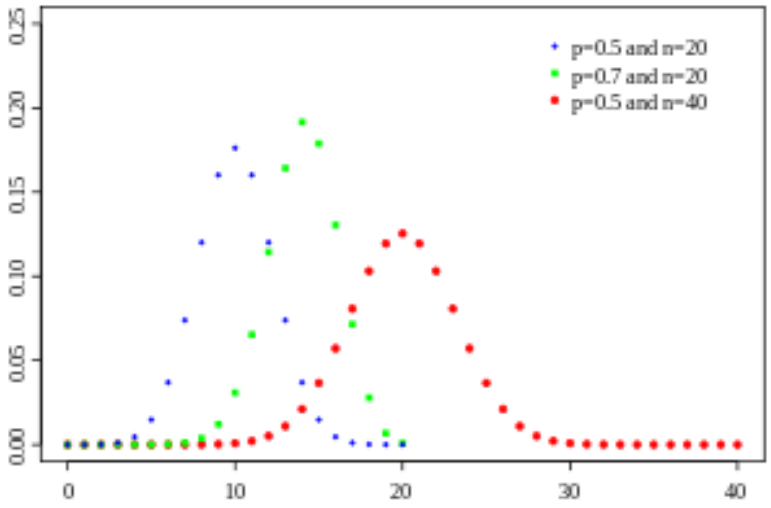

- This is the discrete probability distribution of the number of successes in a sequence of n independent yes/no experiments, each of which yields success with probability p.

Poisson

- Probability density function f(k) = $\frac{\lambda^k}{k!} e^{-\lambda}$
- This is the probability of a given number of events occurring in a fixed interval of time and/or space if these events occur with a known average rate λ and independently of the time since the last event.

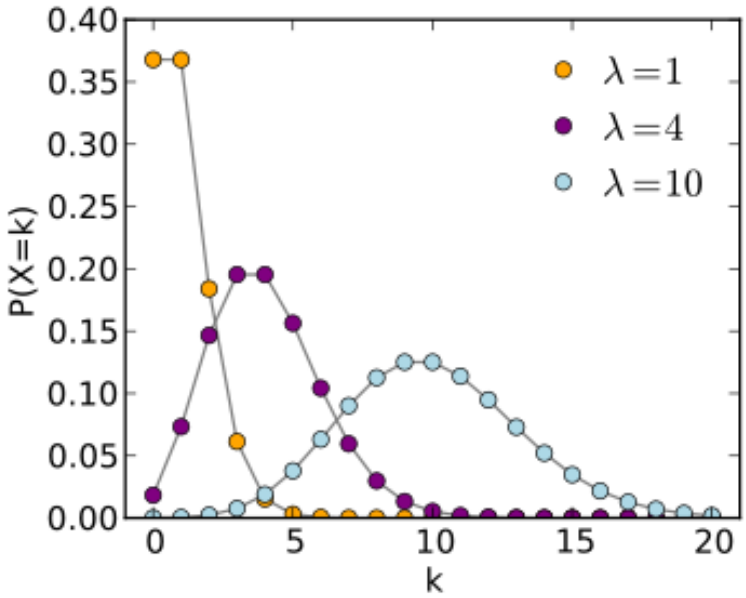
0.40
0.35
0.30
0.25
0.20
0.15
0.10
0.05
0.00
P(X=k)
0
5
10
15
20
k
λ=1
λ=4
λ=10

F Kinetics parameters predicted with MCNP5-1.6

Recently the Monte Carlo code MCNPX has been extended to predict kinetic parameters of reactors. These kinetic parameters are the generation time (Λ), the delayed neutron fraction (β) and the decay constant in a critical reactor ($\alpha = \beta/\Lambda$). Their evaluations require the computation of the adjoint flux (i.e. the importance of a given neutron to the power generated in a critical reactor). Although routinely calculated in deterministic codes using the multi-group formalism, this quantity is not easily accessible to continuous energy Monte-Carlo codes. Instead the adjoint flux is evaluated using the iterated fission probability which approximate the adjoint flux and is essentially the number of fission generated in the N following cycle of the calculation by a neutron in the present generation [18].

The critical configuration of CROCUS that you are using today has been simulated with MCNPX. The geometry is shown in the Figure below. With the new code capability we calculated $\alpha = 154.4 \pm 1.6\ s^{-1}$, $\beta = 736 \pm 7$ pcm and $\Lambda = 47.68 \pm 0.05\ \mu s$.

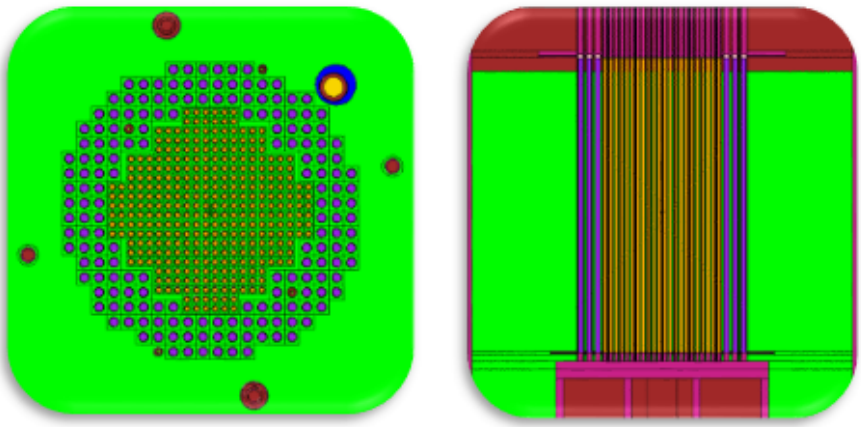

Figure F.1: MCNPX description of the CROCUS reactor in the critical configuration investigated for Exp. 9.

Bibliography

[1] Glenn. F. Knoll, *Radiation Detection and Measurement.* John Wiley and sons New York, 2005.

[2] Operation Manual, *Tri-Carb liquid scintillation analyzer 1900TR.* Packard Instrument company, USA.

[3] B. Baramsai, B. Steinetz, L. Forsley, R. Martin, P. Ugorowski, M. Becks, T. Benyo, A. Chait, R. Hendricks, G. Fralick, *et al.*, "Fast neutron spectroscopy with organic scintillation detectors in a high-radiation environment," tech. rep., 2020.

[4] S. S. Kapoor and V.S. Ramamurthy, *Nuclear Radiation Detectors.* Wiley Eastern Limited, New Delhi, 1986.

[5] J. R. Lamarsh, *Introduction to Nuclear Reactor Theory.* Addison-Wesley, Reading Massachusetts, USA, 1972.

[6] V. C. Wislon et al., *The Temperature Coefficient of the Diffusion Length for Thermal Neutrons m Water.* CP-23Q6, October, 1944.

[7] J. M. Paratte et al, *A benchmark on the calculation of kinetic parameters based on reactivity effect experiments in the CROCUS reactor.* Annals of Nuclear Energy 33, 2006.

[8] R. C. Runkle, A. Bernstein, and P. Vanier, "Securing special nuclear material: Recent advances in neutron detection and their role in nonproliferation," *Journal of Applied Physics*, vol. 108, no. 11, 2010.

[9] F. B. Darby, M. Y. Hua, O. V. Pakari, S. D. Clarke, and S. A. Pozzi, "Multiplicity counting using organic scintillators to distinguish neutron sources: An advanced teaching laboratory," 2023.

[10] J. F. Briesmeister, *MCNP- A general Monte Carlo N-particle transport code, version 4C.* Los Alamos National Laboratory, Report LA-13709-M, 2000.

[11] Los Alamos National Laboratory, Report LA-13709-M, *A short extract of various sections of the MCNP manual, relevant for the experiment 7*, 2000.

[12] A. E. Profio, *Experimental Reactor Physics.* John Wiley & sons Inc., 1976.

[13] R. Keepin, *Physics of Nuclear Kinetics.* Addison-Wesley Publishing company, inc. Reading, Massachusettes, U.S.A, 1965.

[14] Früh, *Réacteur CROCUS- Détermination de la puissance absolue.* Internal report, LPR-179, 1990.

[15] http://www3.nd.edu/ wzech/Genie%202000%20Operations%20Manual.pdf.

[16] http://en.wikipedia.org/wiki/Probability_distribution.

[17] K. Protassov, *Probabilite et incertitudes dans l'analyse des données expérimentales.* Université Joseph Fourier, 1999.

[18] B.C. Kiedrowski, T.E. Booth, F.B. Brown, J.S. Bull, J.A. Favorite, R.A. Forster, and R.L. Martz, *MCNP5-1.60 Feature Enhancements & Manual Clarifications.* Los Alamos National Laboratory, Report LA-UR-10-06217, 2010.